Syntheses and Properties of Branched Sulfonated Poly(arylene ether ketone sulfone)s for Proton Exchange Membranes

Zur Erlangung des akademischen Grades eines

DOKTORS DER NATURWISSENSCHAFTEN

(Dr. rer. nat.)

von der KIT-Fakultät für Chemie und Biowissenschaften

des Karlsruher Instituts für Technologie (KIT)

genehmigte

DISSERTATION

von

M.Sc. Yunji Xie

geboren in Jilin, China

1. Referent:	Prof. Dr. Patrick Théato
2. Referent:	Prof. Dr. Pavel Levkin
Tag der mündlichen Prüfung:	14.07.2023

Die vorliegende Arbeit wurde vom Januar 2019 bis April 2023 unter Anleitung von Prof. Dr. Patrick Théato am Karlsruher Institut für Technologie (KIT) angefertigt.

Erklärung

Ich versichere hiermit, dass ich diese Arbeit selbstständig angefertigt habe und keine anderen, als die angegebenen Quellen und Hinweise benutzt, sowie die wörtlich oder inhaltlich übernommenen Stellen als solche kenntlich gemacht und die Satzung des Karlsruher Instituts für Technologie (KIT) zur Sicherung guter wissenschaftlicher Praxis in der gültigen Fassung beachtet habe. Die elektronische Version der Arbeit stimmt mit der schriftlichen überein und die Abgabe und Archivierung der Primärdaten gemäß Abs. A (6) der Regeln zur Sicherung guter wissenschaftlicher Praxis des KIT beim Institut ist gesichert.

Ort, Datum, Unterschrift

Abstract

Over the course of more than two decades, sulfonated aromatic polymers, exemplified by sulfonated poly(arylene ether)s, have demonstrated substantial potential for application as proton exchange membranes (PEMs). Introducing a small molar fraction of tri-functional monomer in the conventional polymerization process of these polymers yields a macroscopic network of polymer branches. Compared to their linear counterparts, the fabricated branched sulfonated polymer PEMs typically exhibit improvements in proton conductivity, dimensional stability, and oxidative stability. Herein, the structure-property relationship of branched sulfonated poly(arylene ether ketone sulfone)s PEMs was explored, with the aim of achieving superior performance to the commercial perfluorosulfonic acid (PFSA) polymer PEMs.

The effects of two fundamental parameters, degree of branching (DB) and ion exchange capacity (IEC), on the branched polymer PEMs were investigated through the synthesis of two series of branched poly(arylene ether ketone sulfone)s featuring different contents of branching sites and sulfonic acid groups, respectively. Increasing the DB and IEC exerted a similar impact on most properties of PEMs, except for distinct discrepancies that occurred in dimensional variation and oxidative stability. An increased DB led to isotropic swelling change and enhanced oxidative stability, whereas the influence of IEC was entirely the opposite. To maximize oxidative stability and ensure satisfactory proton conductivity of PEMs, increasing DB to 12.5% and then suitably raising IEC was inferred to be a good option.

Moreover, the impact of sulfonic acid group positioning within the branched polymer architecture on PEMs was studied. A series of branched poly(arylene ether ketone sulfone)s with ultra-densely sulfonated branched centers was synthesized, with a maximum DB value of

12.5% being achieved. In comparison to the analogous branched polymer with relatively random sulfonation along branched arms, concentrating sulfonic acid groups on the branched centers resulted in improved dimensional stability (in-plane direction and volumetric) and proton conduction ability under identical water content. However, the oxidative stability was significantly inferior due to the increased risk of polymer chain degradation.

Expanding upon the results from the above-mentioned investigations, a series of branched poly(arylene ether ketone sulfone)s bearing sulfoalkyl side chains on the branched arms was synthesized, with a consistent DB value of 12.5%. The flexibility of the side chains enhanced the mobility of sulfonic acid groups in the fabricated PEMs. The PEM with an IEC value of 1.73 meq g^{-1} demonstrated proton conductivity and dimensional stability comparable to Nafion 117, a PFSA membrane, as well as decent oxidative stability. Furthermore, the proton conductivity of the PEM with an IEC value of 1.96 meq g^{-1} significantly surpassed that of Nafion 117, resulting in superior H_2/air single-cell performance to Nafion 117.

In summary, the polymer architecture of the branched sulfonated poly(arylene ether ketone sulfone)s was progressively optimized, achieving superior performance to commercial PFSA membranes ultimately. The work presented in this thesis is expected to serve as a guide for the structural design and application of branched sulfonated aromatic polymers as PEMs.

Kurzzusammenfassung

Im Laufe von mehr als zwei Jahrzehnten haben sulfonierte aromatische Polymere, wie zum Beispiel sulfonierte Poly(arylether), ein erhebliches Potenzial für die Anwendung als Protonenaustauschmembranen (PEM) gezeigt. Die Einführung eines kleinen molaren Anteils eines trifunktionalen Monomers in den herkömmlichen Polymerisationsprozess dieser Polymere führt zu einem makroskopischen Netzwerk von Polymerverzweigungen. Im Vergleich zu ihren linearen Analoga weisen die hergestellten verzweigten sulfonierten Polymer-PEMs in der Regel eine verbesserte Protonenleitfähigkeit, Dimensionsstabilität und oxidative Stabilität auf. In diesem Beitrag wurde die Struktur-Eigenschafts-Beziehung von verzweigten sulfonierten Poly(aryletherketonsulfon)-PEMs mit dem Ziel untersucht, eine bessere Leistung als die kommerziellen Perfluorsulfonsäure (PFSA)-Polymer-PEMs zu erzielen.

Die Auswirkungen von zwei grundlegenden Parametern, dem Verzweigungsgrad (DB) und der Ionenaustauschkapazität (IEC), auf die verzweigten Polymer-PEMs wurden durch die Synthese von zwei Serien von verzweigten Poly(arylenetherketonsulfonen) mit unterschiedlichem Gehalt an Verzweigungsstellen bzw. Sulfonsäuregruppen untersucht. Eine Erhöhung des DB und der IEC hatte einen ähnlichen Einfluss auf die meisten Eigenschaften der PEMs, mit Ausnahme deutlicher Unterschiede in der Dimensionsstabilität und der oxidativen Stabilität. Ein erhöhter DB führte zu isotropen Quellungsänderungen und erhöhter oxidativer Stabilität, während die IEC genau das Gegenteil bewirkte. Um die oxidative Stabilität zu maximieren und eine zufriedenstellende Protonenleitfähigkeit der PEMs zu gewährleisten, wurde eine Erhöhung des DB auf 12,5 % und eine anschließende Erhöhung der IEC als sinnvolle Option abgeleitet.

Darüber hinaus wurde der Einfluss der Positionierung der Sulfonsäuregruppe innerhalb der verzweigten Polymerarchitektur auf die PEMs untersucht. Es wurde eine Serie von verzweigten Poly(arylenetherketonsulfonen) mit extrem dicht sulfonierten verzweigten Zentren synthetisiert, wobei ein maximaler DB-Wert von 12,5 % erreicht wurde. Im Vergleich zum analogen verzweigten Polymer mit relativ zufälliger Sulfonierung entlang der verzweigten Arme, führte die Konzentration von Sulfonsäuregruppen an den verzweigten Zentren zu einer verbesserten Dimensionsstabilität (in der Ebene und volumetrisch) und Protonenleitfähigkeit bei gleichem Wassergehalt. Die oxidative Stabilität war jedoch aufgrund der erhöhten Empfindlichkeit der Polymerkette deutlich geringer.

Aufbauend auf den Ergebnissen der oben genannten Untersuchungen wurde eine Reihe von verzweigten Poly(arylenetherketonsulfonen) mit Sulfoalkyl-Seitenketten an den verzweigten Armen synthetisiert, wobei der DB-Wert konstant auf 12,5 % gehalten wurde. Die Flexibilität der Seitenketten verbesserte die Mobilität der Sulfonsäuregruppen in den hergestellten PEMs. Die PEM mit einem IEC-Wert von 1,73 meq g^{-1} zeigte eine mit Nafion 117, einer PFSA-Membran, vergleichbare Protonenleitfähigkeit und Dimensionsstabilität sowie eine gute oxidative Stabilität. Darüber hinaus übertraf die Protonenleitfähigkeit der PEM mit einem IEC-Wert von 1,96 meq g^{-1} deutlich die von Nafion 117, was zu einer besseren H_2 /Luft-Einzelzellenleistung im Vergleich zu Nafion 117 führte.

Zusammenfassend lässt sich sagen, dass die Polymerarchitektur der verzweigten sulfonierten Poly(arylenetherketonsulfone) schrittweise optimiert wurde, so dass letztlich eine bessere Leistung als bei kommerziellen PFSA-Membranen erzielt wurde. Die in dieser Arbeit vorgestellte Arbeit soll als Leitfaden für das strukturelle Design und die Anwendung

verzweigter sulfonierter aromatischer Polymere als PEMs dienen.

Contents

1. Theoretical Background

Energy is a vital resource for human survival, evolving and being utilized in tandem with advancements in science and technology. [1] The Industrial Revolution, commencing in the mid-18th century, spurred the rapid expansion of the coal industry, establishing it as the foremost energy source in the world. In the early 20th century, the electrification revolution profoundly altered human lifestyles, positioning petroleum as the primary energy form. [2]

As the global population experienced exponential growth, energy consumption and demand escalated. Concerns regarding the potential depletion of fossil fuels and the environmental degradation resulting from their combustion drove the pursuit of alternative clean energy sources. [3] The European Union's Horizon 2020 plan integrates safe, efficient, and clean energy into its framework, endorsing the transition from existing energy systems to reliable, sustainable, and competitive alternatives while promoting research and innovation. [4]

1.1. Fuel Cells

Fuel cells are energy conversion devices that directly transform chemical energy into electrical energy through an electrochemical reaction involving a fuel and oxidant. [5, 6] In contrast to traditional heat engines, which derive electrical energy via multiple energy conversions, fuel cells exhibit a superior energy conversion efficiency of up to 60%. Furthermore, fuel cells generate only non-polluting emissions, pure water, and reusable thermal energy. [7, 8]

The first fuel cell device was invented by William Grove in 1839. Exploiting the different redox potentials of oxygen and hydrogen, this apparatus conducted an electrochemical reaction upon the catalyzation of platinum, yielding an electromotive force and supplying voltage to the

external circuit. [9] Following over a century of progress, various types of fuel cells have been developed, primarily categorized into five types based on their electrolytes: solid oxide fuel cells (SOFCs), molten carbonate fuel cells (MCFCs), phosphoric acid fuel cells (PAFCs), proton exchange membrane fuel cells (PEMFCs), and alkaline fuel cells (AFCs), as illustrated in **Figure 1.1**. [10, 11]

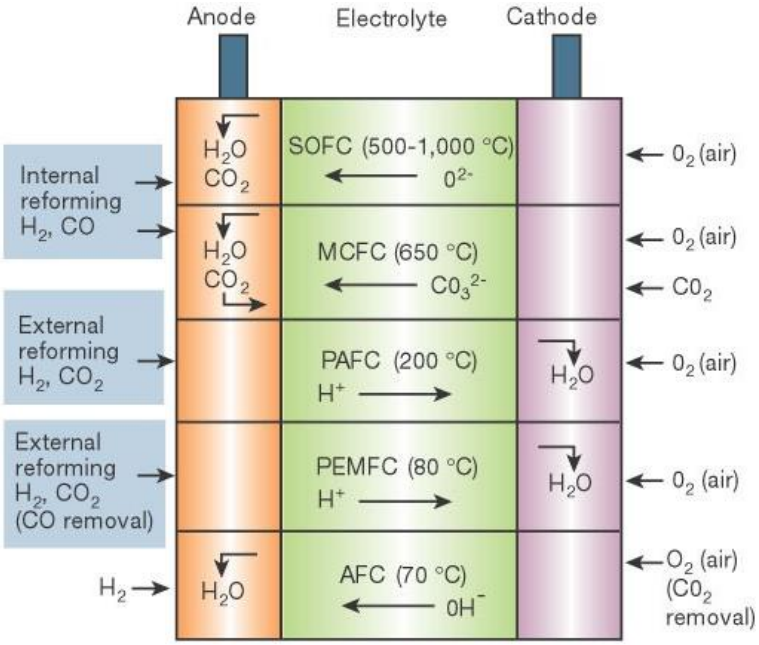

Figure 1.1. Overview of the various types of fuel cells. Reproduced with permission from Ref. [10]. Copyright 2001 Springer Nature.

All types of fuel cells adhere to the same fundamental principle: fuel undergoes an oxidation reaction at the anode, generating electrons. These electrons traverse an external circuit and reach the cathode, where they engage in a reduction reaction with the oxidant. Simultaneously, different forms of ions transport through the electrolyte and/or membrane that separates the cathode and anode. The reaction products for SOFCs, MCFCs, and AFCs form at the anode, whereas those for PAFCs and PEMFCs form at the cathode. [12, 13] In a theoretical term, fuel cells operate as a medium for the conversion of chemical energy from fuel into electrical energy,

provided that reactants are continuously supplied, fuel cells may consistently produce power. [14, 15]

1.2. Proton Exchange Membrane Fuel Cells

PEMFCs employ ion exchange membranes with the ability of proton conduction, i.e., proton exchange membranes as the electrolyte. [16] In comparison to other liquid electrolytes, the solid electrolyte renders PEMFCs more convenient regarding sealing and assembly. Moreover, the operating temperature of PEMFCs typically remains below 100°C, enabling rapid startup. Additionally, the energy density of PEMFCs surpasses that of most other fuel cells. Consequently, PEMFCs are deemed the principally promising candidate for fuel cells as portable and automotive devices. [17, 18] **Figure 1.2** exhibits the schematic structure of PEMFCs, comprising the proton exchange membrane, catalyst layers, gas diffusion layers, and bipolar plates. [19]

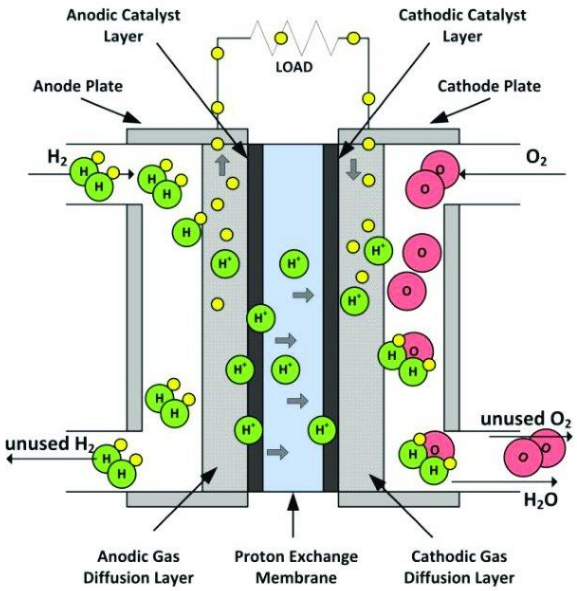

Figure 1.2. The schematic diagram of proton exchange membrane fuel cells. Reproduced with permission from Ref. [19]. Copyright 2014 Elsevier.

With hydrogen utilized as the fuel, the fundamental operation process of PEMFCs is as follows: Hydrogen diffuses through the gas diffusion layer and reaches the anode, where it undergoes an oxidation reaction under the catalyzation, dissociating into protons and electrons. The electrons traverse the external circuit to the cathode, while the protons directly pass through the proton exchange membrane. At the cathode, protons engage in a reduction reaction with oxygen and electrons, facilitated by the catalyst, to yield water. The reactants involved in the system are hydrogen and oxygen, with water being the sole product. [20, 21]

1.3. Proton Exchange Membranes

As one of the core components of PEMFCs, the proton exchange membranes (PEMs) are primarily composed of polymer electrolytes containing sulfonic acid groups, [22, 23] which perform several functions: conducting protons from the anode to the cathode; impeding the transit of electrons, thereby compelling electrons to reach the cathode exclusively through the external circuit; preventing direct contact between electrodes to avoid short circuits; and serving as a scaffold to support the catalyst layer. [24, 25] Consequently, to fulfill these requirements, qualified PEMs ought to exhibit outstanding proton conductivity and insulation capability, low fuel permeability, robust mechanical properties, and excellent stability. [26]

1.3.1. Perfluorosulfonic Acid Polymers

Perfluorosulfonic acid (PFSA) polymers, developed by DuPont in the 1960s, have been the most successful PEM materials thus far, with Nafion and its derivatives serving as predominant examples. [27] As illustrated in **Figure 1.3**, the representative chemical structure of Nafion consists of a hydrophobic polytetrafluoroethylene backbone and hydrophilic perfluorosulfonic

acid side chains. [28] The perfluorinated main chain structure provides PFSA polymers with exceptional chemical stability, while the highly acidic side chains confer outstanding proton conductivity. However, the operation temperature range of PFSA membranes is significantly constrained due to the relatively low glass transition temperature (around 130 °C), leading to a substantial decline in mechanical properties above 100°C. Moreover, PFSA membranes exhibit high fuel permeability, diminishing the efficiency and durability of PEMFCs. Critically, the high cost resulting from the complex synthesis process and the severe environmental pollution generated during waste material incineration limit the large-scale commercial deployment of PFSA membranes. [29] Additionally, recent regulatory considerations by the European Union to ban fluoropolymers may further hinder their widespread adoption. [30]

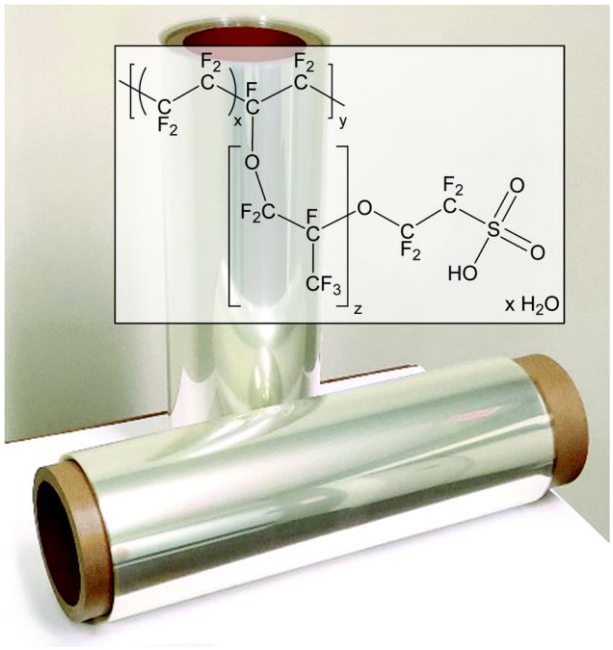

Figure 1.3. Representative chemical structure and roll of a Nafion® membrane. Reproduced with permission from Ref. [28]. Copyright 2021 Royal Society of Chemistry.

1.3.2. Sulfonated Aromatic Polymers

Owing to the limitations mentioned above, massive research has been devoted to the

development of alternative materials for PFSA membranes, with sulfonated aromatic polymers emerging as the most promising candidates. [31] Due to the rigid polymer backbone, sulfonated aromatic polymers maintain excellent thermal stability and mechanical properties above 200°C. Additionally, reduced fuel permeability and lower cost further enhance their suitability for commercialization. [32] Among the most extensively studied sulfonated aromatic polymers, classified by the main chain structure, are sulfonated poly(arylene ether)s, [33-36] sulfonated polyimides, [37, 38] sulfonated polybenzimidazoles, [39, 40] and sulfonated poly(phenylene)s [41, 42]. Nonetheless, the imide ring of sulfonated polyimides demonstrates instability toward hydrolysis, triggering degradation of the main chain and thereby reducing the lifespan of PEMFCs. [43, 44] Due to the acid-base interactions, sulfonated polybenzimidazoles typically manifest markedly low proton conductivity. And polybenzimidazoles doped with inorganic acid H_3PO_4 are generally used as the electrolyte for PAFCs. [45, 46] Furthermore, the synthesis process of sulfonated poly(phenylene)s involves relative complexity and the employment of costly transition metal catalysts. [47, 48] Therefore, sulfonated poly(arylene ether)s have gained prominence among these sulfonated aromatic polymers.

1.4. Sulfonated Poly(arylene ether)s

Poly(arylene ether)s (PAEs) composed of alternating rigid aromatic rings and flexible ether bonds, are a class of high-performance thermoplastic materials with exceptional thermal stability, robust mechanical properties, and remarkable chemical resistance. [49] These attributes find extensive application in diverse high-tech domains, including the aerospace industry, medical equipment, automobile production, and electronic manufacturing. [50, 51] The introduction of sulfonic acid groups into the PAEs is a requisite step to endow PEMs with a

proton conduction ability. [52] The synthesis of sulfonated poly(arylene ether)s (SPAEs) is typically divided into two categories based on the variation in reaction substrates: polymerization of sulfonated monomers or post-sulfonation of polymers. [53]

The polymerization of sulfonated monomers refers to the preliminary synthesis of sulfonated monomers, which are subsequently polymerized with other non-sulfonated monomers to yield SPAEs. [54] This method offers a well-controlled degree of sulfonation and a precisely ordered monomeric structure of the polymer, eliminating the risk of polymer backbone degradation upon post-sulfonation. [55] However, the variety of sulfonated monomers is limited, resulting in a reduced variation of architecture for SPAEs. Moreover, the steric hindrance of sulfonated monomers declines their reactivity during condensation polymerization, thereby restraining the potential for increasing the molecular weight of the polymer. [55, 56]

The post-sulfonation of polymers primarily involves electrophilic aromatic substitution reaction on PAEs. [57] This reaction tends to occur preferably on aromatic rings associated with electron-donating groups, replacing hydrogen atoms with sulfonic acid groups. Conversely, when aromatic rings are linked with electron-withdrawing groups, the post-sulfonation reaction is hampered. [58] Consequently, the integration of monomers with diverse structures into the polymer, followed by post-sulfonation, leads to SPAEs with versatile architectures. However, this process potentially exposes the polymer to degradation and other side reactions, rendering the precise control over the degree of sulfonation and the positioning of sulfonic acid groups challenging. Hence, the appropriate selection of a sulfonation agent that aligns with the polymer structure, coupled with meticulous control over reaction conditions, is crucial. [59, 60]

1.4.1. Proton Conduction

Initially developed SPAEs with relatively simple architectures generally demonstrated inferior proton conduction abilities at lower ion exchange capacity (IEC) values. To achieve proton conductivity comparable to PFSA membranes, a high IEC is generally necessary, leading to massive water absorption and consequentially excessive swelling change. [61, 62]

It is widely accepted that there are three types of mechanisms for proton conduction within PEMs: the *vehicle*, the *Grotthuss*, and the *surface* mechanisms. [63, 64] As shown in **Figure 1.4**, upon dissociating from sulfonic acid groups, protons form associations with water molecules. The *vehicle* mechanism suggests that protons diffuse alongside the water molecule carriers, while a counterflow of the nonionic carriers arises. In contrast, the *Grotthuss* mechanism theorizes that protons move through the rupture and reformation of hydrogen bonds with water molecules in a "hopping" fashion. Additionally, the *surface* mechanism enables protons to transport between sulfonic acid groups, mediated by water molecules. Typically, these three mechanisms coexist and one of the mechanisms may act dominant based on the water content within the PEMs. As the water content increases, the prevailing mechanism transitions from the *surface* to the *vehicle*, and ultimately to the *Grotthuss* mechanism. [65, 66]

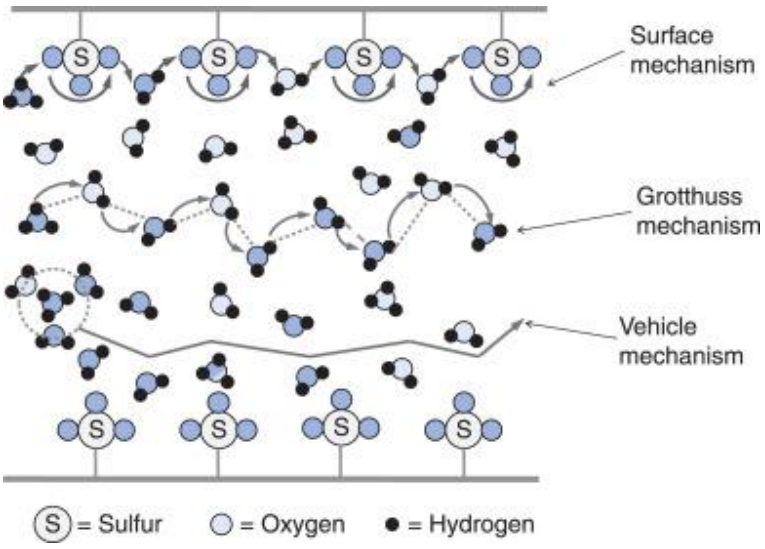

Figure 1.4. Simplified schematic representation of proton conduction in hydrated proton exchange membranes. Reproduced with permission from Ref. [64]. Copyright 2012 Elsevier.

Due to the dependency on the water molecules, proton conduction typically occurs in the hydrated ionic domains, thus the interconnectivity of the hydrophilic nanochannels is the decisive factor for proton conductivity. [67, 68] In a pioneering work, Kreuer performed a comparative analysis of the microscopic morphology of Nafion and sulfonated polyetherketone (SPEEKK) by small-angle X-ray scattering (SAXS). [69] As depicted in **Figure 1.5**, a pronounced hydrophilic-hydrophobic phase separation morphology forms within Nafion, with interconnected hydrophilic phases constructing wide proton transportation channels. This is attributed to the significant difference in polarity between the highly hydrophobic perfluorinated main chain and the strongly acidic perfluorosulfonic acid side chains, which promotes the formation of well-defined microscopic morphology. Conversely, the hydrocarbon-based backbone of SPEEKK displays weaker hydrophobicity and the acidity of the aryl sulfonic acid groups is less pronounced, resulting in less-developed hydrophilic-hydrophobic phase separation and narrow proton transport channels, which hinder effective proton conduction.

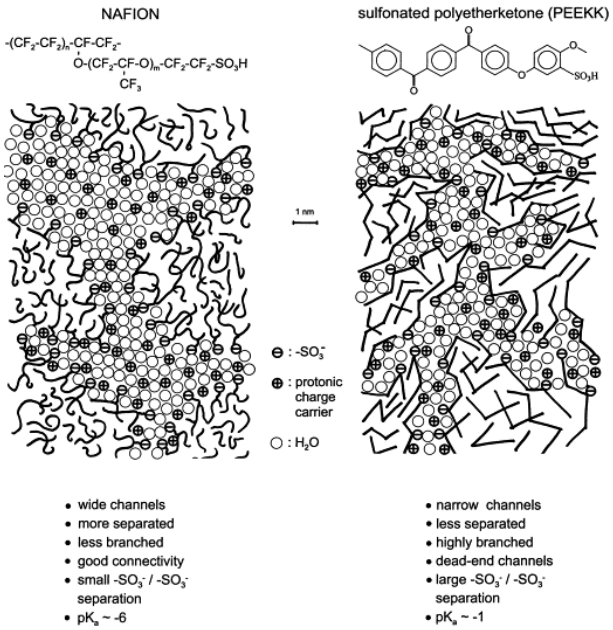

Figure 1.5. Schematic representation of the microscopic morphology of Nafion and sulfonated polyetherketone. Reproduced with permission from Ref. [69]. Copyright 2001 Elsevier.

Therefore, strategically designing and optimizing the polymer architecture of the SPAEs and constructing a well-developed microscopic morphology are imperative, thereby achieving comparable or even superior performance to those of PFSA membranes. [70, 71] The following sections introduce several types of SAPEs with representative polymer architectures. The nanoscale morphology is characterized by transmission electron microscope (TEM), atomic force microscope (AFM), and small-angle X-ray scattering (SAXS).

1.4.2. Sulfonated Random Copolymers

In the early stages of PEMs development, sulfonated random copolymers were a focal point of interest due to their straightforward preparation. [72, 73] However, the distribution of the hydrophilic and hydrophobic structural units is disorganized, and both the hydrophobicity of the hydrocarbon-based polymer backbone and the acidity of the sulfonic acid groups are limited. [74, 75] This results in a less-developed hydrophilic-hydrophobic phase separation morphology. Although appropriate monomer selection may lead to the formation of hydrophilic ionic

clusters, which are disorderly dispersed within the hydrophobic matrix and exhibit poor connectivity, culminating in fabricated PEMs with inferior proton conductivity. [76]

Watanabe and Miyatake et al. investigated the impact of the size and structure of hydrophobic structural units on the performance of sulfonated polyether random copolymer PEMs. [77] The result revealed an inverse relationship between the size of the hydrophilic microphase and the size of the hydrophobic structural unit. As shown in **Figure 1.6**, compared to other hydrophobic units, naphthalene was not only smaller but also more inclined to stack due to its planar structure, thus fostering the formation of larger hydrophilic ionic clusters. Therefore, among the four PEMs, the SPE4 exhibited the highest proton conductivity over a wide range of temperature and relative humidity (RH) level.

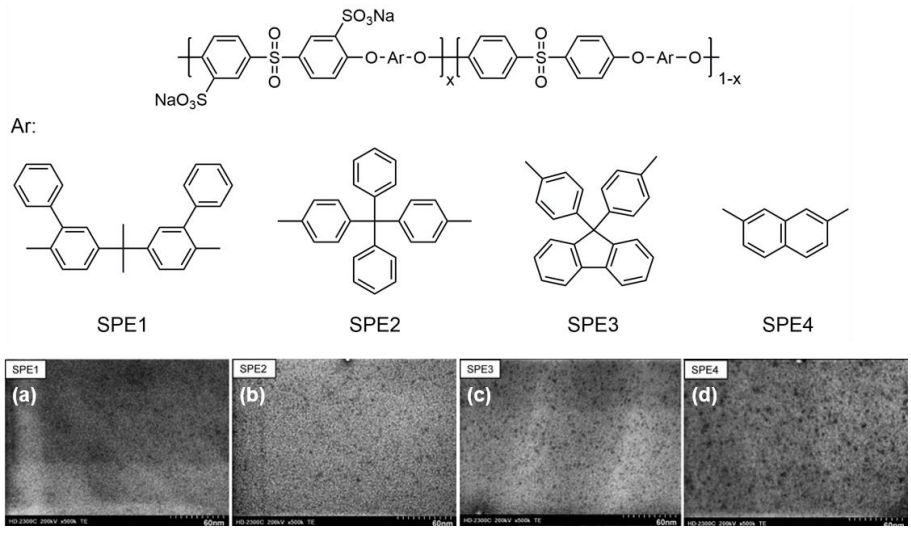

Figure 1.6. Chemical structure of sulfonated polyether random copolymers with different hydrophobic structural units, and TEM images of **(a)** SPE1, **(b)** SPE2, **(c)** SPE3, and **(d)** SPE4. Adapted with permission from Ref. [77]. Copyright 2009 American Chemical Society.

Na and Wang et al. synthesized two types of sulfonated poly(arylene ether ketone sulfone) random copolymers, namely SPEEKS and SPEEKKS, with 4,4'-difluorobenzophenone and 1,4-bi(4-fluorobenzoyl) benzene as non-sulfonated monomers, respectively. [78] The aim was to

investigate the relationship between the structure of the polymer backbone and the physical and electrochemical behaviors of the prepared PEMs. As depicted in **Figure 1.7**, the distance between hydrophilic ionic clusters in SPEEKKS-3 was larger than that of SPEEKS-3 at an identical degree of sulfonation, attributed to the larger size of the hydrophobic structural unit within the former. Consequently, SPEEKKS-3 indicated better mechanical strength. In contrast, the higher density of ionic clusters improved the proton conductivity of SPEEKS-3. Furthermore, an increase in the degree of sulfonation led to a noticeable aggregation of these clusters from SPEEKS-3 to SPEEKS-5, which consequently enhanced proton conductivity even further.

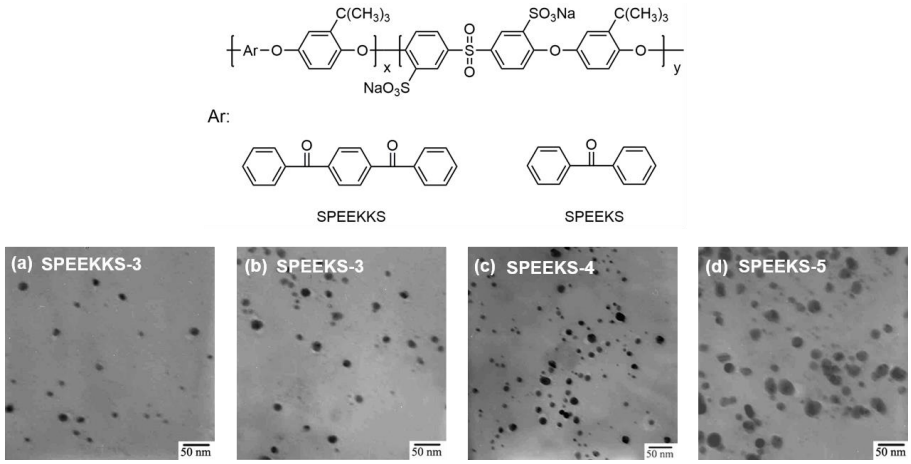

Figure 1.7. Chemical structure of sulfonated poly(arylene ether ketone sulfone) random copolymers with different hydrophobic structural units, and TEM images of **(a)** SPEEKKS-3, **(b)** SPEEKS-3, **(c)** SPEEKS-4, and **(d)** SPEEKS-5. Adapted with permission from Ref. [78]. Copyright 2009 John Wiley and Sons.

1.4.3. Sulfonated Block Copolymers

Sulfonated block copolymers are composed of alternating hydrophilic and hydrophobic chain segments, thus enabling forming a well-defined microphase separation morphology between the hydrophilic and hydrophobic domains. [79, 80] By manipulating parameters such as

dissimilarity, chain length, and volume ratio of each block, the microscopic morphology of the sulfonated block polymer is readily regulated. The fabricated PEMs typically demonstrate superior proton conductivity, even under low relative humidity. [81, 82] However, the synthesis process involved in this type of polymer is considerably complicated, necessitating the preparation of oligomers with varying molecular weights prior to polymerization, inducing significant consumption of time and cost. [83, 84]

McGrath and his colleagues synthesized two types of hydrophobic oligomers end-capped with hexafluorobenzene (BPS0-HFB) and decafluorobiphenyl (BPS0-DFBP), respectively, as illustrated in **Figure 1.8**. [85] Given the high reactivity of perfluorinated aromatic compounds in nucleophilic aromatic substitution reaction, the ensuing coupling reaction with hydrophilic oligomer (BPS-100) may proceed at a relatively low temperature (80 ℃). This process effectively avoided side reactions such as ether-ether exchange reaction. The synthesized sulfonated poly(arylene ether sulfone) multi-block copolymers for PEMs, BPS0-HFB-BPS100 and BPS0-DFBP-BPS100, both exhibited a pronounced microphase separation morphology and coherent proton transportation channels. The incorporation of fluorine not only intensified the hydrophobicity of the polymer backbone but also heightened the acidity of the sulfonic acid groups. Both fabricated PEMs demonstrated outstanding proton conductivity within an RH range of 30-100%. Noteworthy, the proton conductivity of BPS0-DFBP-BPS100 slightly exceeded that of BPS0-HFB-BPS100 at a similar IEC level, due to the higher fluorine content.

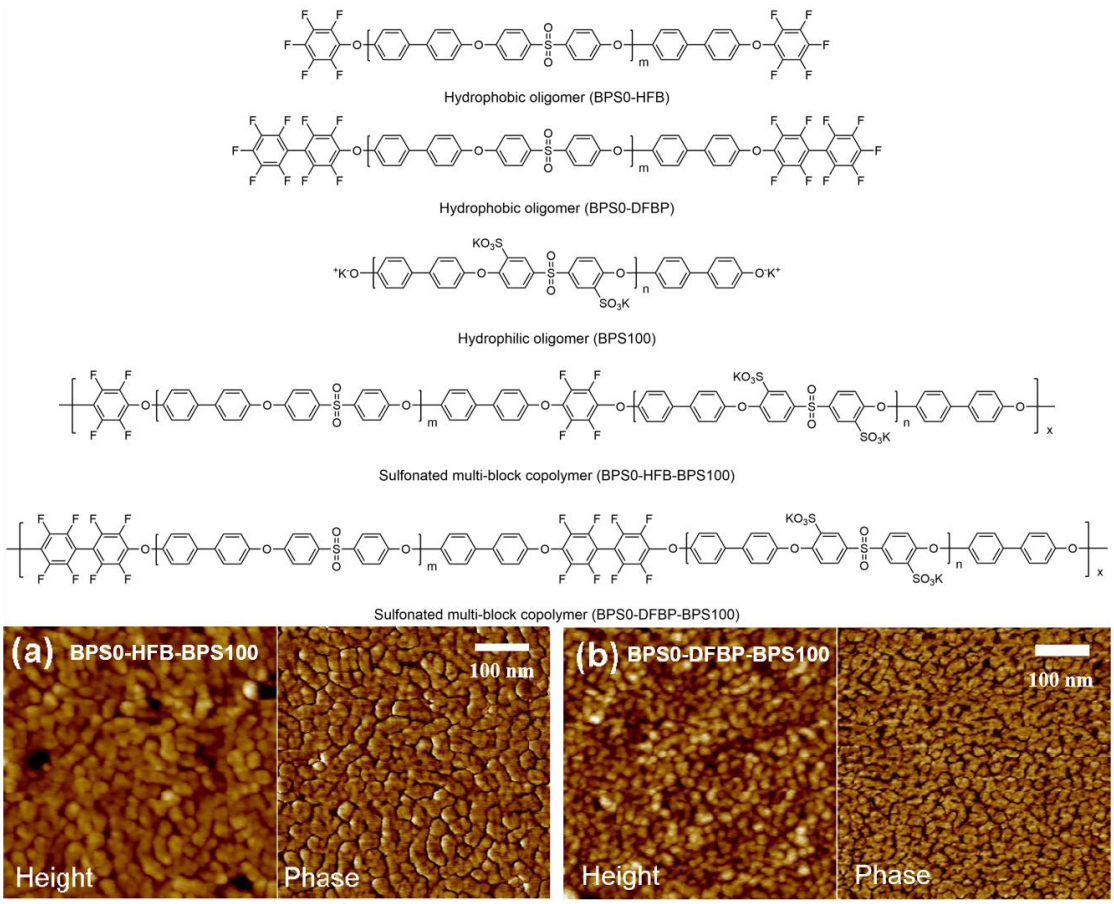

Figure 1.8. Chemical structure of hydrophobic (BPS0-HFB and BPS0-DFBP) and hydrophilic (BPS100) oligomers, and AFM images (tapping mode) of sulfonated poly(arylene ether sulfone) multi-block copolymers **(a)** BPS0-HFB-BPS100 and **(b)** BPS0-DFBP-BPS100. Adapted with permission from Ref. [85]. Copyright 2009 Elsevier.

This group further explored the impact of block length on the properties of sulfonated multi-block copolymer PEMs, with the results indicated in **Figure 1.9**. [86, 87] Decafluorobiphenyl was incorporated in hydrophobic oligomer (BisSF), with the aim to enhance the hydrophobicity of the polymer backbone. As the length of hydrophilic and hydrophobic blocks increased, the microphase separation between these two regions became more pronounced, and the connectivity between the hydrophilic regions tightened. Lengthening the hydrophilic block tended to elevate the proton conductivity of the PEMs, while extending the hydrophobic block exhibited a counteracting effect. Ultimately, the BisSF-BPS100 (17K-12K) achieved optimal

performance, surpassing the commercial Nafion 112 membrane.

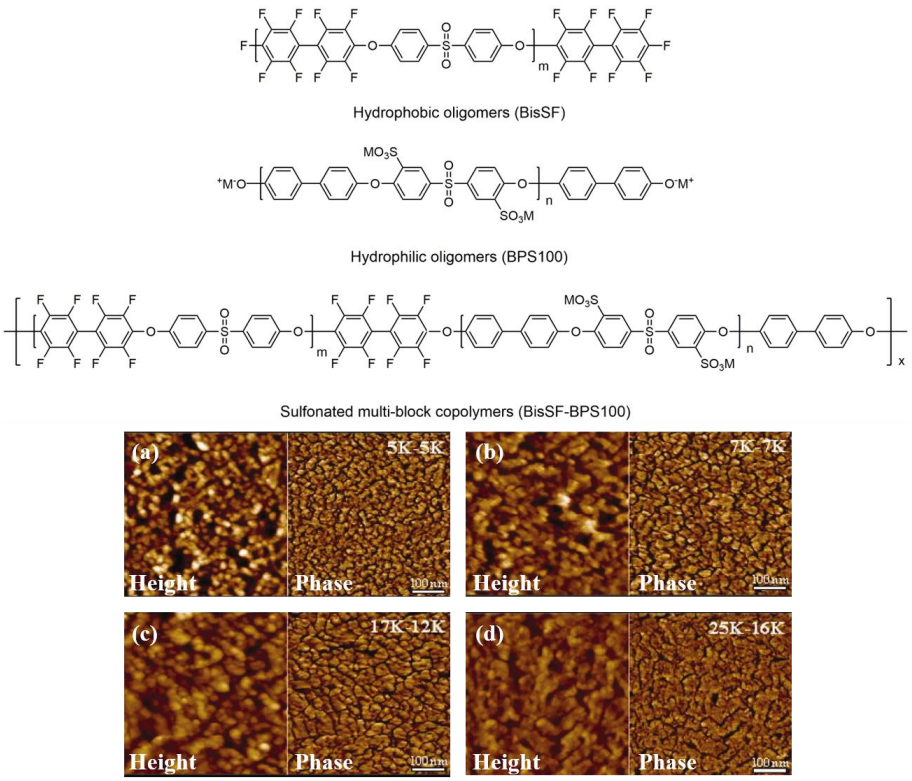

Figure 1.9. Chemical structure of hydrophobic (BisSF) and hydrophilic (BPS100) oligomers, and AFM images (tapping mode) of sulfonated poly(arylene ether sulfone) multi-block copolymers **(a)** BisSF-BPS100 (5K-5K), **(b)** BisSF-BPS100 (7K-7K), **(c)** BisSF-BPS100 (17K-12K), and **(d)** BisSF-BPS100 (25K-16K). Adapted with permission from Ref. [86]. Copyright 2009 John Wiley and Sons.

In a similar research, Jannasch and his team analyzed the influence of the hydrophobic block length on the properties of sulfonated multi-block copolymer PEMs. [88] As detailed in **Figure 1.10**, the sulfonic acid groups in the hydrophilic oligomer were attached to the *ortho* position of the sulfonyl group, which created an electron-deficient environment, thereby enhancing the acidity and stability of sulfonic acid groups. Considering that s1PAES-*b*/*a* possessed an identical length of the hydrophilic block, the size of the hydrophilic region in the AFM images remained nearly unchanged. However, as the length of the hydrophobic block diminished, the size of the hydrophobic region notably contracted. The s1PAES-11k/10k exhibited the

minimum volume fraction of the hydrophobic phase and the highest IEC value, yielding superior proton conductivity to commercial Nafion 212.

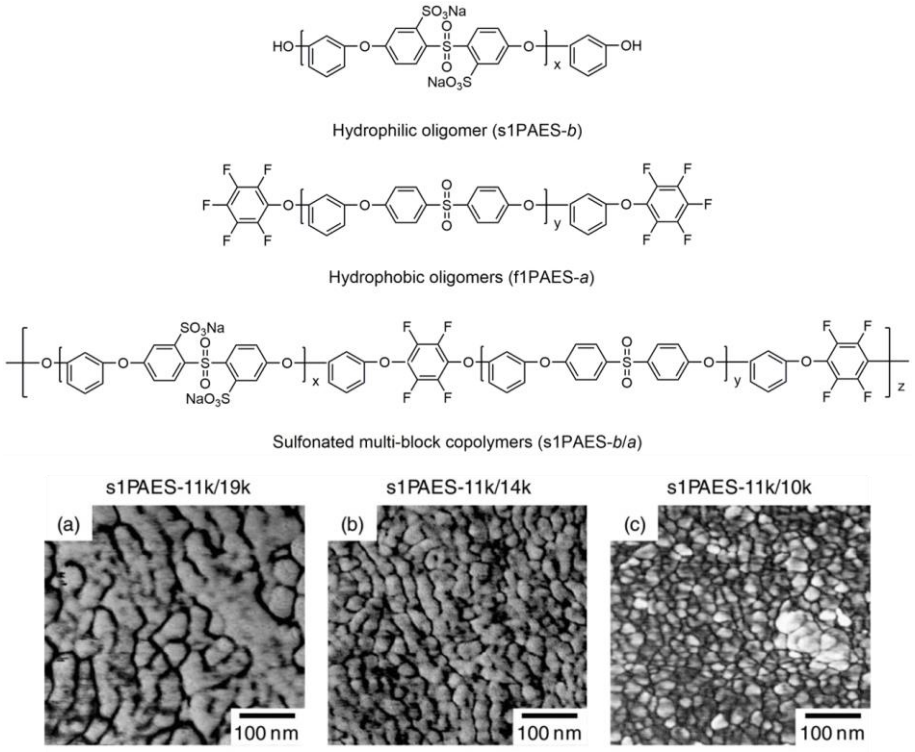

Figure 1.10. Chemical structure of hydrophilic (s1PAES-*b*) and hydrophobic (f1PAES-*a*) oligomers, and AFM phase images (tapping mode) of sulfonated poly(arylene ether sulfone) multi-block copolymers **(a)** s1PAES-11k/19k, **(b)** s1PAES-11k/14k, and **(c)** s1PAES-11k/10k. Adapted with permission from Ref. [88]. Copyright 2012 John Wiley and Sons.

1.4.4. Densely Sulfonated Copolymers

Densely sulfonated copolymers represent a class of polymers featuring the attachment of more than two sulfonic acid groups to a single structural aromatic unit. [89, 90] The strong polarity contrast between the hydrophilic and hydrophobic units promotes the formation of a pronounced microphase separation morphology, even when these units are randomly distributed along the polymer backbone, the proton conductivity of fabricated PEMs is significantly enhanced. [91-93]

Ueda et al. synthesized a series of densely sulfonated poly(ether sulfone) (SPES) random copolymers for PEMs, with eight sulfonic acid groups attaching to a single structural unit. [94] As displayed in **Figure 1.11**, the strong polarity contrast between the hydrophilic and hydrophobic units promoted the development of well-developed microphase separation. Moreover, one of the fabricated PEMs, SPES-5b with an IEC value of 2.03 meq g^{-1} demonstrated a remarkable proton conductivity. Even though the RH reduced to 30%, its proton conductivity remained in the same order of magnitude as that of commercial Nafion 117.

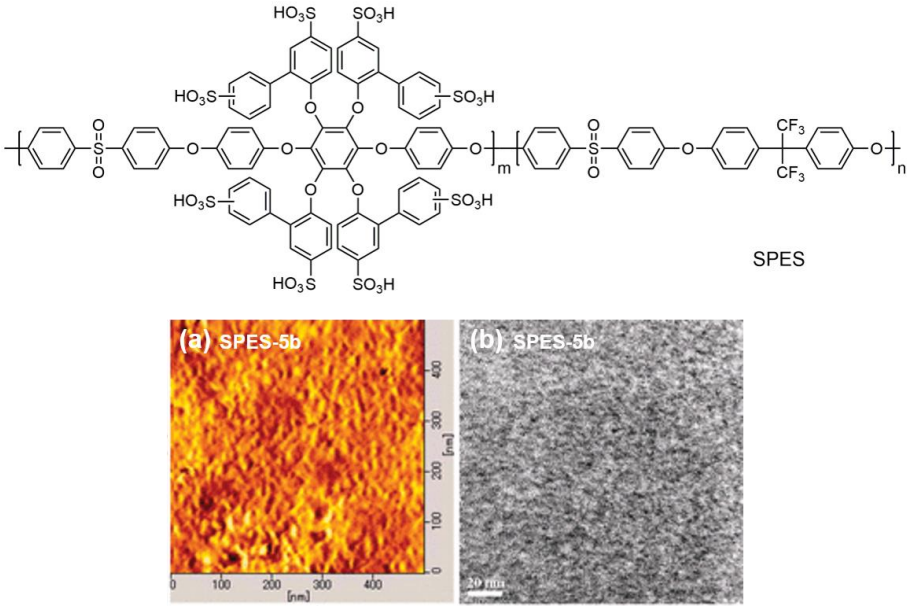

Figure 1.11. Chemical structure of densely sulfonated poly(ether sulfone) random copolymers, and **(a)** AFM tapping phase image and **(b)** cross-section TEM image of SPES-5b. Adapted with permission from Ref. [94]. Copyright 2009 American Chemical Society.

Hay and Meng et al. prepared two types of sulfonated poly(aryl ether) (SPAE) random copolymer PEMs, each featuring nanoclusters endowed with either 6 or 12 sulfonic acid groups, as illustrated in **Figure 1.12**. [95] At an equivalent IEC level, a more distinctive hydrophilic-hydrophobic phase separation morphology along with enlarged hydrophilic ionic clusters was observed from the TEM image of the SPAE-3b. Thus, the proton conductivity of SPAE-3b was

approximately 20% superior to that of SPAE-3a. These results demonstrated that enhancing the densification degree of sulfonic acid groups within a single structural unit promoted the formation of better microscopic morphology, consequently boosting the proton conductivity of PEMs.

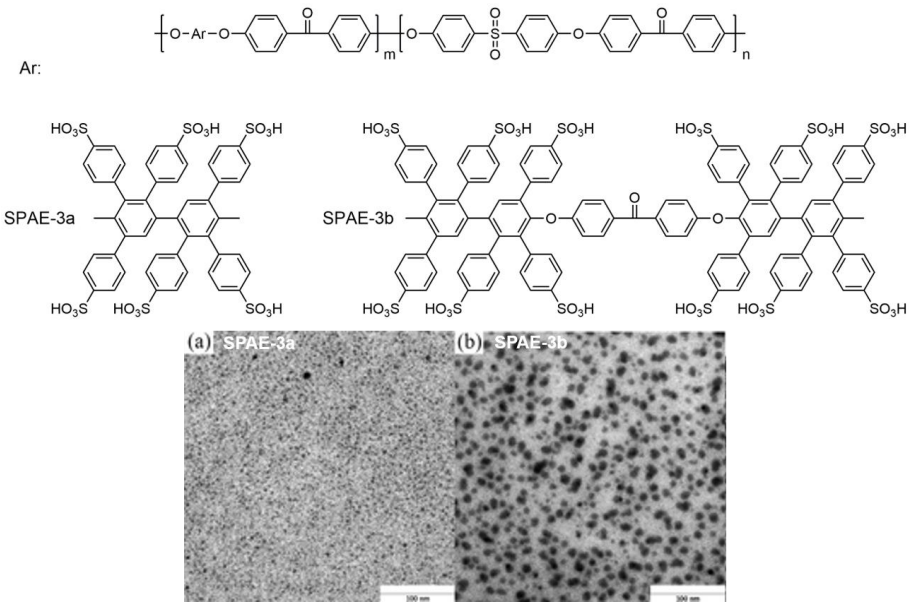

Figure 1.12. Chemical structure of densely sulfonated poly(aryl ether) random copolymers, and TEM images of **(a)** SPAE-3a and **(b)** SPAE-3b. Adapted with permission from Ref. [95]. Copyright 2009 American Chemical Society.

Watanabe and Miyatake et al. combined the strategies of densely sulfonated and multi-block, resulting in the development of a type of densely sulfonated poly(arylene ether sulfone ketone) multi-block copolymers for PEMs, as depicted in **Figure 1.13**. [96] Compared with the conventional sulfonated multi-block copolymers previously synthesized by this team, the novel PEMs exhibited an enhanced hydrophilic-hydrophobic microphase separation morphology and improved proton conductivity. These results underlined the effectiveness of escalating the sulfonation density. By maintaining the dimension of the hydrophobic block constant and elevating the size of the hydrophilic block, the size of the hydrophilic microphase was

effectively increased, which thus elevated the proton conductivity of PEMs. However, when the sizes of both hydrophilic and hydrophobic blocks were simultaneously increased, while keeping their ratio constant, this approach also enlarged the hydrophilic microphase, but disrupted the continuity of the hydrophobic microphase, leading to a decrease in the mechanical strength of PEMs. As a result, the polymer X30Y8 performed optimal performance, achieving proton conductivity surpassing that of commercial Nafion 212 across a range of 30%-90% RH at 80 °C.

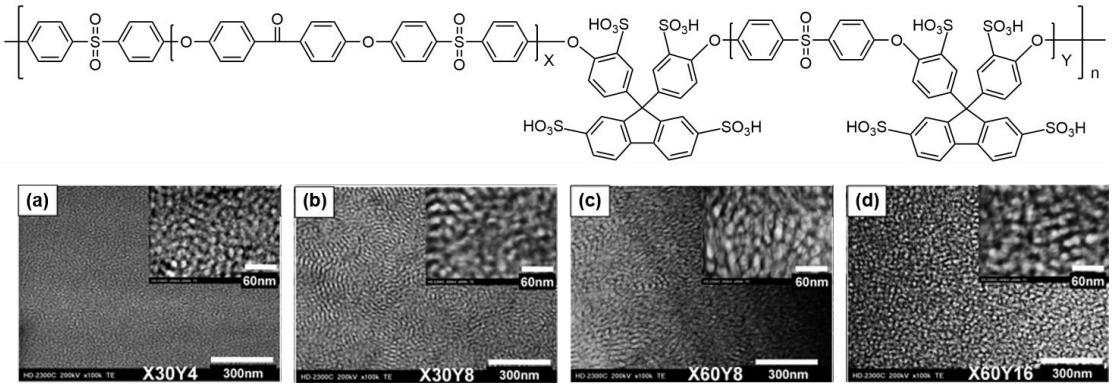

Figure 1.13. Chemical structure of densely sulfonated poly(arylene ether sulfone ketone) multi-block copolymers, and TEM images of **(a)** X30Y4, **(b)** X30Y8, **(c)** X60Y8, and **(d)** X60Y16. Adapted with permission from Ref. [96]. Copyright 2010 American Chemical Society.

1.4.5. Sulfonated Graft Copolymers

Inspired by the chemical structure of PFSA polymers, sulfonated graft polymers are synthesized by attaching sulfonic-acid-groups-functionalized aromatic or aliphatic side chains to the physically and chemically stable main chain. [97, 98] The separated arrangement of hydrophilic and hydrophobic sequences contributes to the formation of a well-defined microphase separation morphology, which is readily modifiable by regulating the length, rigidity, and periodicity of the side chains. [99] The length and rigidity of the side chains impact the size of

the hydrophilic phase, while the grafting frequency of the side chains determines the count of hydrophilic ionic clusters per unit volume. [100, 101]

Guiver and Lee et al. synthesized a series of poly(arylene ether sulfone) (PAES) random copolymers grafted with sulfonated (polyphenylene oxide) (SPPO) side chains for PEMs, as depicted in **Figure 1.14**. [102] The results of TEM presented a distinct microphase separation morphology between the hydrophobic phase constituted by the PAES main chain and the hydrophilic phase formed by the SPPO side chains. Enlarging the side chain size and increasing the grafting frequency both expanded the hydrophilic microphase, thereby constructing interconnected channels for proton transportation and enhancing proton conductivity. The X5-Y14 exhibited superior proton conductivity, outperforming Nafion 112 across an RH range of 30% to 90% at 90 ℃. Noteworthy, the impact of elevating the grafting frequency was more pronounced. Under similar IEC values, the proton conductivity of X5-Y9 markedly exceeded that of X3-Y14.

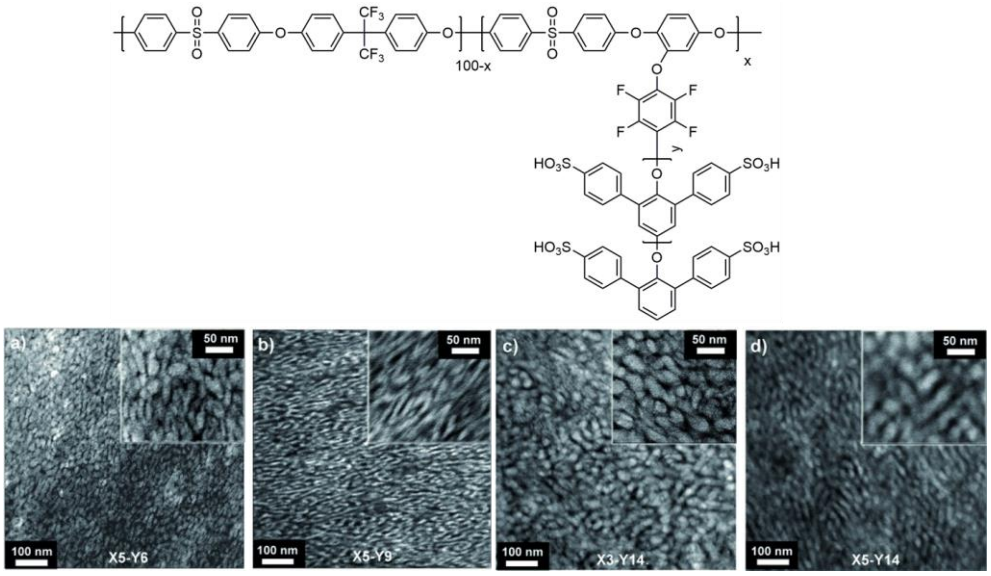

Figure 1.14. Chemical structure of poly(arylene ether sulfone) random copolymers grafted with sulfonated poly(phenylene oxide)s, and TEM images of **(a)** X5-Y6, **(b)** X5-Y9, **(c)** X3-Y14, and **(d)** X5-Y14. Adapted with permission from Ref. [102]. Copyright 2011 John Wiley and Sons.

Flexible alkyl side chains, as compared to rigid aromatic counterparts, may effectively promote the aggregation of sulfonic acid groups, thus forming hydrophilic channels with remarkable connectivity. A series of poly(phenylene ether ketone) multi-block copolymers featuring flexible sulfoalkyl side chains for PEMs was prepared by Wang and Zhang et al., as shown in **Figure 1.15**. [103] The M_xN_y-SO_3H exhibited enhanced hydrophilic-hydrophobic microphase separation morphologies than the analogous random copolymer. Concurrent augmentation in the length of hydrophilic and hydrophobic blocks, while maintaining their ratio constant, a tendency to expand both the hydrophilic and hydrophobic phases was observed. If the length of the hydrophilic block remained unchanged while the hydrophobic block was lengthened, the size of the hydrophobic phase expanded and those of the hydrophilic phase diminished. In the end, irrespective of the diverse chemical composition ratios among the three copolymers, they all demonstrated outstanding proton conductivity, exceeding that of Nafion 212 in a range of 30%-95% RH at 80 ℃.

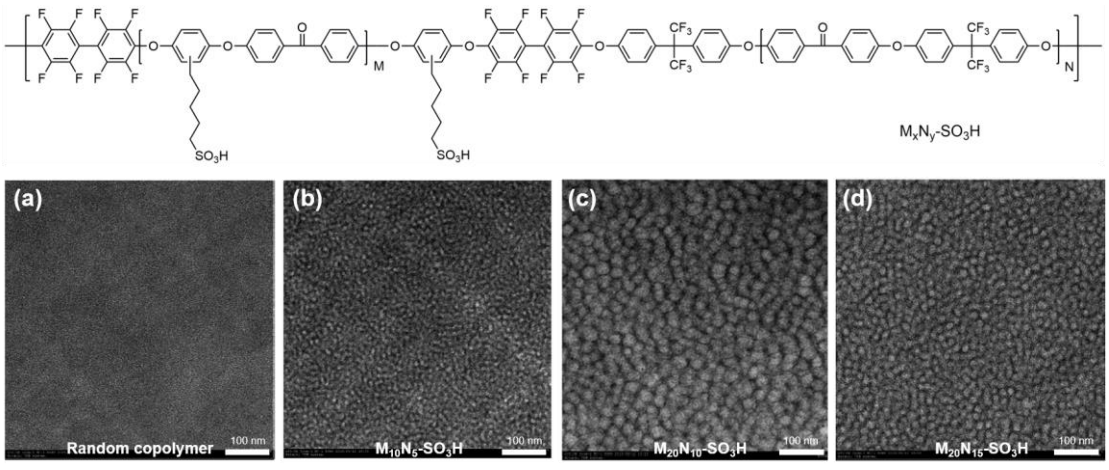

Figure 1.15. Chemical structure of poly(phenylene ether ketone) (M_xN_y-SO_3H) multi-block copolymers grafted with sulfoalkyl side chains, and TEM images of **(a)** sulfonated random copolymer, **(b)** $M_{10}N_5$-SO_3H, **(c)** $M_{20}N_{10}$-SO_3H, and **(d)** $M_{20}N_{15}$-SO_3H. Adapted with permission from Ref. [103]. Copyright 2016 Royal Society of Chemistry.

The combination of graft and densely sulfonated strategies also yields beneficial results. Pang's group synthesized two types of poly(arylene ether) random copolymers with sulfonated tetraarylmethane (SPAE-*x*) and sulfonated hexaarylbenzene (SP-20) as side chains, respectively, as illustrated in **Figure 1.16**. [104] In the relevant SAXS profiles, all the polymer PEMs displayed similar characteristic scattering peaks to that of Nafion 117, indicating the construction of a well-defined hydrophilic-hydrophobic phase separation morphology. Furthermore, the characteristic separation length of the SPAE-*x* was higher than that of SP-20, presumably due to the formation of larger hydrophilic ionic clusters resulting from the higher sulfonation density within a single structural unit. Therefore, the SPAE-15 exhibited better proton conductivity than the SP-20 with a similar IEC level. Additionally, under a fully hydrated state, the proton conductivity of SPAE-18 was approximately 20% higher than that of Nafion 117.

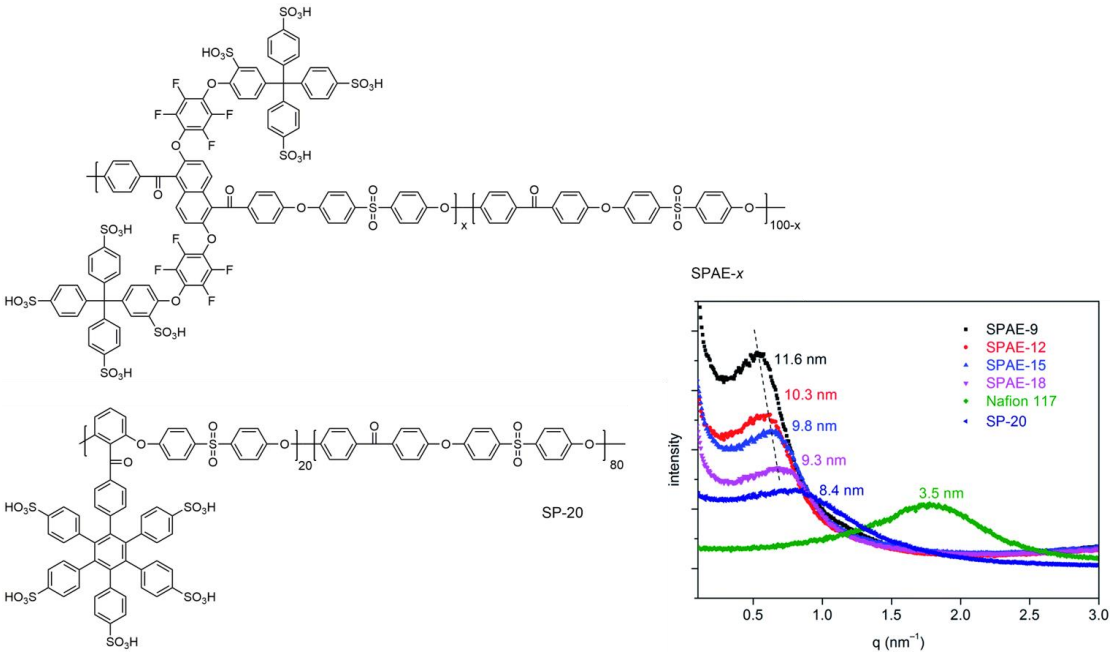

Figure 1.16. Chemical structure of two types of poly(arylene ether) random copolymers featuring densely sulfonated sides chains and the relevant SAXS profiles. Adapted with permission from Ref. [104]. Copyright 2015 Royal Society of Chemistry.

1.4.6. Crosslinked Sulfonated Copolymers

To ensure the long-term operation of PEMFCs, several essential characteristics are required for PEMs, including robust oxidation stability, mechanical performance, and stable dimensions following water absorption without significant variations. [105, 106] Crosslinked sulfonated copolymers enhance these performances by incorporating strengthened interactions between polymer chains, such as covalent bonds. [107] However, the restriction of polymer chain mobility may disrupt the phase separation between hydrophilic and hydrophobic domains and the formation of continuous proton transportation channels, thereby compromising proton conductivity. [108, 109] Currently, no universally optimal solution has been identified. Therefore, it is imperative to select appropriate crosslinkers, degree of crosslinking, and crosslinking methods, based on the distinctive structures of copolymers to improve stability and mechanical performance while sustaining or even augmenting proton conductivity. Moreover, crosslinked sulfonated copolymers are insoluble in organic solvents, which limits the recycling or reprocessing of this type of copolymer. [110, 111]

Wang and Chen et al. utilized sulfonated poly(arylene ether sulfone) (SPAES) oligomers as crosslinkers to react with poly(arylene ether ketone) (PAEK) random copolymers containing active side groups, thereby synthesizing a series of crosslinked PAEK(*a*/*b*)-SPAES(*m*) copolymers for PEMs. [112] As depicted by TEM images in **Figure 1.17**, by preserving the molar ratio of PAEK repeating units connected with crosslinkers, while extending the length of SPAES, both the IEC values and the size of the hydrophilic phase increased. In contrast, maintaining the SPAES length constant and reducing the proportion of repeating units connected by crosslinkers triggered a reverse trend. Despite all the crosslinked copolymer

PEMs displaying superior dimensional stability compared to the analogous linear copolymer, their proton conductivity was deficient. Only the proton conductivity of PAEK(1/5)-SPAES(15) matched the level observed prior to crosslinking.

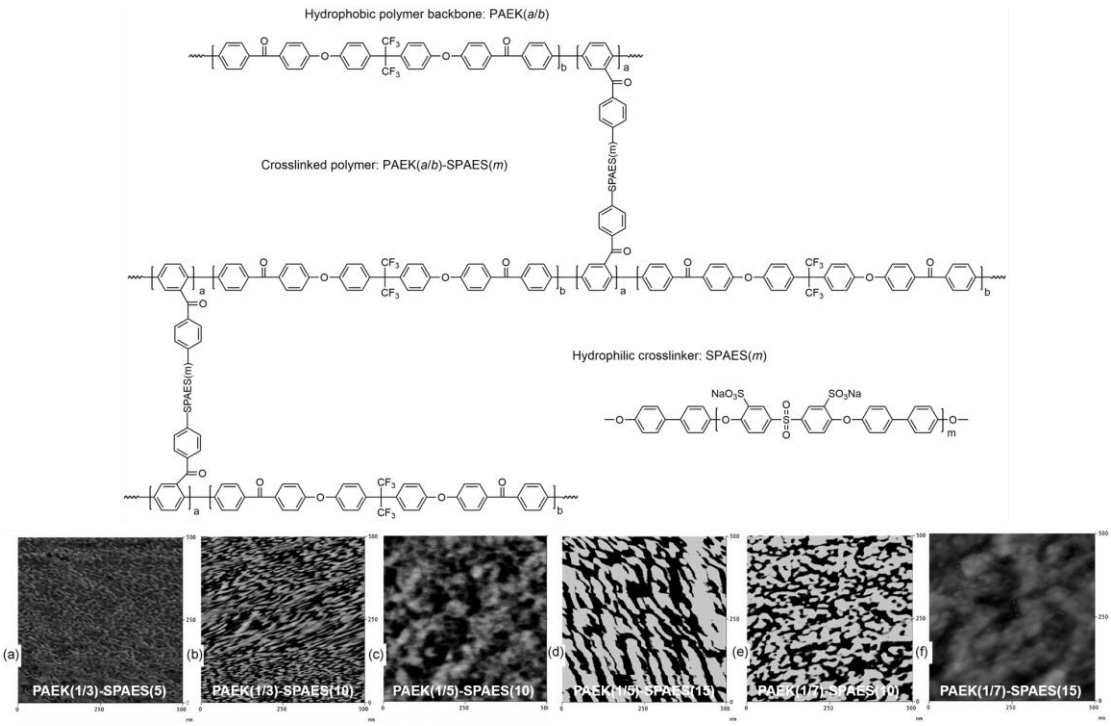

Figure 1.17. Chemical structure of poly(arylene ether ketone) random copolymers crosslinked by sulfonated poly(arylene ether sulfone) oligomers, and AFM images (tapping mode) of **(a)** PAEK(1/3)-SPAES(5), **(b)** PAEK(1/3)-SPAES(10), **(c)** PAEK(1/5)-SPAES(10), **(d)** PAEK(1/5)-SPAES(15), **(e)** PAEK(1/7)-SPAES(10), and **(f)** PAEK(1/7)-SPAES(15). Adapted with permission from Ref. [112]. Copyright 2011 John Wiley and Sons.

Lee and Hong et al. fabricated four semi-interpenetrating polymer network PEMs composed of crosslinked poly(2,6-dimethyl-1,4-phenylene oxide) (PPO) and linear sulfonated PPO (SPPO), in which the crosslinked PPO was synthesized by thermally crosslinking with four distinct types of epoxy resin crosslinkers. [113] As illustrated in **Figure 1.18**, given an identical degree of crosslinking, the size of the hydrophilic ionic clusters formed by BDE-0.5 was smaller. This is due to the ability of aliphatic crosslinkers to develop a denser hydrophobic skeleton, limiting

the mobility of SPPO. Conversely, aromatic crosslinkers formed a looser hydrophobic skeleton, promoting the aggregation of SPPO. As a result, the hydrophilic ionic clusters of RDE-0.5, BADE-0.5, and PBAE-0.5 were significantly larger, becoming gradually sparse with the increasing length of the crosslinker. The BDE-0.5 displayed better connectivity of the hydrophilic phase, leading to the best proton conductivity. Furthermore, the oxidative and dimensional stability of all crosslinked PEMs improved as the degree of crosslinking increased. However, proton conductivity peaked at a crosslinking degree of 0.2, exceeding that of the linear counterpart, before showing a gradual decline.

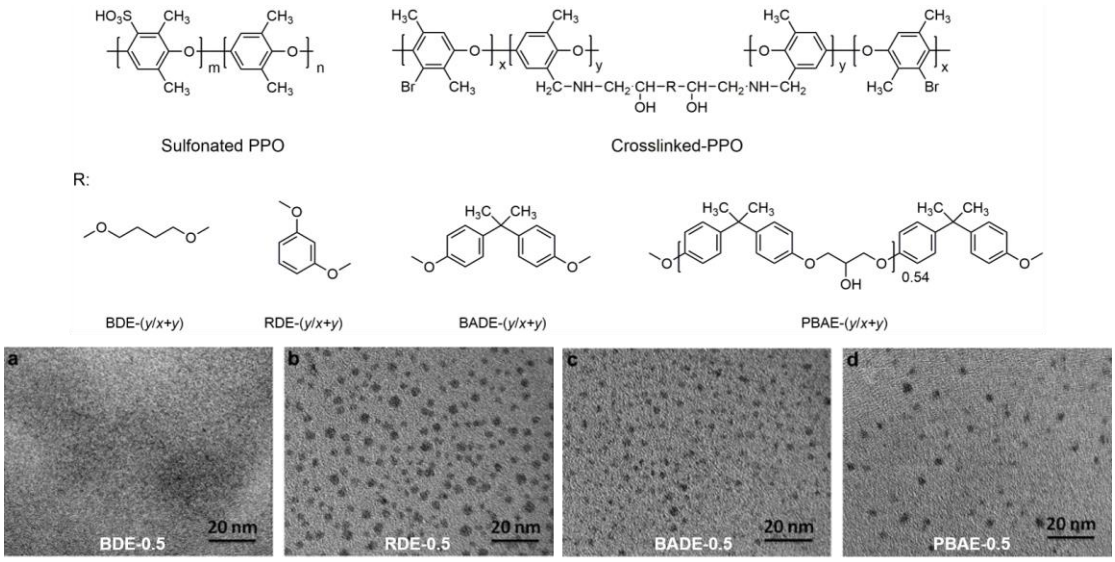

Figure 1.18. Chemical structure of linear sulfonated PPO and crosslinked PPO featuring four types of crosslinkers, and TEM images of **(a)** BDE-0.5, **(b)** RDE-0.5, **(c)** BADE-0.5, and **(d)** PBAE-0.5. Adapted with permission from Ref. [113]. Copyright 2013 Elsevier.

Lee's research group incorporated acetylene groups onto the termini of linear sulfonated poly(phenylene sulfide nitrile) random copolymers. Subsequently, a series of crosslinked copolymer PEMs (XESPSN-*n*) was prepared through the thermal crosslinking of the end groups during the membrane formation process, as shown in **Figure 1.19**. [114] Compared to the

analogous linear copolymer, ESPSN50, all crosslinked copolymers displayed more well-defined microscopic morphology, and the size of the hydrophilic phase expanded with increasing IEC values. At similar IEC values, XESPSN50 surpassed ESPSN50 in proton conductivity, dimensional stability, oxidative stability, and mechanical properties. Notably, the proton conductivity of XESPSN-70 was considerably higher than that of Nafion 212 across an RH range of 30% to 100% at 80 °C.

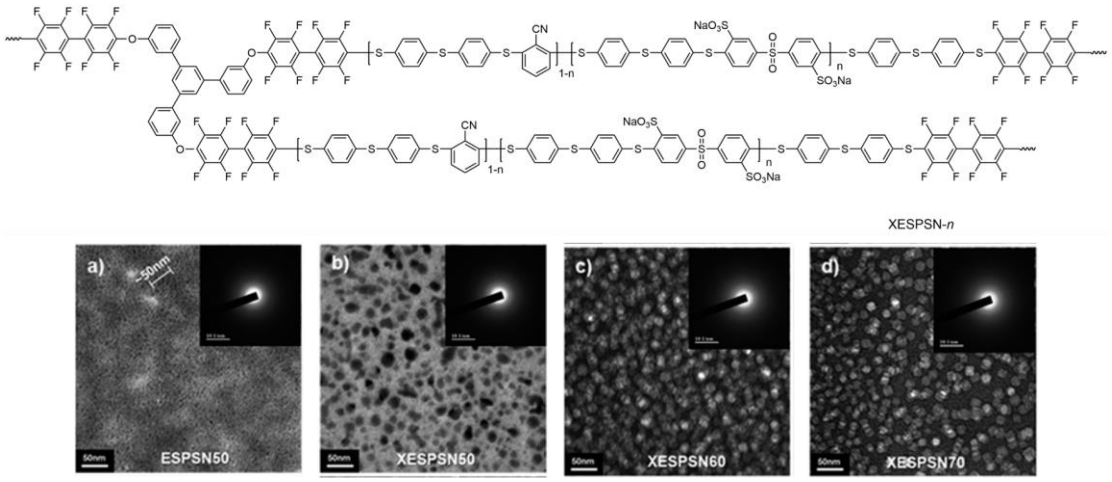

Figure 1.19. Chemical structure of crosslinked sulfonated poly(phenylene sulfide nitrile) copolymers, and TEM images of **(a)** ESPSN50, **(b)** XESPSN50, **(c)** XESPSN60, and **(d)** XESPSN70. Adapted with permission from Ref. [114]. Copyright 2012 Royal Society of Chemistry.

1.4.7. Branched Sulfonated Copolymers

Introducing a small molar fraction of tri-functional monomer to a regular polymerization process enables the transformation of polymer architecture from linear chains to a macroscopic network of polymer branches. [115] The resultant branched sulfonated copolymers exhibit a three-dimensional macromolecular structure similar to crosslinked sulfonated copolymers, leading to the enhancement of oxidative stability and dimensional stability of fabricated PEMs. Furthermore, these polymers retain the characteristics of linear sulfonated copolymers, such as

desirable solubility in common organic solvents and well-defined microscopic morphology. [116, 117] Due to the increased free volume compared to their linear counterparts, branched sulfonated copolymers typically exhibit higher water absorption, consequently improving proton conductivity. [118, 119] Despite the promising potential of branched sulfonated copolymers demonstrated, the related research remains limited as of now.

Wang's research group investigated the effect of various B_3 monomers, acting as branching agents, on the degree of branching (DB) of the resultant branched sulfonated copolymers. The results revealed that employing B_3 monomers equipped with long and rigid arms enhanced the DB values along with preventing macroscopic crosslinking during the polymerization process. Consequently, a series of branched sulfonated poly(fluorenyl ether ketone sulfone) copolymers featuring different DB values was synthesized, as illustrated in **Figure 1.20**. [120] The fabricated PEMs showed an increase in water uptake, proton conductivity, dimensional stability, and oxidative stability with the rise in DB values, outperforming the analogous linear sulfonated copolymer. Notably, the PEM with the maximum DB (10%) demonstrated a well-defined hydrophilic-hydrophobic phase separation morphology in the AFM image, achieving superior proton conductivity to Nafion 117 under a fully hydrated condition.

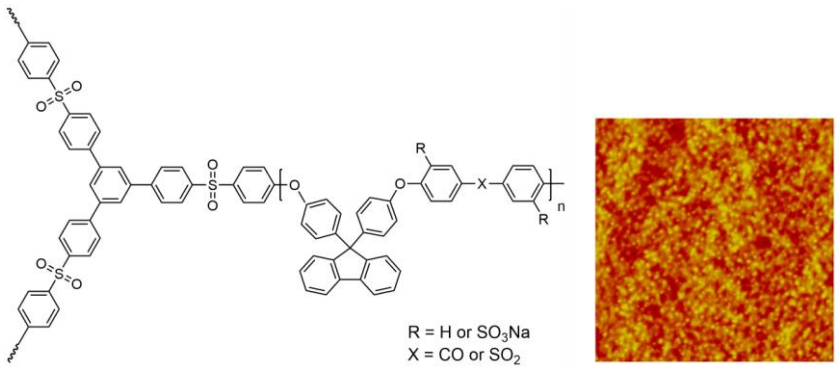

Figure 1.20. Chemical structure of branched sulfonated poly(fluorenyl ether ketone sulfone) copolymers, and the AFM image (tapping mode) of the PEM with a DB value of 10%. Adapted with permission from

Ref. [120]. Copyright 2014 Elsevier.

Subsequently, this team prepared two types of branched sulfonated block poly(arylene ether) copolymer PEMs, referred to as P1 and P2. P1 comprised the hydrophilic block enveloped by the hydrophobic block, whereas, in P2, the arrangement was reversed. [121] As displayed in **Figure 1.21**, both PEMs presented pronounced microscopic morphology. With identical DB values and similar IEC values, the hydrophilic block of P2 characterized better mobility, facilitating the connectivity of the hydrophilic domains, thereby leading to improved proton conductivity. In contrast, P1 exhibited greater dimensional and oxidative stability compared to P2, attributed to the shielding of the hydrophilic block by the surrounding hydrophobic block.

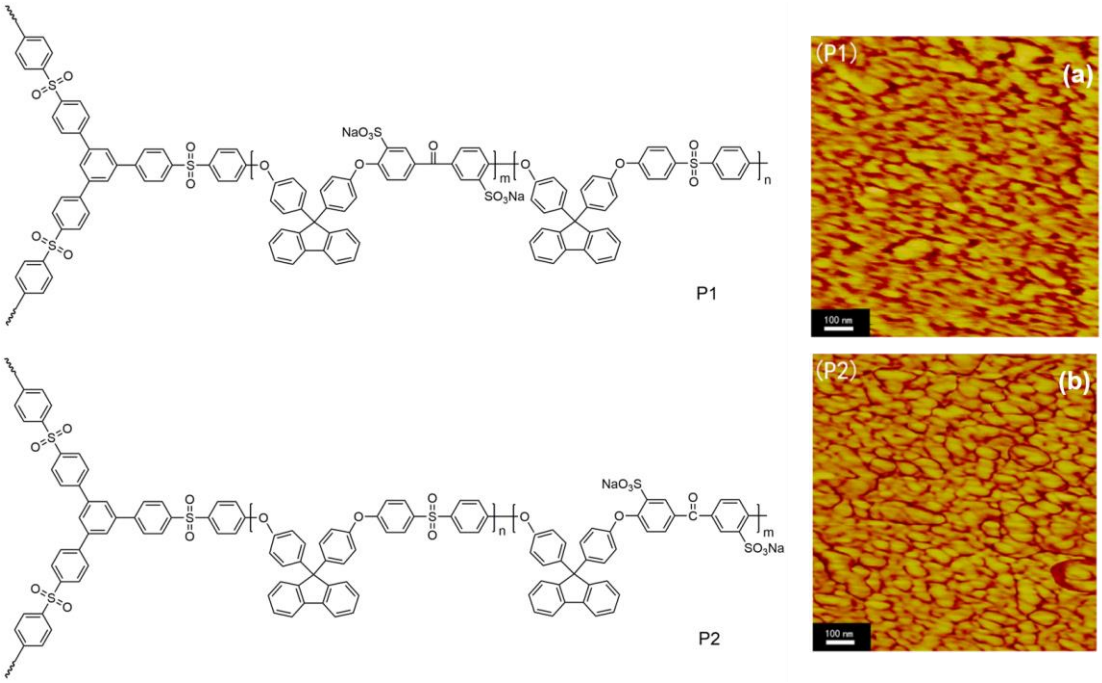

Figure 1.21. Chemical structure of two types of branched sulfonated block poly(arylene ether) copolymers, and AFM images (tapping mode) of **(a)** P1 and **(b)** P2. Adapted with permission from Ref. [121]. Copyright 2015 Elsevier.

Wang and his colleagues further synthesized a class of branched sulfonated poly(arylene ether sulfone) copolymers grafted with flexible sulfoalkyl side chains (SPAES-side). [122] Compared

with the analogous branched copolymers with sulfonic acid groups directly attached to the main chain (SPAEKS-main), the flexible side chains enhanced the mobility of the sulfonic acid groups, promoting the formation of interconnected hydrophilic phases. As illustrated in **Figure 1.22**, the size of the hydrophilic phase of the SPAES-side substantially exceeded that of the SPAEKS-main, resulting in superior proton conductivity. Furthermore, the flexible side chains, by increasing the chain entanglement, also heightened the dimensional stability, oxidative stability, and mechanical strength of the SPAES-side, surpassing that of the SPAEKS-main.

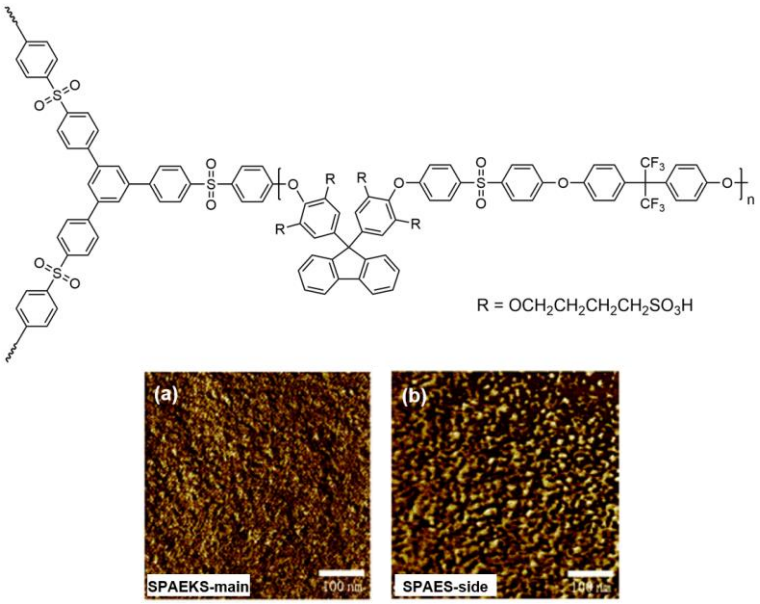

Figure 1.22. Chemical structure of branched sulfonated poly(arylene ether sulfone) copolymers grafted with sulfoalkyl side chains, and TEM images of **(a)** SPAEKS-main and **(b)** SPAES-side. Adapted with permission from Ref. [122]. Copyright 2016 Royal Society of Chemistry.

2. Motivation

Sulfonated aromatic polymers represented by sulfonated poly(arylene ether)s have been investigated as potential alternatives to PFSA polymers. However, most PEMs composed of these polymers are typically trapped in a trade-off between proton conductivity, dimensional stability, and durability. Introducing a branching architecture into the polymer emerges as a promising structural solution to it.

The present work explores the structure-property relationship of branched sulfonated aromatic polymer PEMs, with the aim of achieving superior performance to that of PFSA membranes through the optimization of structural design. Specifically, based on branched poly(arylene ether ketone sulfone) as the polymer skeleton, the impacts of three factors on the properties of PEMs are investigated: (i) the contents of branching sites and sulfonic acid groups, (ii) the positions of the sulfonic acid groups within the polymer architecture, and (iii) the linkage of the sulfonic acid groups to the polymer backbone.

The contents of the branching sites and sulfonic acid groups, the two most fundamental and crucial parameters for branched sulfonated polymers, are generally represented by the degree of branching (DB) and ion exchange capacity (IEC), respectively. In **Chapter 3**, two series of branched sulfonated poly(arylene ether ketone sulfone)s with varying DB and IEC values, respectively, are synthesized to investigate their effects and accordingly pave the way for subsequent research. The properties of the prepared PEMs are systematically investigated and compared with their linear counterpart and a commercially available PFSA membrane, i.e., Nafion 117.

With the objective of studying the effect of sulfonic acid groups positioning within the branched polymer architecture, **Chapter 4** presents the synthesis of a series of branched poly(arylene ether ketone sulfone)s containing ultra-densely sulfonated branched centers. The properties of the fabricated PEMs are thoroughly investigated and compared with the analogous polymer featuring sulfonated branched arms, with part key data from Nafion 117 also included for reference.

Building on the results from the preceding two chapters, **Chapter 5** aims to surpass the fuel cell performance of PFSA membranes. To accomplish this, a series of branched poly(arylene ether ketone sulfone)s bearing sulfobutyl side chains is synthesized, with the mobility of sulfonic acid groups improved by the flexible alkyl chains. Various properties of the obtained PEMs, particularly proton conductivity and H_2/air single-cell performance, are investigated and compared to those of Nafion 117.

3. Branched poly(arylene ether ketone sulfone)s containing sulfonated tetraarylmethane units for proton exchange membranes: Effects of degree of branching and ion exchange capacity

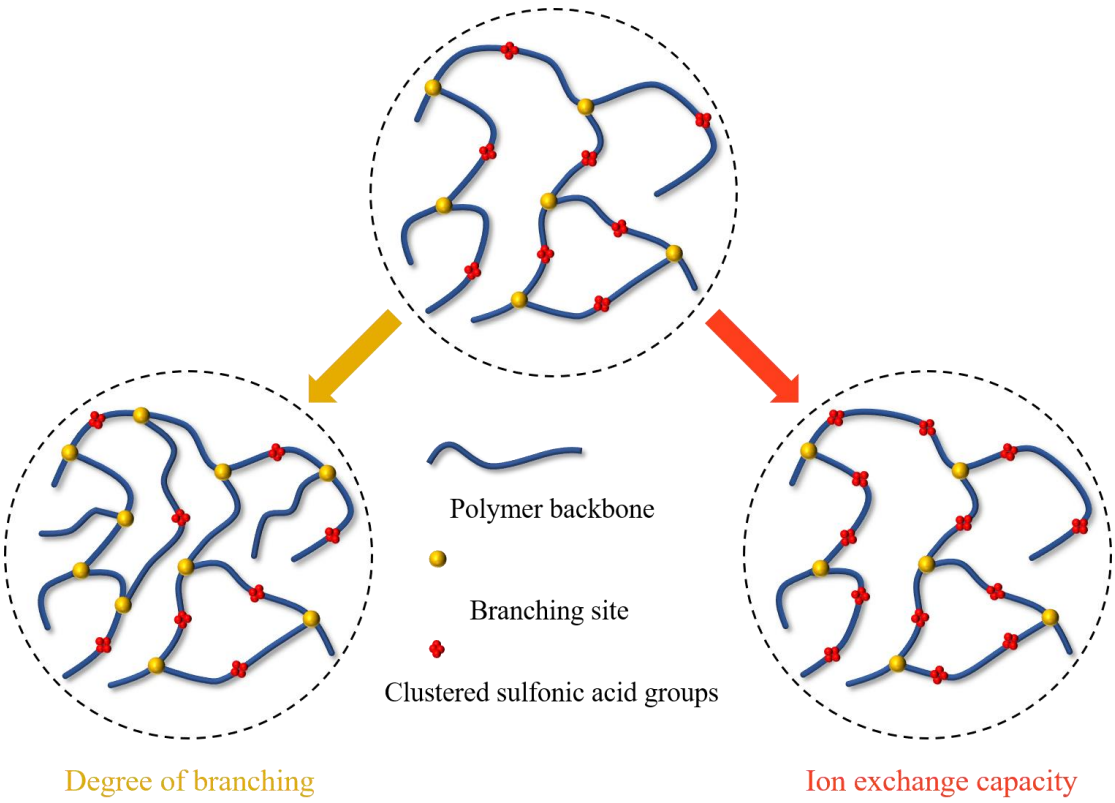

This chapter and the corresponding parts in the experimental section are adapted with permission from Ref. [123]: Yunji Xie, Anna Ringuette, Di Liu, Jinhui Pang, Hatice Mutlu, Dominik Voll, and Patrick Théato*. Sulfonated branched poly(arylene ether ketone sulfone) proton exchange membranes: Effects of degree of branching and ion exchange capacity, *European Polymer Journal*, 2023, 186, 111837.

3.1. Introduction

Branched sulfonated aromatic polymers have risen as a promising option for PEMs, many reports have achieved excellent performance by regulating the molar ratio of branching monomer (typically a tri-functional group monomer) during the polymerization, which is donated as the degree of branching (DB). However, most studies have overlooked another critical factor, i.e., the ion exchange capacity (IEC), which represents the accessible number of sulfonic acid groups within the PEMs, directly determining various properties. [115] Therefore, a systematical comparison and discussion regarding the effects of DB and IEC values on branched sulfonated aromatic polymer PEMs is highly required.

Poly(arylene ether ketone sulfone), a subclass of poly(arylene ether)s, has been demonstrated to serve as an excellent backbone for branched polymers. Wang's group developed a type of branched poly(arylene ether ketone sulfone) that incorporates sulfonated fluorenyl. The prepared PEM, with a maximum DB of 10%, exhibited superior proton conductivity (0.42 S cm^{-1}), limited swelling change (16.2 %), and outstanding chemical stability (immersion in Fenton's reagent for more than 300 min without breakage) at 80 °C. [120] Furthermore, as introduced previously, among various structural strategies aiming to form well-defined microscopic morphology, densely sulfonated copolymers are comparatively straightforward in synthesis and readily combined with other structures. Hence, with branched poly(arylene ether ketone sulfone) containing densely sulfonated structural units as the fundamental architecture, investigating the effects of DB and IEC values is meaningful.

3.2. Strategy

In this chapter, a trifluoride monomer and a tetraarylmethane bisphenol monomer were

synthesized and subsequently copolymerized with 4,4'-difluorobenzophenone and 4,4'-dihydroxydiphenylsulfone, followed by post-sulfonation. By adjusting the molar ratio of these two monomers during the polymerization, two series of branched sulfonated poly(arylene ether ketone sulfone)s with different DB and IEC values, respectively, were prepared. In addition, the sulfonated tetraarylmethane units form a densely sulfonated structure. Various properties of prepared PEMs including water uptake, swelling ratio, microscopic morphology, proton conductivity, thermal and oxidative stability, mechanical properties, and H_2/air single-cell performance were investigated, and further compared to those of the analogous linear sulfonated polymer PEM and a commercially available PFSA membrane, i.e., Nafion 117.

3.3. Results and Discussion

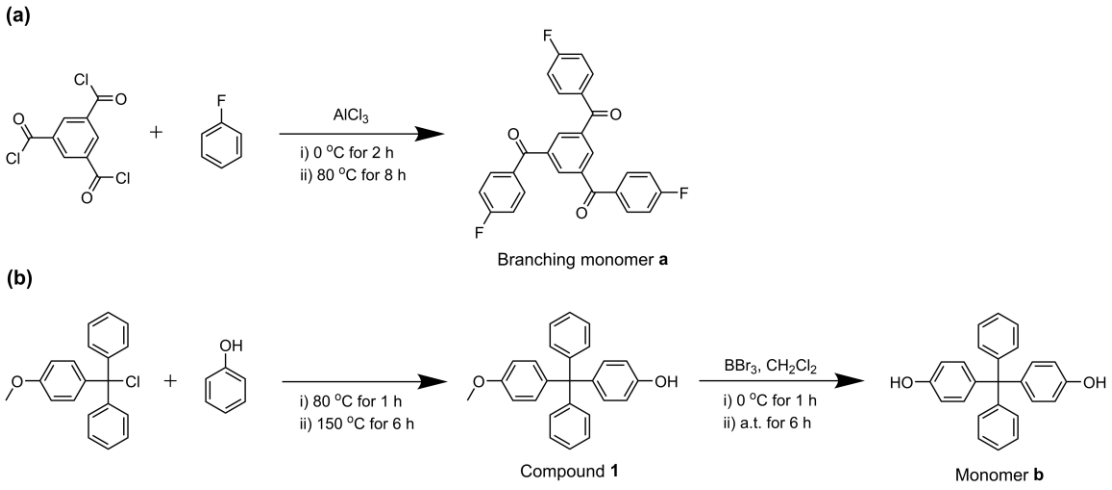

Scheme 3.1. Synthesis of **(a)** branching monomer **a** and **(b)** monomer **b**. Adapted with permission from Ref. [123]. Copyright 2023 Elsevier.

3.3.1. Synthesis of Monomers

The synthetic routes of branching monomer **a** and tetraarylmethane monomer **b** are depicted in **Scheme 3.1**. A Friedel-Crafts reaction between 1,3,5-benzenetricarbonyl trichloride and fluorobenzene was conducted to produce branching monomer **a**. [124] And the monomer **b** was

afforded by an aromatic electrophilic substitution of phenol with 4-methoxytriphenylmethyl chloride, followed by a demethoxylation reaction. [125] None of the above synthesis steps involved complex reactions, and the resulting yields were considerably high, exceeding 80%. The chemical structures of branching monomer **a**, compound **1,** and monomer **b** were confirmed by ^{1}H NMR spectroscopy. As shown in **Figure 3.1**, the integral area ratio of peaks of branching monomer **a** at 8.24 ppm (H_1), 7.93-8.01 ppm (H_2), 7.41-7.49 ppm (H_3) was 1: 2: 2, revealing the Friedel-Crafts reaction proceeded successfully. Moreover, the peak of the methoxy group at 3.72 ppm had vanished completely from compound **1** to monomer **b**, and the integral area of the peak representing the hydroxyl group significantly increased, indicating that the methoxy group was successfully converted to the hydroxyl group.

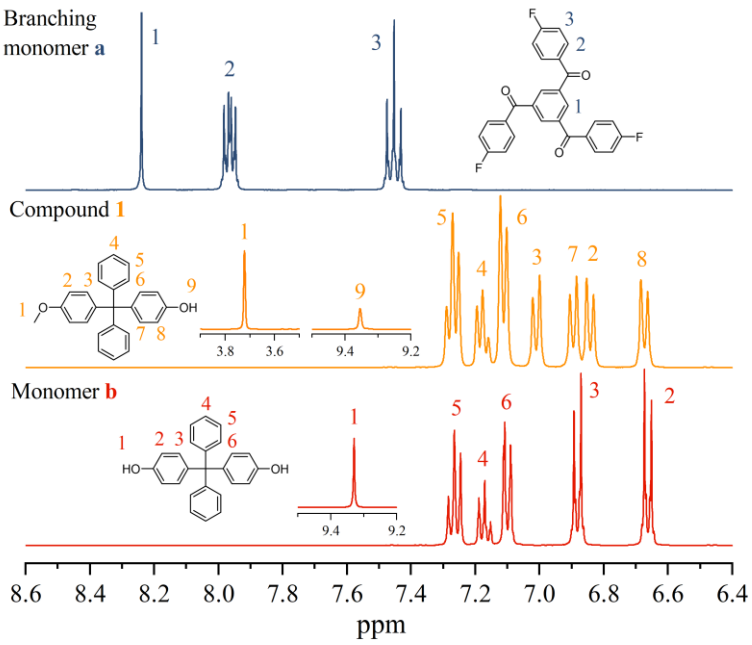

Figure 3.1. ^{1}H NMR spectra (DMSO-d_6) of branching monomer **a**, compound **1**, and monomer **b**. Adapted with permission from Ref. [123]. Copyright 2023 Elsevier.

3.3.2. Synthesis of Copolymers

As depicted in **Scheme 3.2**, branched and linear poly(arylene ether ketone sulfone)s were

successfully synthesized by conventional nucleophilic polycondensation, donated as "B-*x*-PAEKS-*y*" and "L-PAEKS-30", respectively, with *x* representing the DB, which was calculated from the molar ratio of branching monomer **a** to the employed bisphenol monomers, ranging from 5% to 10% (**Table 3.1**), and *y* and 30 representing the molar ratio of monomer **b** to the employed bisphenol monomers, ranging from 25% to 35%. The ceiling DB value of B-*x*-PAEKS-*y* copolymers was determined as 10% because a higher than 10% DB resulted in macroscopic crosslinking during polymerization. [120]

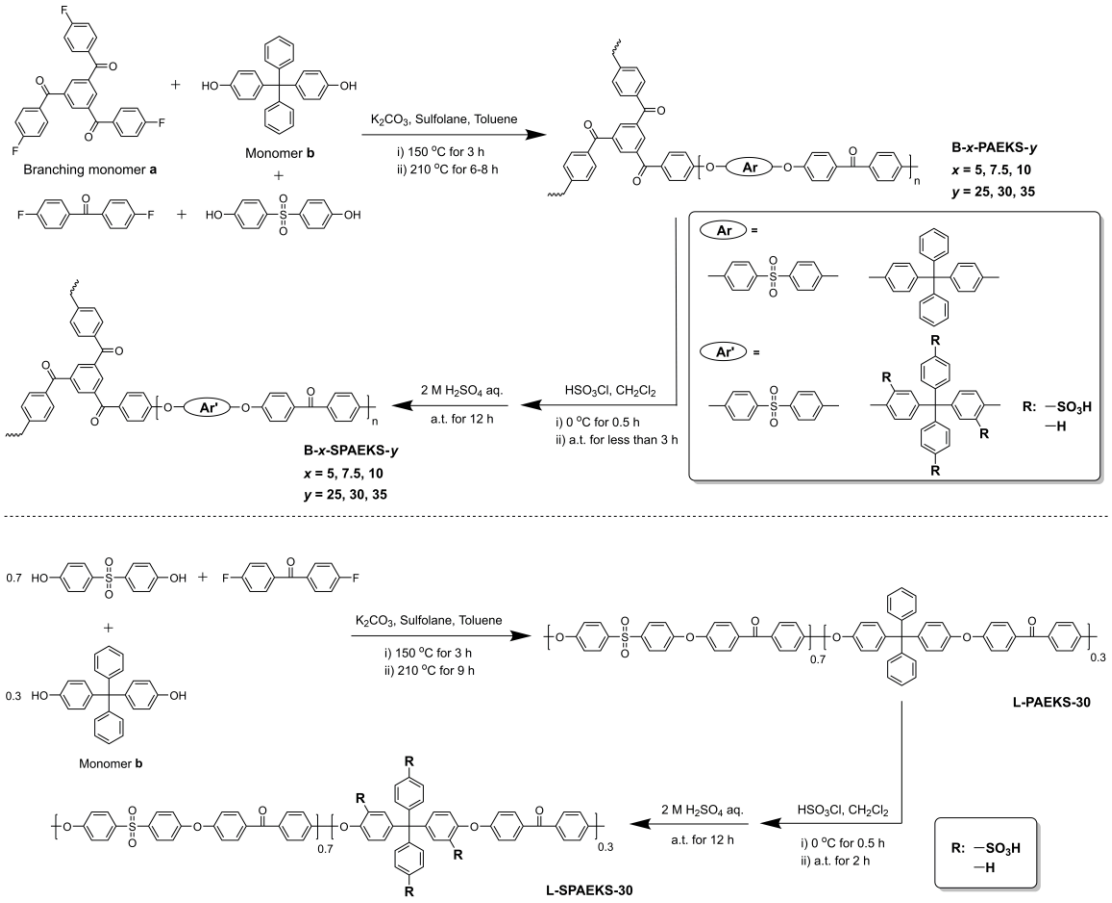

Scheme 3.2. Synthesis of branched copolymers (B-*x*-PAEKS-*y*, B-*x*-SPAEKS-*y*) and linear copolymers (L-PAEKS-30 and L-SPAEKS-30), with *x* and *y* representing the molar ratio of branching monomer **a** and monomer **b** to the employed bisphenol monomers, respectively. Adapted with permission from Ref. [123]. Copyright 2023 Elsevier.

The chemical structures of the copolymers were verified by ^{1}H NMR spectroscopy as shown in

Figure 3.2. A characteristic peak belonging to branching monomer **a** was observed at 8.23-8.31 ppm (H_1) in the spectra of B-*x*-PAEKS-*y* when compared with L-PAEKS-30. According to the integral area ratios of peaks at 8.23-8.31 ppm (H_1), 7.83-7.91 ppm (H_5 or $H_{5'}$), 7.68-7.83 ppm ($H_{2,\ 12}$ or $H_{12',\ 12''}$), and 6.82-6.94 ppm (H_6 or $H_{6'}$), the compositions of B-*x*-PAEKS-*y* and L-PAEKS-30 were confirmed. Indeed, the results were nearly consistent with the initial feeding ratios, indicating that the branching monomer **a** was quantitatively incorporated into the B-*x*-PAEKS-*y*.

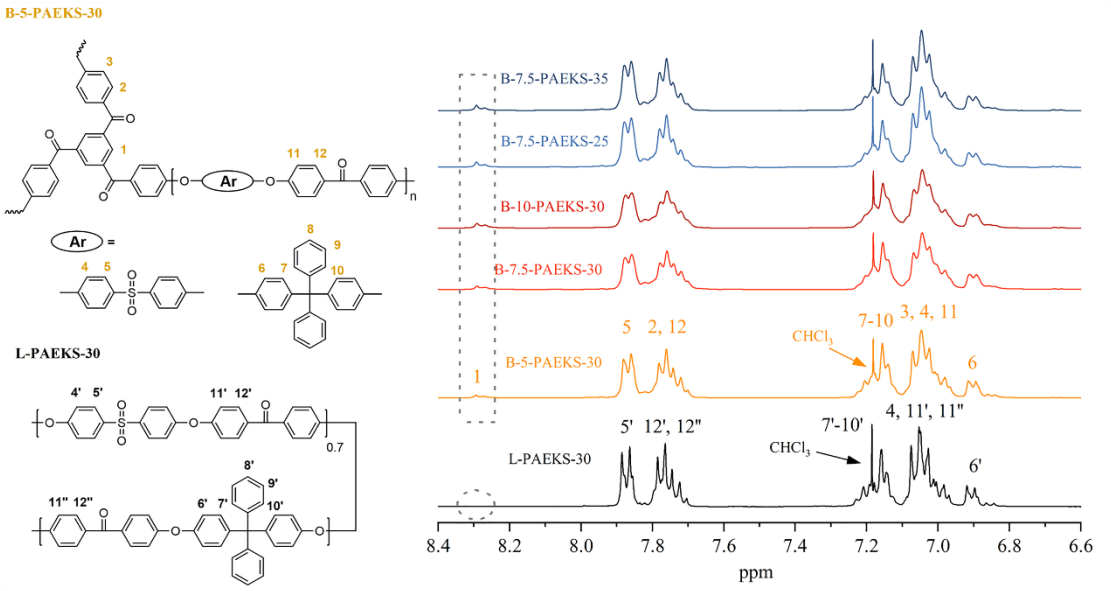

Figure 3.2. ^{1}H NMR spectra ($CDCl_3$) of B-*x*-PAEKS-*y* and L-PAEKS-30. Adapted with permission from Ref. [123]. Copyright 2023 Elsevier.

The B-*x*-PAEKS-*y* exhibited similar solubility with L-PAEKS-30, as both dissolved well in *N*-methyl-2-pyrrolidone (NMP), *N, N*-dimethylacetamide (DMAc), dimethyl sulfoxide (DMSO), and chloroform, demonstrating that no macroscopic crosslinking had occurred. Nonetheless, upon filtering these polymer solutions with 0.45 μm organic phase syringe filters, the B-*x*-PAEKS-*y* exhibited resistance to passing through the filters, which was not observed from the L-PAEKS-30. The underlying reason is the enlarged volumetric size of the branched polymer

compared to the linear polymer in solution, resulting from the presence of the branching architectures. Consequently, to accurately characterize the integral molecular weights of copolymers without losing any possible parts, size exclusion chromatography (SEC) was dismissed in favor of viscosity measurements. For this, the copolymers were dissolved in NMP and filtered using G4 glass sand core funnels with an average pore diameter between 5-15 μm. This method allowed for smooth passage of the polymer solutions and remove potential impurities such as dust. The inherent viscosities of the copolymers were in the range of 0.71-1.03 dL g^{-1}, as listed in **Table 3.1**, proving that copolymers with high molar weights were obtained.

3.3.3. Sulfonation of Copolymers

The post-sulfonation of copolymers was conducted with chlorosulfonic acid, a milder sulfonation reagent than concentrated sulfuric acid, [126] and the resulting branched and linear sulfonated copolymers were named "B-*x*-SPAEKS-*y*" and "L-SPAEKS-30", respectively. The sulfonation reaction occurred selectively on the tetraarylmethane units due to their electron-rich nature, forming a densely sulfonated structure (more than two sulfonic acid groups within a single structural unit), while the remaining polymer skeleton was protected by the strong electron-withdrawing effect of carbonyl and sulfonyl groups. [104] The conditions of the sulfonation reaction were elaborately controlled to realize an approximately identical degree of sulfonation (DS) among the sulfonated copolymers. For this, the molar ratio of chlorosulfonic acid to tetraarylmethane unit was kept constant at 16 to 1, and the sulfonation time at ambient temperature was slightly extended as the DB value increased. Most importantly, the sulfonation time of all copolymers had to be limited to less than 3 h, otherwise, an insoluble gel tended to

form, similar phenomenon is also reported in other literature, [127, 128] which is presumably due to the formation of the sulfone bridge between polymer chains [53, 107].

The ^{1}H NMR spectra of B-*x*-SPAEKS-*y* and L-SPAEKS-30 are depicted in **Figure 3.3**, attributing to the introduction of sulfonic acid groups, the new peaks of protons locating in the *ortho* position of sulfonic acid groups arose at 7.53-7.63 ppm (H_9 or $H_{9'}$) and 7.72-7.91 ppm (H_8 or $H_{8'}$) (overlapped). Since the composition of the copolymers had been confirmed, the DS values were calculated by the integral area ratios of signal peaks at 7.91-8.10 ppm ($H_{2,5}$ or $H_{5'}$), 7.72-7.91 ppm ($H_{8,12}$ or $H_{8',12'}$) and 7.53-7.63 ppm (H_9 or $H_{9'}$). The obtained DS values ranged from 77.6-79.6%, indicating that around 3 out of 4 aryl sites had been sulfonated on each tetraarylmethane unit. The incomplete sulfonation of the tetraarylmethane unit might be caused by insufficient sulfonation time (< 3 h). However, as stated above, the sulfonation time had been optimized to its maximum, with crosslinking occurring once surpassing the upper limit.

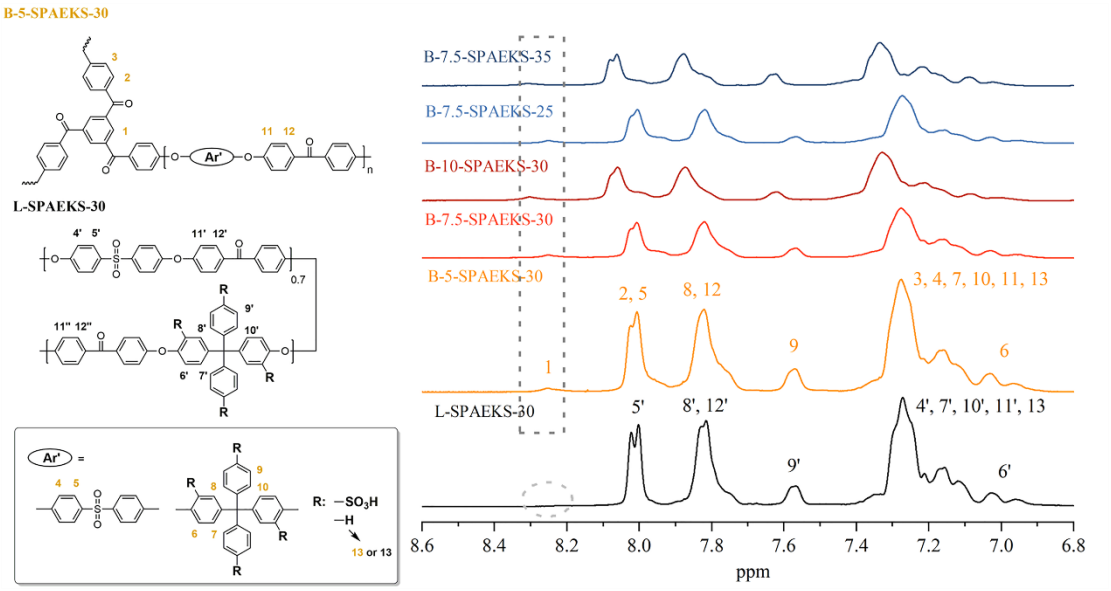

Figure 3.3. ^{1}H NMR spectra (DMSO-d_6) of B-*x*-SPAEKS-*y* and L-SPAEKS-30. Adapted with permission from Ref. [123]. Copyright 2023 Elsevier.

The FT-IR spectra of B-*x*-SPAEKS-*y* and L-SPAEKS-30 copolymers were further analyzed,

with the FT-IR spectrum of B-7.5-PAEKS-30 shown in **Figure 3.4** for comparison. The characteristic IR absorption band of the C=O occurred at 1658 cm^{-1}, and the band of sulfonic acid groups (S=O) was observed at 1033 cm^{-1}, indicating that the sulfonic acid groups were successfully introduced to the sulfonated copolymers.

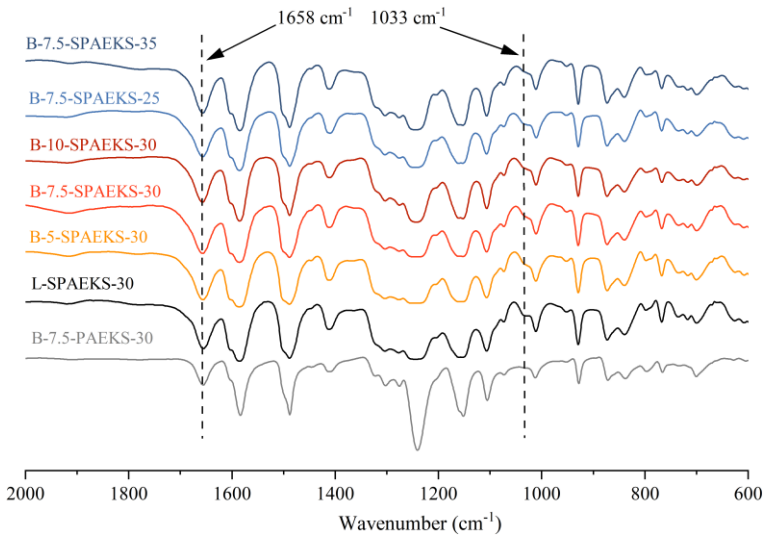

Figure 3.4. FT-IR spectra of B-*x*-SPAEKS-*y*, L-SPAEKS-30, and B-7.5-PAEKS-30. Adapted with permission from Ref. [123]. Copyright 2023 Elsevier.

All sulfonated copolymers exhibited good solubility in conventional polar solvents, such as NMP, DMAc, and DMSO, and no insoluble gel was observed. The inherent viscosity values (0.84-2.03 dL g^{-1}) of sulfonated copolymers were higher than those of corresponding unsulfonated copolymers (**Table 3.1**), presumably owing to the polyelectrolyte effect.

3.3.4. Preparation of Membranes and Ion Exchange Capacity

The B-*x*-SPAEKS-*y* and L-SPAEKS-30 membranes with thicknesses of 40-50 μm (**Table 3.1**) were obtained by solution casting from DMAc, and subsequently immersed in 2 M H_2SO_4 aqueous solution for 12 h to fully protonate. The visual images of dry B-10-SPAEKS-30 and L-SPAEKS-30 membranes at ambient temperature are representatively shown in **Figure A.1**

(**Appendix**). The ion exchange capacity (IEC) values of B-*x*-SPAEKS-*y* and L-SPAEKS-30 membranes were evaluated by ^{1}H NMR and acid-based titration, yielding IEC_{Theo} and IEC_{Titr}, respectively. As presented in **Table 3.1**, both demonstrated decent consistency, indicating most of the sulfonated groups were successfully converted to proton form. Therefore, the IEC_{Theo} is represented hereinafter as IEC. Owing to the same content of tetraarylmethane units and careful control of sulfonation reaction conditions, the series of B-*x*-SPAEKS-30 and L-SPAEKS-30 membranes achieved a similar IEC level (1.66-1.72 meq g^{-1}). Whereas the IEC values of the series of B-7.5-SPAEKS-*y* membranes elevated from 1.41 to 1.94 meq g^{-1} with the increase of sulfonated tetraarylmethane moieties. The effects of DB and IEC on the properties of PEMs were evaluated and compared according to the behavior of these two series of membranes in the following.

Table 3.1. Degree of branching, inherent viscosity, ion exchange capacity, thickness, and density of B-*x*-SPAEKS-*y* and L-SPAEKS-30 membranes. Adapted with permission from Ref. [123]. Copyright 2023 Elsevier.

Membrane	DB (%)	η^{a} (dL g^{-1})	IEC (meq g^{-1})		Thickness^{d} (μm)	Density^{e} (g cm^{-3})
			Theo^{b}	Titr^{c}		
L-SPAEKS-30	0	0.84 (0.71)	1.72	1.69	40 ± 2	1.50 ± 0.04
B-5-SPAEKS-30	5	1.63 (0.73)	1.68	1.65	46 ± 2	1.34 ± 0.04
B-7.5-SPAEKS-30	7.5	1.85 (0.88)	1.67	1.63	49 ± 2	1.13 ± 0.05
B-10-SPAEKS-30	10	2.03 (1.03)	1.66	1.62	47 ± 3	0.88 ± 0.03
B-7.5-SPAEKS-25	7.5	1.31 (0.84)	1.41	1.39	41 ± 1	1.17 ± 0.04
B-7.5-SPAEKS-35	7.5	1.77 (0.63)	1.94	1.91	45 ± 2	1.10 ± 0.03

[a] The inherent viscosity of B-*x*-SPAEKS-*y* and L-SPAEKS-30, number in parenthesis represents that of B-*x*-PAEKS-*y* and L-PAEKS-30.

[b] Calculated from the integrated area ratio of the signal peaks in ^{1}H NMR.

[c] Obtained by acid-base titration.

[d] Thickness of dry membrane.

[e] Density of dry membrane.

3.3.5. Water Uptake and Swelling Ratio

The generally accepted mechanisms of proton conduction in PEMs are mainly vehicle and Grotthuss, and surface mechanisms, all relying on water molecules to proceed. [129] Therefore, sufficient water absorption of PEMs generally improves proton conductivity, while excessive water content within membranes leads to considerable swelling variation. [130] The water uptake (WU) of B-*x*-SPAEKS-*y* and L-SPAEKS-30 membranes as a function of temperature is depicted in **Figure 3.5a** and relative key data are summarized in **Table 3.2**. The WU curves of all membranes increased with rising temperature, exhibiting a smooth trend from 20 to 80 ℃ but a dramatic change above 80 ℃. The enhancement of DB and IEC values also facilitated the water absorption of the membranes, with this kind of positive effect intensifying as the temperature elevated. Consequently, 80 ℃ was selected as a representative temperature for a more intuitive comparison of the effects of DB and IEC on WU. Besides, 80 ℃ is the typical operating temperature of PEMFCs, which is therefore most important to consider. [131]

The variations of WU with the DB and IEC values at 80 ℃ are shown in **Figure 3.5b**. As can be observed, the WU of B-7.5-SPAEKS-*y* membranes rapidly rose from 24.6 to 65.1%, accompanied by the IEC ranging from 1.41 to 1.94 meq g^{-1}, which is attributed to the increasing number of accessible hydrophilic sulfonic acid groups inside the membrane. However, even

though the L-SPAEKS-30 membrane possessed a slightly higher IEC (1.72 meq g^{-1}) than B-*x*-SPAEKS-30 membranes (1.66-1.68 meq g^{-1}), the branched copolymers membranes still exhibited greater WU, and gradually increased with the growth of DB. The WU of the B-10-SPAEKS-30 reached 43.3% at 80 °C, which was almost 1.5 times that of L-SPAEKS-30 with a WU of only 30.0%. This tendency was presumably due to the formation of a larger free volume within the membrane when the branching architecture increased, enabling it to hold more water. [121] The densities of dry B-*x*-SPAEKS-30 and L-SPAEKS-30 (**Table 3.1**) further supported this assumption, where those of B-*x*-SPAEKS-30 were significantly lower than that of the latter, and an obvious decrease was displayed in the range of 1.34-0.88 g cm^{-3} as the DB increased, demonstrating the expansion effect of the branching architecture on the free volume.

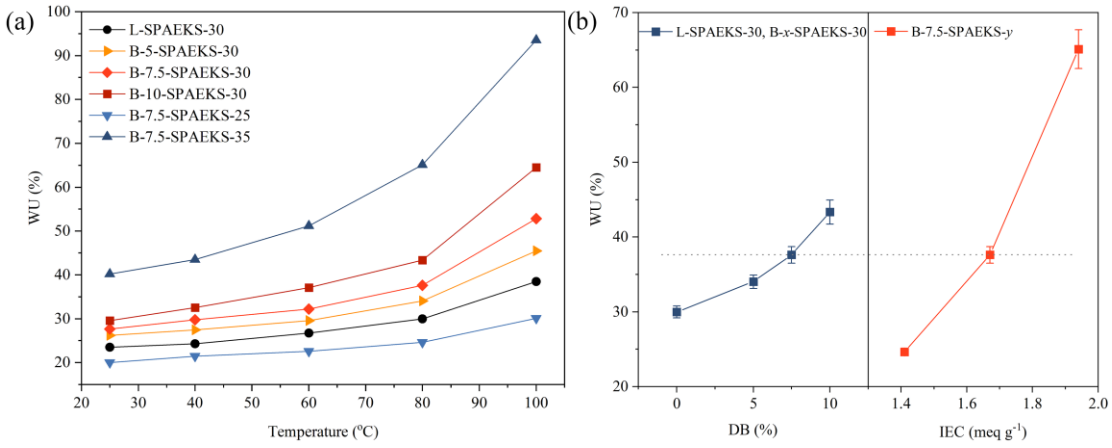

Figure 3.5. (a) Water uptake of B-*x*-SPAEKS-*y* and L-SPAEKS-30 membranes as a function of temperature; **(b)** water uptake of L-SPAEKS-30 and B-*x*-SPAEKS-30 membranes as a function of the degree of branching at 80 °C (left) and water uptake of B-7.5-SPAEKS-*y* membrane as a function of ion exchange capacity at 80 °C (right). Adapted with permission from Ref. [123]. Copyright 2023 Elsevier.

The swelling variation of PEMs is an inevitable consequence caused by the water absorption, and the unrestrained dimensional change results in a serious reduction of the mechanical properties and durability of the PEMs, as well as worse compatibility with the catalyst layer of

the electrode. [132] The swelling ratios (SRs) of B-*x*-SPAEKS-*y* and L-SPAEKS-30 membranes in in-plane (IP), through-plane (TP), volume as functions of temperature were measured, and the results are depicted in **Figure 3.6a**, **Figure 3.6b**, **Figure 3.6c**, respectively, and part of key data are summarized in **Table 3.2**. As expected, the trends of all curves were consistent with WU behavior, which increased with the rising temperature. Interestingly, the effects of elevating IEC on both SR-IP and SR-TP were the same, but the influences from the enhancement of DB on the SR-IP and SR-TP were the opposite.

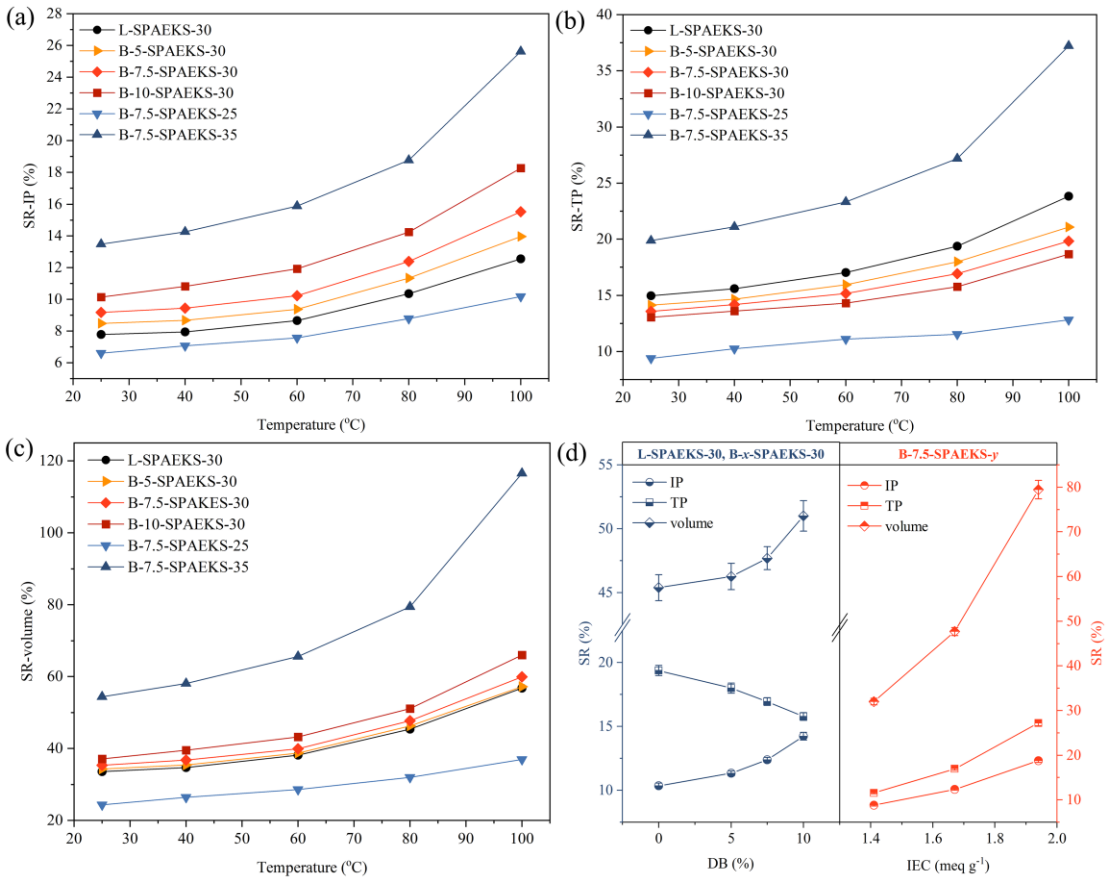

Figure 3.6. (a) Swelling ratio-in plane, **(b)** swelling ratio-through plane, and **(c)** swelling ratio-volume of B-*x*-SPAEKS-*y* and L-SPAEKS-30 membranes as a function of temperature, respectively; **(d)** swelling ratios in all the directions of L-SPAEKS-30 and B-*x*-SPAEKS-30 membranes as a function of the degree of branching at 80 °C (left), and the swelling ratios in all the directions of B-7.5-SPAEKS-*y* membranes as a function of on exchange capacity at 80 °C (right). Adapted with permission from Ref. [123]. Copyright 2023 Elsevier.

The SR-IP and SR-TP of membranes as functions of DB and IEC at 80 ℃, respectively, are therefore compared in **Figure 3.6d**. The SR-IP and SR-TP of B-7.5-SPAEKS-*y* membranes exhibited upward profiles in the range of 8.8-18.8% and 11.5-27.2%, respectively, when the IEC rose from 1.41 to 1.94 meq g^{-1}. However, the SR-TP of L-SPAEKS-30 and B-*x*-SPAEKS-30 membranes decreased from 19.4 to 15.8% with the increase of DB from 0 to 10%, meanwhile, the SR-IP increased from 10.4 to 14.2%. The special tendency is derived from the inhibiting effect of the branching architecture on the anisotropic dimensional change of PEMs. The sulfonic acid groups aggregate regularly in sulfonated multi-block or densely sulfonated linear polymers rather than random distribution, leading to the formation of a distinct morphological orientation within the membrane, which thus results in the anisotropic dimensional change, i.e., higher SR-TP than SR-IP. [133, 134] However, the introduction of branching architecture into the polymer reduces the orientation and then induces an isotropic dimensional change of the membrane. The ratios of SR-TP to SR-IP of all the membranes at 80 ℃ are listed in **Table 3.2**. Among them, the L-SPAEKS-30 exhibited a strong anisotropy on dimensional variation due to the occurrence of densely sulfonated tetraarylmethane units, whereas the anisotropy of the B-*x*-SPAEKS-*y* was much weaker, and this phenomenon aggravated with the increase of DB. Besides, the slight upward trend of the ratios in B-7.5-SPAEKS-*y* is due to the larger amount of sulfonated tetraarylmethane units. Hence, the impacts of DB on SR-IP and SR-TP were different from that of IEC.

The profiles of SR-volume with the change of DB and IEC at 80 ℃ are also displayed in **Figure 3.6d**. The SR-volume of B-7.5-SPAEKS-*y* presented a rapidly rising tendency from 32.0 to 79.5% over the whole IEC range, while the uptrend of L-SPAEKS-30 and B-*x*-SPAEKS-30 was

relatively steady, with a range of 45.4-51.1%. Both curves performed similarly to their corresponding WU, as shown in **Figure 3.5b**.

In summary, elevating DB and IEC both promote WU, which in turn enlarges the SR-IP and SR-volume of the membranes. The significant difference is that increasing DB reduces the SR-TP, leading the membranes towards isotropic swelling, whereas the augment of IEC remains the anisotropic dimensional variation by expanding the SR-TP. Additionally, in comparison with the WU and SRs of Nafion 117 at 80 ℃ listed in **Table 3.2**, the B-*x*-SPAEKS-*y* membranes demonstrated comparable or even better water affinity and dimensional stability.

Table 3.2. Water uptake, swelling ratios in in-plane, through-plane, and volume, and anisotropic swelling change of B-*x*-SPAEKS-*y*, L-SPAEKS-30, and Nafion 117 membranes. Adapted with permission from Ref. [123]. Copyright 2023 Elsevier.

Membrane	WU (%)		SR						
			IP (%)		TP (%)		volume (%)		TP/IP
	25 ℃	80 ℃	25 ℃	80 ℃	25 ℃	80 ℃	25 ℃	80 ℃	80 ℃
L-SPAEKS-30	23.5 ± 0.4	30.0 ± 0.8	7.8 ± 0.1	10.4 ± 0.2	15.0 ± 0.3	19.4 ± 0.4	33.6 ± 0.6	45.4 ± 1.0	1.87
B-5-SPAEKS-30	26.2 ± 0.4	34.0 ± 0.9	8.5 ± 0.2	11.3 ± 0.2	14.2 ± 0.3	18.0 ± 0.4	34.4 ± 0.9	46.3 ± 1.0	1.59
B-7.5-SPAEKS-30	27.7 ± 0.6	37.6 ± 1.1	9.2 ± 0.2	12.4 ± 0.2	13.6 ± 0.2	17.0 ± 0.3	35.5 ± 0.7	47.7 ± 0.9	1.37
B-10-SPAEKS-30	29.6 ± 0.8	43.3 ± 1.6	10.1 ± 0.2	14.2 ± 0.3	13.1 ± 0.2	15.8 ± 0.3	37.1 ± 0.7	51.1 ± 1.2	1.11
B-7.5-SPAEKS-25	20.0 ± 0.2	24.6 ± 0.5	6.6 ± 0.1	8.8 ± 0.2	9.4 ± 0.3	11.5 ± 0.2	24.3 ± 0.6	32.0 ± 0.7	1.31
B-7.5-SPAEKS-35	40.2 ± 1.4	65.1 ± 2.6	13.5 ± 0.3	18.8 ± 0.4	19.9 ± 0.5	27.2 ± 0.6	54.5 ± 1.5	79.5 ± 2.1	1.45
Nafion 117	19.2 ± 0.4	29.4 ± 0.9	13.1 ± 0.5	20.2 ± 0.6	15.0 ± 0.4	23.1 ± 0.7	47.1 ± 1.8	77.86 ± 2.8	-

3.3.6. Microscopic Morphology

The microscopic morphology of PEMs is a decisive factor that affects the various macroscopic properties including water absorption, dimensional change, and especially proton conductivity. [135] Hence, small-angle X-ray scattering (SAXS) was utilized to analyze the nanoscale morphology of B-*x*-SPAEKS-*y* and L-SPAEKS-30 membranes, which have been dried in vacuum, and the results are displayed in **Figure 3.7**. All membranes exhibited obvious characteristic scattering peaks, indicating the formation of a well-defined phase separation between the hydrophilic phase composed of densely sulfonated tetraarylmethane moieties and the hydrophobic phase formed by polymer backbone. [136] The characteristic separation length, i.e., the *d* value of each membrane is listed next to the scattering curves. As can be observed, increasing DB and IEC resulted in the decline of the *d* value in the range from 6.30 nm to 5.66 nm and from 6.06 nm to 5.22 nm, respectively.

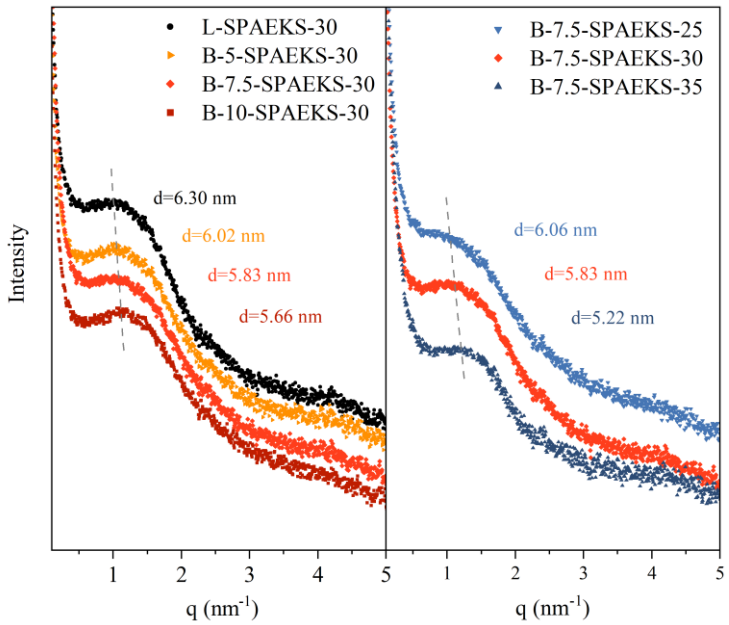

Figure 3.7. The small-angle X-ray scattering profiles of the L-SPAEKS-30, B-*x*-SPAEKS-30 (left), and B-7.5-SPAEKS-*y* (right) membranes (stained with Pb^{2+}). Adapted with permission from Ref. [123]. Copyright 2023 Elsevier.

To intuitively reveal the impact of DB and IEC on the microphase morphology of membranes, transmission electron microscope (TEM) measurements were further conducted, and the images are shown in **Figure 3.8**. The hydrophilic phase (dark region) in the shape of ionic clusters was dispersed evenly throughout the membranes, and presented distinct phase separation from the hydrophobic phase (bright region). [93] Furthermore, the size of ionic clusters of L-SPAEKS-30 and B-*x*-SPAEKS-30 membranes gradually decreased with the increase of DB value, leading to a denser distribution. This is presumably attributed to the branching architecture hampering the aggregation of the hydrophilic phase, which reduces the formation of larger ionic clusters. In contrast, the size of ionic clusters of B-7.5-SPAEKS-*y* membranes remained nearly consistent, but the number of ionic clusters grew with an increase of IEC, resulting in a closer arrangement as well. Although increasing DB and IEC exert different influences on the state of the individual ionic clusters of two series of membranes, the impact on the overall distribution trend was the same, thus inducing declined *d* value.

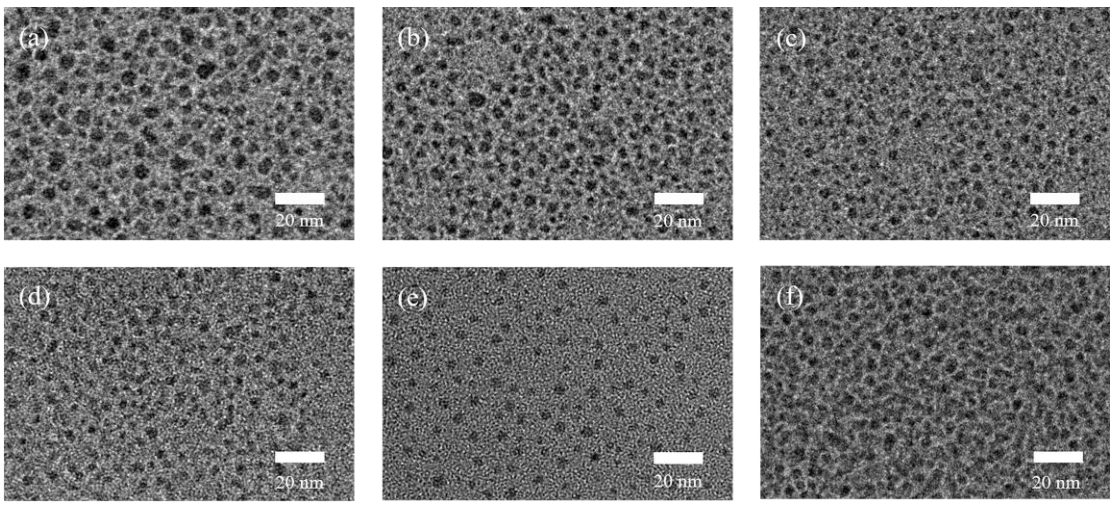

Figure 3.8. The transmission electron microscope images of **(a)** L-SPAEKS-30, **(b)** B-5-SPAEKS-30, **(c)** B-7.5-SPAEKS-30, **(d)** B-10-SPAEKS-30, **(e)** B-7.5-SPAEKS-25, and **(f)** B-7.5-SPAEKS-35 membranes (stained with Pb^{2+}). Adapted with permission from Ref. [123]. Copyright 2023 Elsevier.

3.3.7. Proton conductivity

Proton conductivity (σ) is a crucial parameter for PEMs that affects the final performance of the PEMFCs. [137] The proton conductivity measurements of B-*x*-SPAEKS-*y* and L-SPAEKS-30 membranes were taken via the four-electrode AC impedance method, and the results as a function of temperature are shown in **Figure 3.9a**, with all the curves presenting an upward tendency as temperature increased. Selected key data is extracted and presented in **Table 3.3**, and the proton conductivity of membranes as functions of DB and IEC values at 80 ℃ is further depicted in **Figure 3.9b**. As can be observed, elevating DB and IEC both effectively improved the proton conduction of membranes, which is due to the denser distribution of ionic clusters and the higher WU. Typically, the hydrophilic phase expands after absorption of water, and the water molecule acts as the carrier of the proton. [138] Therefore, the membrane with a higher DB or IEC is likely to form a more continuous proton transport channel, in which protons bind to sufficient water molecules and thus enhancing transportation. However, despite B-10-SPAEKS-30 with the highest DB exhibiting proton conductivity of 94.5 mS cm^{-1} at 80 ℃, such performance was worse than that of Nafion 117 (122.0 mS cm^{-1}). Consequently, the B-7.5-SPAEKS-35 membrane was the only membrane presenting satisfactory proton conductivity (134.5 mS cm^{-1}), i.e., performing better than Nafion 117.

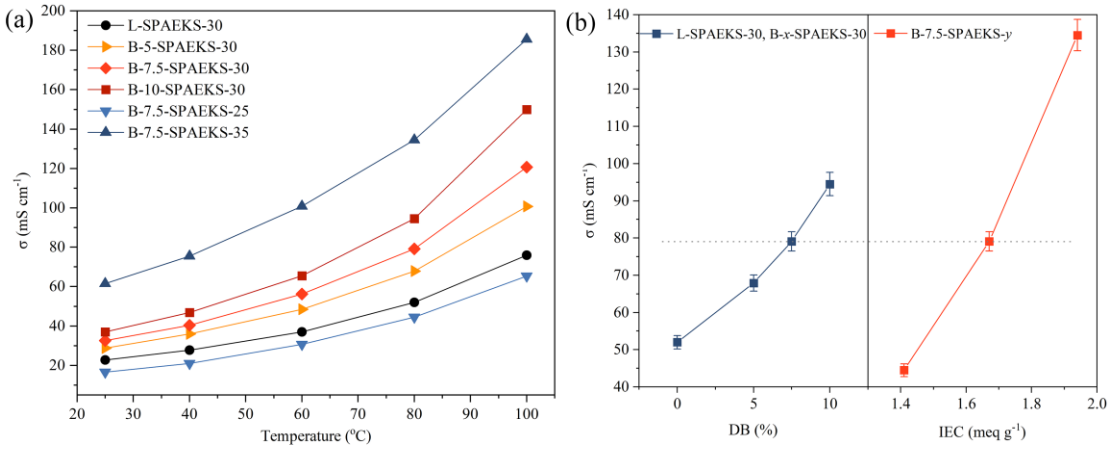

Figure 3.9. (a) Proton conductivity of B-*x*-SPAEKS-*y* and L-SPAEKS-30 membranes as a function of temperature; **(b)** proton conductivity of L-SPAEKS-30 and B-*x*-SPAEKS-30 membranes as a function of the degree of branching at 80 °C (left), and proton conductivity of B-7.5-SPAEKS-*y* membranes as a function of ion exchange capacity at 80 °C (right). Adapted with permission from Ref. [123]. Copyright 2023 Elsevier.

Table 3.3. Proton conductivity, thermal and oxidative stability, mechanical properties of B-*x*-SPAEKS-*y*, L-SPAEKS-30, and Nafion 117 membranes. Adapted with permission from Ref. [123]. Copyright 2023 Elsevier.

Membrane	σ (mS cm^{-1})		T_d[a] (°C)	τ[b] (min)	Mechanical properties	
	25 °C	80 °C			Tensile Strength (MPa)	Elongation at break (%)
L-SPAEKS-30	22.8 ± 1.2	52.0 ± 1.8	314.1	360 ± 15	45.4 ± 3.0	30.3 ± 2.4
B-5-SPAEKS-30	28.7 ± 1.4	67.9 ± 2.2	314.0	465 ± 15	34.1 ± 1.7	14.4 ± 0.4
B-7.5-SPAEKS-30	32.6 ± 1.7	79.1 ± 2.6	313.9	495 ± 15	29.0 ± 2.1	12.5 ± 1.5
B-10-SPAEKS-30	37.1 ± 1.4	94.5 ± 3.1	312.6	510 ± 15	24.9 ± 2.7	10.8 ± 1.6
B-7.5-SPAEKS-25	16.5 ± 0.9	44.5 ± 1.7	325.3	555 ± 15	32.9 ± 3.0	11.5 ± 1.7
B-7.5-SPAEKS-35	61.6 ± 2.8	134.5 ± 4.2	308.3	360 ± 15	20.2 ± 0.9	8.9 ± 1.1
Nafion 117	59.0 ± 3.0	122.0 ± 4.5	-	> 600	15.5 ± 0.6	106.3 ± 6.3

[a] 5% weight loss temperature.

[b] τ is the time required for the sample immersed in Fenton's reagent to start to rupture.

3.3.8. Stabilities and Mechanical Properties

Sufficient thermal and oxidative stabilities, as well as mechanical robustness of the PEMs, are essential to maintain the long-term operation of PEMFCs. [139] Thermogravimetric analysis (TGA) was utilized to evaluate the thermal stability of B-*x*-SPAEKS-*y* and L-SPAEKS-30 membranes. As can be observed from **Figure 3.10**, the initial degradation temperatures of all membranes were higher than 250 ℃. Two major degradation steps were observed, with the first degradation occurring at ~280 ℃, which was attributed to the loss of sulfonic acid groups. Further decomposition took place at ~480 ℃, due to the fragmentation of the polymer main chain. In the end, upon heating to 800 ℃, a residual char of more than 45 wt % was retained. Moreover, the 5% weight loss temperature values (T_d) of all the membranes are listed in **Table 3.3**, exhibiting a downward trend as the IEC increased, which is due to the introduction of sulfonic acid groups reducing the thermal stability of membranes. However, the typical operating temperature of PEMFCs is 80 ℃, as a result, the B-*x*-SPAEKS-*y* membranes displayed excellent thermal stability.

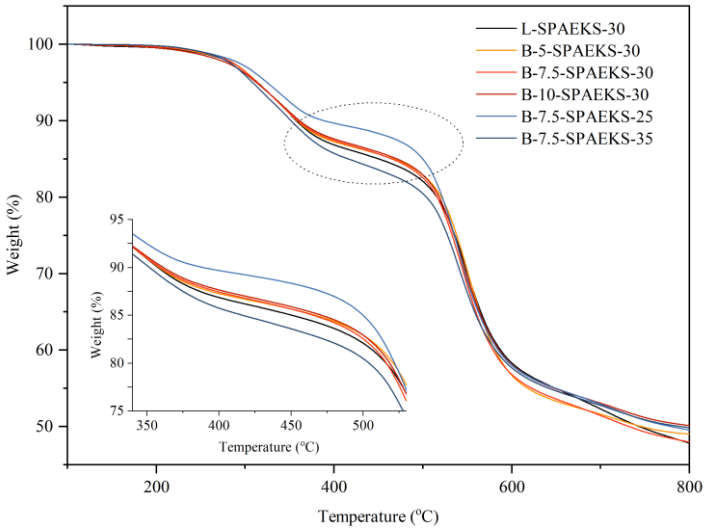

Figure 3.10. The thermogravimetric analysis curves of B-*x*-SPAEKS-*y* and L-SPAEKS-30 membranes. Adapted with permission from Ref. [123]. Copyright 2023 Elsevier.

During the operation of H_2/air PEMFCs, it is widely accepted that free radicals ($HO\cdot$ or $HO_2\cdot$) are generated because of the gas crossover, resulting in the chemical degradation of polymer chains. [140] To simulate an accelerated degradation condition, the membranes were immersed in Fenton's reagent at 80 °C. The time (τ) when the sample began to rupture upon exposure to Fenton's reagent was recorded to evaluate the oxidative stability of the membrane. Sample breakage was checked by gently shaking the container holding the sample every 15 min. The results are listed in **Table 3.3** and depicted as functions of DB and IEC in **Figure 3.11**. As can be observed, the oxidative stability of B-*x*-SPAEKS-30 membranes was substantially improved when compared to L-SPAEKS-30 membrane and further enhanced with increasing DB. Different from the linear polymer, even though some segments of branched polymer were attacked by radicals and then broken, the branching architecture is still capable to maintain the main integrity of the polymer chain. Thus, the peak τ value of B-10-SPAEKS-30 reached 510 min, almost 1.5 times that of the L-SPAEKS-30 membrane (360 min). However, such a positive effect gradually diminished, which is presumably due to the incremental water absorption of the B-*x*-SPAEKS-30, raising the risk of polymer degradation upon attack of free radicals. [141] Noteworthy, according to the tendency of the curve, the maximum DB value possible to preserve the enhancement of oxidative stability is 12.5%.

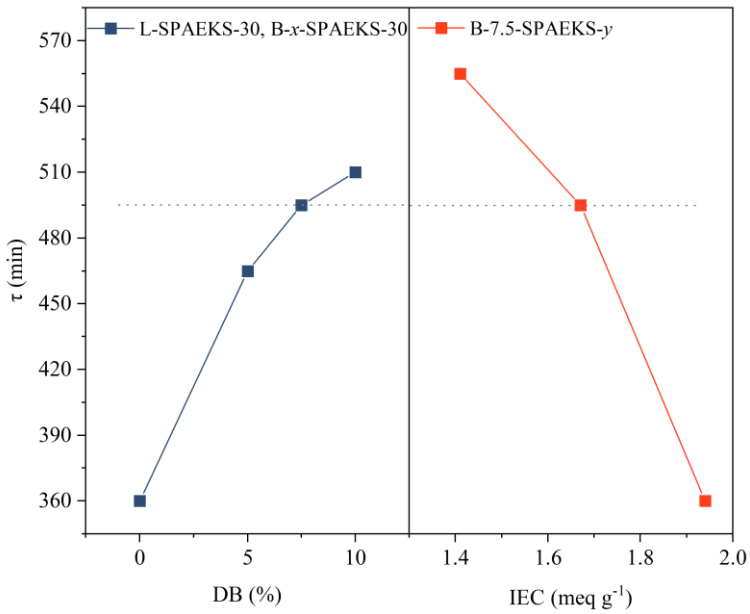

Figure 3.11. Oxidative stability of L-SPAEKS-30 and B-*x*-SPAEKS-30 membranes as a function of the degree of branching at 80 °C (left), and the oxidative stability of B-7.5-SPAEKS-*y* membranes as a function of ion exchange capacity at 80 °C (right). Adapted with permission from Ref. [123]. Copyright 2023 Elsevier.

The effect of the augment of IEC on oxidative stability was opposite to that of DB. The τ value of B-7.5-SPAEKS-*y* membranes dramatically dropped from 555 to 360 min over the whole IEC range (1.41-1.94 meq g^{-1}), owing to the rapidly increased water uptake. It is worth noting that the B-7.5-SPAEKS-35 possessed twice the WU (65.1%) of L-SPAEKS-30 (30.0%) at 80 °C, but the τ values of these two membranes were in the same range, demonstrating the strong reinforced effect of branching architecture on oxidative stability of membranes. Although the oxidative stability of B-*x*-SPAEKS-*y* membranes was not as excellent as Nafion 117 (τ > 600 min), a τ value of 200 min is typically considered as a standard to guarantee sufficient oxidative stability of PEMs to survive in PEMFCs, which the B-*x*-SPAEKS-*y* membranes fulfill.

Excellent mechanical properties are another factor that ensures the long-term operation of PEMs under actual working conditions. [142] The tensile testing experiments of hydrated B-*x*-

SPAEKS-*y* and L-SPAEKS-30 membranes were performed at 25 ℃. The results are listed in **Table 3.3** and the stress-strain curves are illustrated in **Figure 3.12**. Notably, the mechanical properties of B-*x*-SPAEKS-*y* were significantly weaker than that of L-SPAEKS-30, which was attributed to less chain entanglement induced by the presence of branching architecture, impairing the strength and toughness of membranes. [143] The tensile strength and elongation at break of B-*x*-SPAEKS-30 continually decreased in the range of 34.1-24.9 MPa and 14.4-10.8%, respectively, when DB increased from 5 to 10%. Similarly, the rise in IEC led to the increasingly inferior performance of B-7.5-SPAEKS-*y*, with a decline of tensile strength from 32.9 to 20.2 MPa and elongation at break from 11.5 to 8.9%, owing to the considerably increasing water absorption. [144] Overall, both DB and IEC are the negative factors influencing the mechanical property of membranes, yet B-*x*-SPARKS-*y* membranes are still sufficiently strong compared with the performance of Nafion 117 (15.5 MPa) under the same conditions.

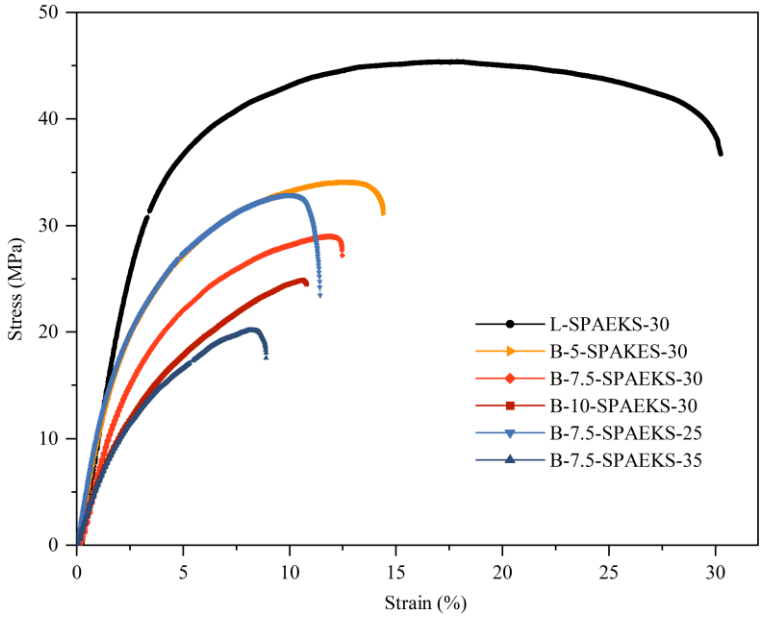

Figure 3.12. The stress-strain curves of B-*x*-SPAEKS-*y* and L-SPAEKS-30 membranes. Adapted with permission from Ref. [123]. Copyright 2023 Elsevier.

3.3.9. H_2/air Single-cell Performance and Durability

The membrane electrolyte assemblies (MEAs) of B-*x*-SPAEKS-*y* and L-SPAEKS-30 membranes were prepared to evaluate the H_2/air fuel cells performance. The resulting polarization curves are depicted in **Figure 3.13a**. As can be observed, enhancing DB and IEC both effectively improved the single-cell performance of membranes, which is consistent with the behavior of proton conductivity. The maximum power density of the L-SPAEKS-30 was 241.2 mW cm^{-2}, but that of the B-10-SPAEKS-30 was promoted to 351.1 mW cm^{-2} with the increase of DB values. Meanwhile, a nearly doubled performance was achieved from B-7.5-SPAEKS-25 to B-7.5-SPAEKS-35 membrane as of IEC value was elevated, with the highest maximum power density at 426.8 mW cm^{-2}.

The durability of the H_2/air fuel cell assembled with B-10-SPAEKS-30 membrane was investigated, and the result is shown in **Figure 3.13b**. The voltage of the membrane exhibited relatively steady performance throughout the test, and approximately 5% attenuation was presented after operation for 48 h, indicating the potential of fabricated B-*x*-SPAEKS-*y* membranes for application in the H_2/air fuel cell.

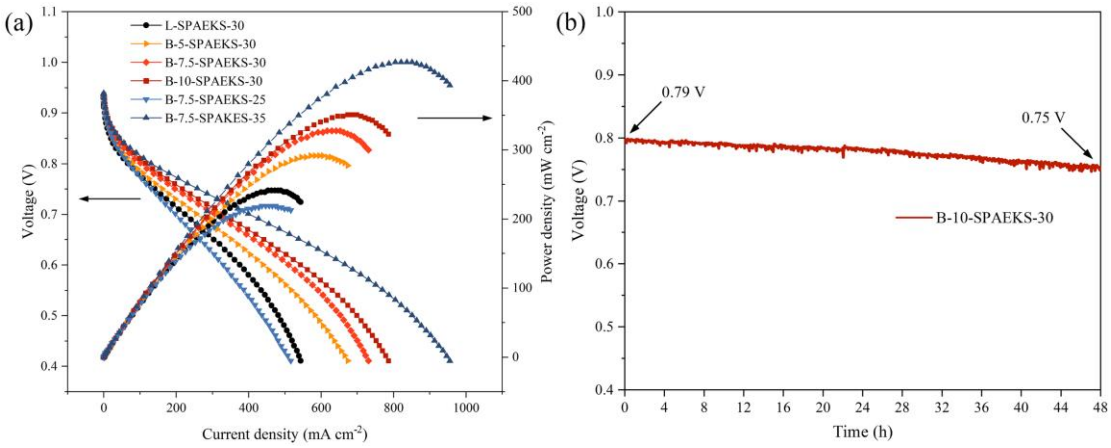

Figure 3.13. (a) The polarization curves of H_2/air fuel cells assembled with B-*x*-SPAEKS-*y* and L-

SPAEKS-30 membranes under 100% relative humidity at 80 °C; **(b)** Durability of H_2/air fuel cell assembled with B-10-SPAEKS-10 membrane under 100% relative humidity at 80 °C. Adapted with permission from Ref. [123]. Copyright 2023 Elsevier.

3.4. Recapitulation

Branching monomer **a** and tetraarylmethane monomer **b** were synthesized and copolymerized with 4,4'-difluorobenzophenone and 4,4'-dihydroxydiphenylsulfone, followed by post-sulfonation. By adjusting the molar ratio of the two monomers during the polymerization, two series of branched sulfonated poly(arylene ether ketone sulfone)s with varying DB and IEC values, respectively, namely B-*x*-SPAEKS-*y* were synthesized. The DB and IEC were controlled in the range of 5-10% and 1.41-1.94 meq g^{-1}, respectively.

Increasing the DB and IEC of B-*x*-SPAEKS-*y* membranes exerted the same impact on promoting water absorption, proton conductivity, single-cell performance, and formation of denser distribution of ionic clusters while reducing the mechanical properties. Distinctly different effects of DB and IEC occurred on dimensional variation and oxidative stability, as elevated DB led to isotropic swelling change and enhanced oxidative stability, whereas the influence of IEC was totally the opposite.

The B-10-SPAEKS-30 membrane presented the best oxidative stability, but its insufficient IEC prevented it from achieving comparable proton conductivity to Nafion 117. In contrast, the B-7.5-SPAEKS-35 membrane realized better proton conductivity than Nafion 117. Besides, the enhancing effect of elevated DB on oxidative stability diminished gradually, with 12.5% deduced as the maximum DB value to maintain the positive effect.

Hence, to optimize oxidative stability while ensuring satisfactory proton conductivity,

increasing DB to 12.5% and then suitably raising IEC appears to be a good option.

4. Branched poly(arylene ether ketone sulfone)s with ultra-densely sulfonated branched centers for proton exchange membranes: Effect of the positions of the sulfonic acid groups

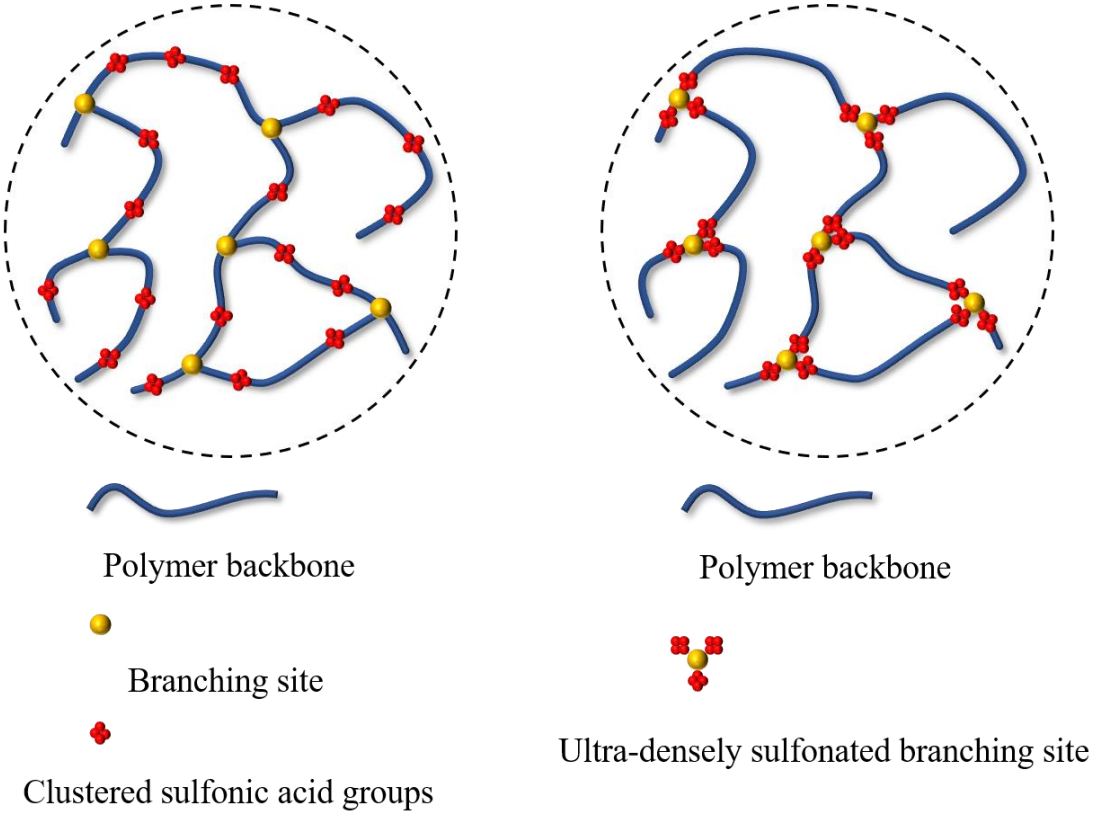

This chapter and the corresponding parts in the experimental section are adapted with permission from Ref. [145]: Yunji Xie, Di Liu, Anna Ringuette, and Patrick Théato*. Branched poly(arylene ether ketone sulfone)s with ultradensely sulfonated branched centers for proton exchange membranes: Effect of the positions of the sulfonic acid groups. *ACS Applied Materials & Interfaces*, 2023, 15 (20), 24517-24527.

4.1. Introduction

Many studies have highlighted the critical impact of the degree of branching (DB) on improving the properties of PEMs. [122, 146] The investigation in **Chapter 3** also demonstrated the promotion of increasing DB on the oxidative stability of PEMs fabricated by branched poly(arylene ether ketone sulfone)s containing sulfonated tetraarylmethane, identifying 12.5% as the optimal DB value to maximize this beneficial effect. However, reported DB values employing the B_3 monomer as the branching agent have not yet surpassed 10% so far, attributed to the tendency for macroscopic crosslinking during polymerization. Wang's group discovered that achieving branched polymer with high DB value is intimately associated with the selection of an appropriate branching agent, with the B_3 monomer featuring long and hard arms allowing for increased DB without inducing crosslinking. [120]

Furthermore, the majority of research has focused on tethering the sulfonic acid groups on the branched arms, with the exception of one example, which reports branched centers modified by sulfonic acid groups. [115] In comparison with the random distribution of sulfonic acid groups on the branched arms, concentrating functional groups on the branched centers considerably promotes regularity and coherence of hydrophilic and hydrophobic polymer segments, respectively, thereby promising benefits for the performance of PEMs. [89, 95] Han et al. prepared a branched poly(arylene ether) with sulfonic-acid-groups-functionalized carbazole derivatives as the branched centers. However, insufficient sulfonated sites on the branched centers limited the ion exchange capacity (IEC) of PEM to 1.12 meq g^{-1}, resulting in an inferior proton conductivity of only 42.1 mS cm^{-1} at 80 °C. [147]

Therefore, the investigation of branched aromatic polymer PEMs with high DB values and

sulfonated branched centers remains to be further advanced, with the crucial aspect being the development of a novel B_3 branching monomer.

4.2. Strategy

In this chapter, a triphenol monomer comprising tri-tetraarylmethane was designed as the branching agent, which was copolymerized with 4,4'-difluorobenzophenone and 4,4'-dihydroxydiphenylsulfone to yield a series of branched poly(arylene ether ketone sulfone)s with DB values ranging from 7.5 to 12.5%. Upon the post-sulfonation, sulfonic acid groups were ultra-densely tethered on the branched centers, achieving satisfactory IEC values for the PEMs. Various properties of prepared PEMs, including water uptake, swelling ratio, microscopic morphology, proton conductivity, thermal and oxidative stability, mechanical properties, and H_2/air single-cell performance, were investigated and compared to B-10-SPAEKS-30 synthesized in **Chapter 3**, which featured sulfonated branched arm. Key data from the commercially available Nafion 117 are also incorporated for reference.

4.3. Results and Discussion

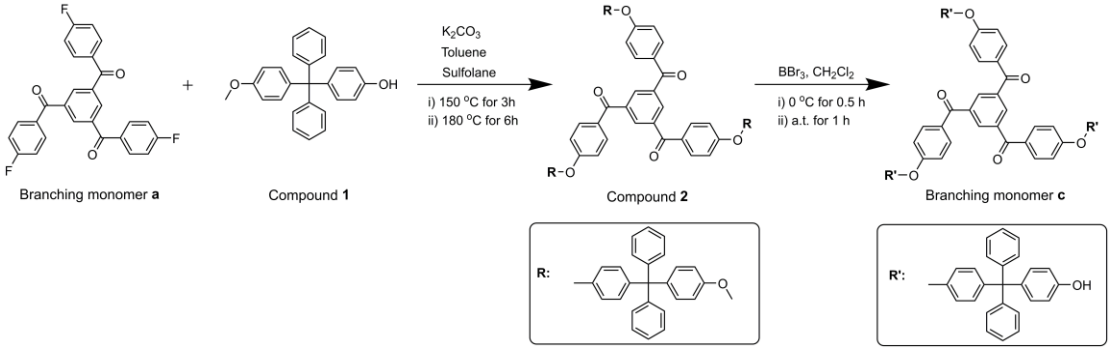

Scheme 4.1. Synthesis of branching monomer **c**. Adapted with permission from Ref. [145]. Copyright 2023 American Chemical Society.

4.3.1. Synthesis of Monomer

The synthetic route of the branching monomer **c** is depicted in **Scheme 4.1**, involving a sequential two-step reaction. A nucleophilic aromatic substitution between branching monomer **a** and compound **1** was first conducted, and a subsequent demethoxylation proceeded to afford branching monomer **c.** None of the above synthesis steps involved complex reactions, and the resulting yields were relatively high, exceeding 75%. The ^{1}H NMR spectra of compound **2** and branching monomer **c** are shown in **Figure 4.1**. The integral area ratio of signal peaks, H_1 (8.20 ppm), H_2 (7.87-7.90 ppm), H_{10} (6.83-6.86 ppm), and H_{11} (3.70 ppm) of compound **2** was 1: 2: 2: 3, indicating all the fluorine atoms of branching monomer **a** had been substituted by compound **1**. Upon demethoxylation, a new peak representing the hydroxyl group arose at 9.38 ppm (H_{11}) in the ^{1}H NMR spectrum of branching monomer **c**, concurrently, the peak associated with the methoxy group vanished, which proves the methoxy group had completely converted to the hydroxyl group.

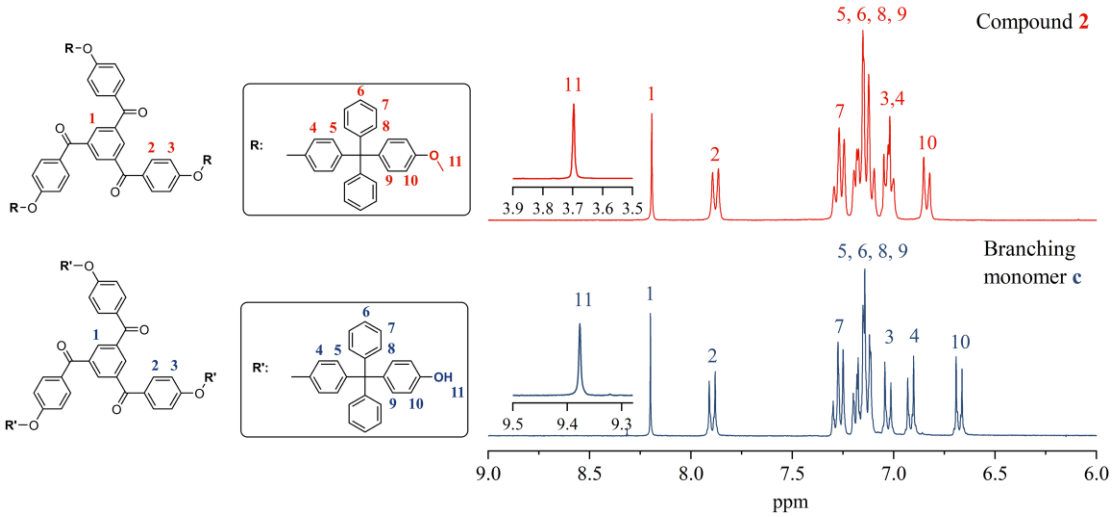

Figure 4.1. ^{1}H NMR spectra (DMSO-d_6) of compound **2** and branching monomer **c**. Adapted with permission from Ref. [145]. Copyright 2023 American Chemical Society.

4.3.2. Synthesis of Copolymers

As depicted in **Scheme 4.2**, branched poly(arylene ether ketone sulfone)s, denoted as B-*x*-PAEKS, were synthesized through nucleophilic polycondensation of branching monomer **c,** 4,4'-dihydroxydiphenylsulfone, and 4,4'-difluorobenzophenone. The *x* represents the degree of branching (DB) value, determined by the molar ratio of the branching monomer **c** to the employed bisfluoride monomer, which ranged from 7.5 to 12.5% (**Table 4.1**). Subsequently, the post-sulfonation mediated by chlorosulfonic acid was performed for less than 2 h to avoid the formation of insoluble gels, yielding B-*x*-SPAEKS with ultra-densely sulfonated branched centers. [148] From the perspective of the chemical architecture, the B-10-SPAEKS presents the same DB, the content of tetraarylmethane units, and polymer backbone as B-10-SPAEKS-30, which was synthesized in **Chapter 3**. The main difference between the two copolymers lay in the position of sulfonic-acid-groups-functionalized tetraarylmethane moieties.

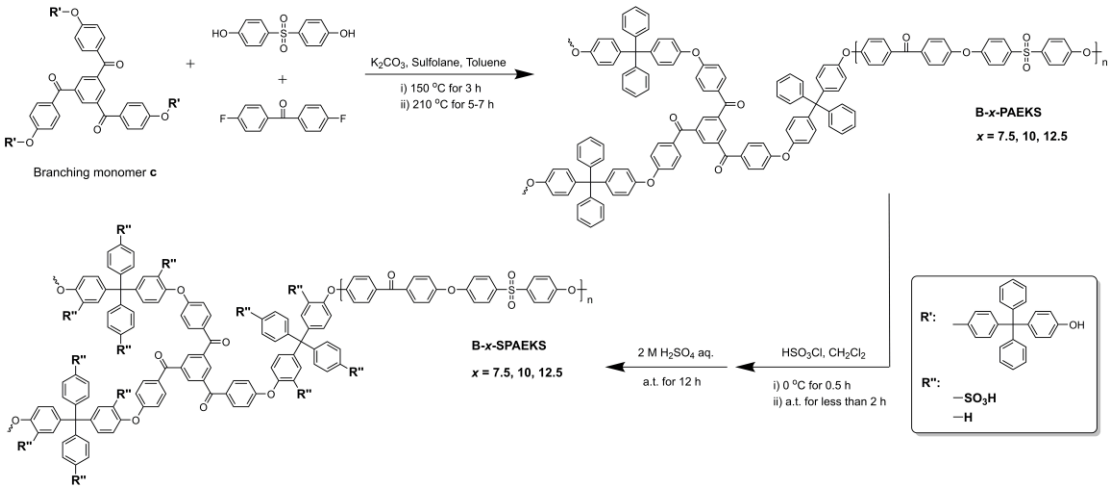

Scheme 4.2. Synthesis of branched copolymers B-*x*-PAEKS and B-*x*-SPAEKS, with *x* representing the molar ratio of the branching monomer **c** to the employed bisfluoride monomer. Adapted with permission from Ref. [145]. Copyright 2023 American Chemical Society.

The chemical structures of copolymers were analyzed with ^{1}H NMR and FT-IR. **Figure 4.2** exhibits the ^{1}H NMR spectra of B-10-PAEKS and B-10-SPAEKS. Signal peaks corresponding to the protons in the *ortho* positions of sulfonyl (H_{12}), carbonyl ($H_{2,10}$), and ether bonds (H_4 and $H_{3,9,11}$) in B-10-PAEKS were identified. Additionally, characteristic peaks associated with branched centers (H_1) arose at around 8.32 ppm. According to the integral area ratio of these peaks, the compositions of B-*x*-PAEKS were demonstrated to be nearly consistent with the theoretical values. After the sulfonation reaction, two new signal peaks representing the protons in the *ortho* positions of the sulfonic acid groups were generated, one of which ($H_{7'}$) arose in the range of 7.51-7.71 ppm, while the other ($H_{6'}$) overlapped by peak ($H_{2,10}$). Consequently, the degree of sulfonation of the B-*x*-SPAEKS was determined to be within 87.9-89.0%, indicating that more than three aryl sites per tetraarylmethane unit were sulfonated.

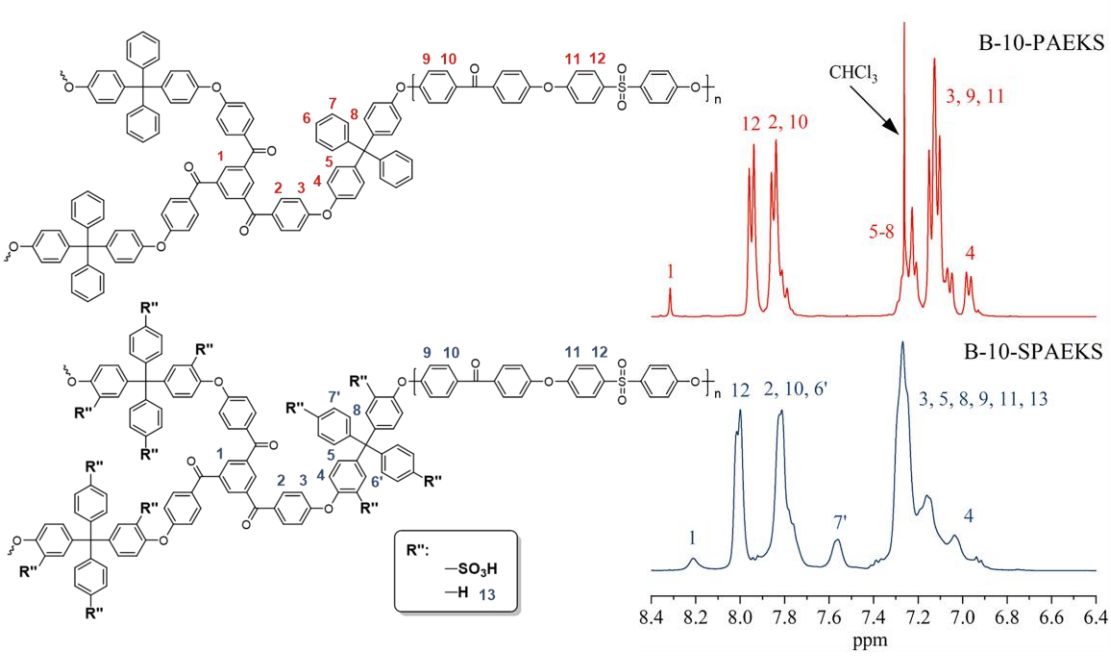

Figure 4.2. ^{1}H NMR spectra of B-10-PAEKS ($CDCl_3$) and B-10-SPAEKS (DMSO-d_6). Adapted with permission from Ref. [145]. Copyright 2023 American Chemical Society.

The FT-IR spectra of B-*x*-SPAEKS and B-10-PAEKS are displayed in **Figure 4.3**. The characteristic absorption band of sulfonic acid groups (S=O) arose at 1035 cm^{-1} in the spectra of B-*x*-SPAEKS, combined with the absence in that of B-10-PAEKS, demonstrating successful sulfonation.

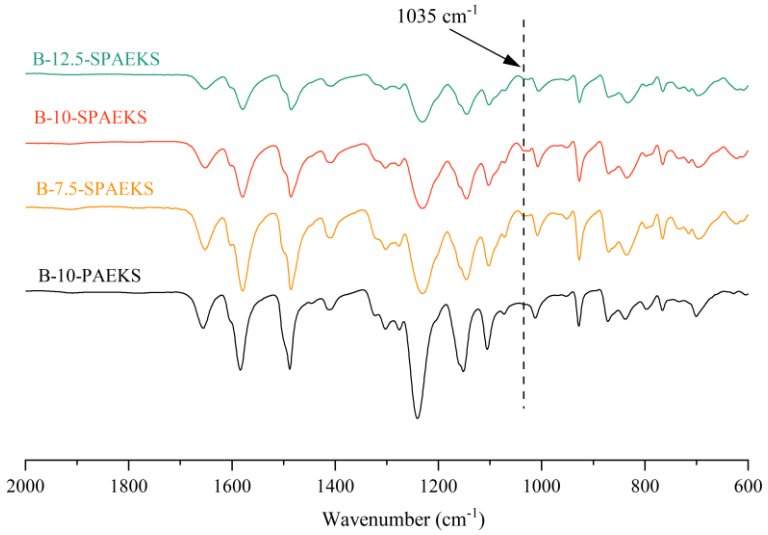

Figure 4.3. FT-IR spectra of B-*x*-SPAEKS and B-10-PAEKS. Adapted with permission from Ref. [145]. Copyright 2023 American Chemical Society.

All copolymers dissolved well in common polar organic solvents, e.g., *N,N*-dimethylacetamide (DMAc), dimethyl sulfoxide (DMSO), and *N*-methyl-2-pyrrolidone (NMP), without forming an insoluble gel. In addition, the inherent viscosities of the copolymers are summarized in **Table 4.1**. B-*x*-SPAEKS presented higher viscosities (1.10-2.03 dL g^{-1}) than B-*x*-PAEKS (0.59-1.03 dL g^{-1}), presumably due to the polyelectrolyte effect.

4.3.3. Preparation of Membranes and Ion Exchange Capacity

The B-*x*-SPAEKS membranes with thicknesses in the range of 38-47 μm, were fabricated via solution casting and subsequently protonated in a 2 M H_2SO_4 aqueous solution for 12 h. The visual image of dry B-10-SPAEKS membrane at ambient temperature is representatively shown

in **Figure A.1** (**Appendix**). **Table 4.1** illustrates the ion exchange capacity (IEC) values of B-*x*-SPAEKS membranes, further including that of B-10-SPAEKS-30. Note, the experimental IEC_{Titr} values were nearly consistent with the theoretical IEC_{Theo} values, indicating a high degree of protonation. Consequently, IEC values shown hereinafter are represented by IEC_{Theo}. Furthermore, due to the deliberate adjustment of sulfonation time, similar IEC values were realized for B-10-SPAEKS and B-10-SPAEKS-30, with respective 1.67 and 1.66 meq g^{-1}. Hence, by comparing the various properties of B-10-SPAEKS and B-10-SPAEKS-30 membranes, the effect of the position of sulfonic acid groups on the branched polymer PEMs enabled investigation.

Table 4.1. Degree of branching, inherent viscosity, ion exchange capacity, thickness, and density of B-*x*-SPAEKS and B-10-SPAEKS-30 membranes. Adapted with permission from Ref. [145]. Copyright 2023 American Chemical Society.

Membrane	DB (%)	η[a] (dL g^{-1})	IEC (meq g^{-1})		Thickness[d] (μm)	Density[e] (g cm^{-3})
			Theo[b]	Titr[c]		
B-7.5-SPAEKS	7.5	1.10 (0.59)	1.38	1.35	38 ± 2	1.41 ± 0.03
B-10-SPAEKS	10	1.38 (0.79)	1.67	1.64	39 ± 2	1.38 ± 0.04
B-12.5-SPAEKS	12.5	1.56 (0.81)	1.95	1.91	42 ± 2	1.35 ± 0.04
B-10-SPAEKS-30	10	2.03 (1.03)	1.66	1.62	47 ± 3	0.88 ± 0.03

[a] The inherent viscosity of B-*x*-SPAEKS and B-10-SPAEKS-30, number in parenthesis represents that of B-*x*-PAEKS and B-10-PAEKS-30.

[b] Calculated from the ^{1}H NMR.

[c] Obtained by acid-base titration.

[d] Thickness of dry membrane.

[e] Density of dry membrane.

4.3.4. Water Uptake and Swelling Ratio

Water molecules, serving as carriers for proton conduction, play a vital role in PEMs. Thus, adequate water absorption of PEMs typically facilitates proton transport, whereas excessive water content within membranes induces significant dimensional variations, thereby impairing the mechanical performance and the practical application capability. [96] The water uptake (WU) of B-*x*-SPAEKS and B-10-SPAEKS-30 membranes as a function of temperature is illustrated in **Figure 4.4a**, in which the WU curves of B-*x*-SPAEKS displayed an upward trend with the increase in temperature. The WU of the B-10-SPAEKS was considerably lower than that of the B-10-SPAEKS-30 over the whole temperature range, despite the DB and IEC values of both being nearly identical. Furthermore, the B-12.5-SPAEKS with higher DB and IEC only achieved a similar WU (43.5%) to the B-10-SPAEKS-30 (43.3%) at 80 ℃.

Such a significant gap in the water affinity between two types of membranes is mainly due to two reasons, one of which is the different regularity in the polymer architecture. Many published articles demonstrate that sulfonated polymers with regular architecture (such as block and densely sulfonated) present less water absorption than the polymer bearing the disordered distribution of sulfonic acid groups. [149, 150] The sulfonic acid groups were ultra-densely tethered on the branched centers of B-*x*-SPAEKS, in contrast, those were relatively randomly modified on the branched arms of B-10-SPAEKS-30. In addition, the discrepancy in free volume is likely the second reason. As listed in **Table 4.1**, the densities of B-*x*-SPAEKS membranes in a dry state were higher than that of the B-10-SPAEKS-30 membrane. Indeed, the sulfonic-acid-groups-functionalized tetraarylmethane units with a large steric hindrance were randomly distributed along the branched arms of B-10-SPAEKS-30, and dominated a high proportion of

the repeating units, resulting in reduced polymer chain entanglement and therefore expanded free volume of the membrane. For B-*x*-SPAEKS, the tetraarylmethane units attached to the sulfonic acid groups are localized on the branched centers, which influences the polymer less and thus results in a smaller free volume. [116]

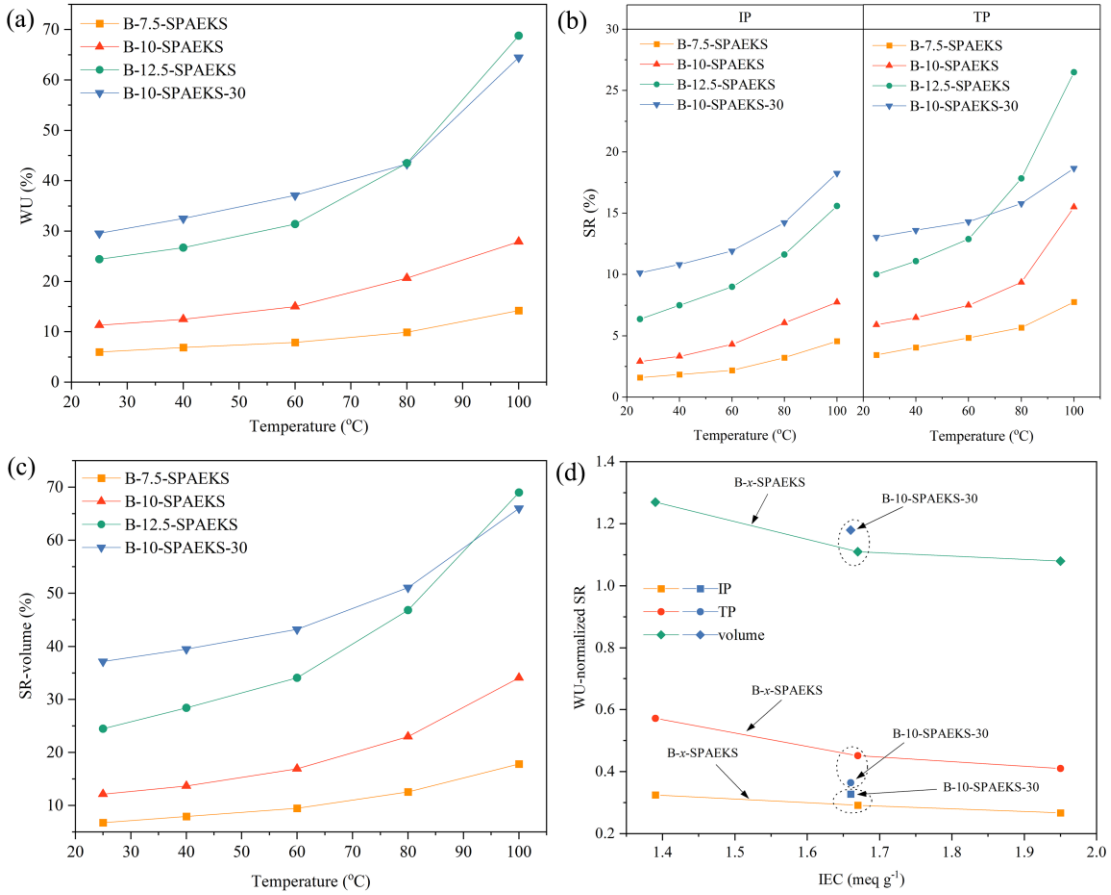

Figure 4.4. (a) Water uptake of B-*x*-SPAEKS and B-10-SPAEKS-30 membranes as a function of temperature; **(b)** Swelling ratios of B-*x*-SPAEKS and B-10-SPAEKS-30 membranes in in-plane (left) and through-plane (right) as functions of temperature; **(c)** Swelling ratio of B-*x*-SPAEKS and B-10-SPAEKS-30 membranes in volume as a function of temperature; **(d)** Water uptake-normalized swelling ratios (in-plane, through-plane, and volume) of B-*x*-SPAEKS and B-10-SPAEKS-30 membranes at 80 °C as a function of IEC. Adapted with permission from Ref. [145]. Copyright 2023 American Chemical Society.

The swelling ratios (SRs) in in-plane (IP) and through-plane (TP) directions of the B-*x*-SPAEKS and B-10-SPAEKS-30 membranes as a function of temperature are indicated in **Figure 4.4b**, where B-*x*-SPAEKS showed a distinct anisotropic swelling phenomenon, i.e., higher SR-TP than SR-IP at the same temperature. Furthermore, the variation of SR-TP was more dependent on temperature, particularly exhibiting a dramatic increment after 80 ℃, whereas the rise in SR-IP was relatively smooth from 25 to 100 ℃. The reason is the morphological orientation within the membranes induced by the regular aggregation of sulfonic acid groups, which frequently occurs in block or densely sulfonated polymer PEMs. [151, 152] The SR-TP/SR-IP values of B-*x*-SPAEKS at 80 ℃ (the typical operating temperature of PEMFCs) are listed in **Table 4.2**, decreasing from 1.78 to 1.53, which is attributed to the weakened orientation by the higher content of branching architectures. The B-10-SPAEKS-30 also displayed an anisotropic dimensional change behavior but it was less pronounced than B-*x*-SPAEKS, and had a stronger dependence on temperature for the growth of the SR-IP than SR-TP. As shown in **Table 4.2**, the SR-TP/SR-IP of B-10-SPAEKS-30 at 80 ℃ was 1.11, considerably lower than those of B-*x*-SPAEKS. The difference is due to the relatively random distribution of the sulfonic acid groups in B-10-SPAEKS-30, which is smaller than those of B-*x*-SPAEKS regarding regularity and density of arrangement. [153, 154] The overall volumetric SR of B-*x*-SPAEKS and B-10-SPAEKS-30 membranes as a function of temperature is depicted in **Figure 4.4c**, demonstrating similar profiles to those of SR-IP and SR-TP.

The swelling variations of the PEMs are directly correlated to water absorption. Accordingly, the SRs of B-*x*-SPAEKS followed a rising trend in terms of IP, TP, and volume as the WU increased. And the B-10-SPAEKS-30 exhibited stronger SRs in any dimension than B-10-

SPAEKS due to a larger WU. However, compared to Nafion 117 (**Table 4.2**), the B-12.5-SPAEKS and B-10-SPAEKS-30 absorbed almost 1.5 times of water but swelled remarkably less in all directions at the same temperature, which is attributed to the branched architecture inhibiting the motion of polymer chains, thereby diminishing the dimensional variations of membranes in water. [119] To standardize the evaluation of the dimensional stability of the B-*x*-SPAEKS, B-10-SPAEKS-30, and Nafion 117 membranes, WU-normalized SR (80 ℃) was employed as an index. As summarized in **Table 4.2**, the SRs/WU in all dimensions of B-*x*-SPAEKS and B-10-SPAEKS-30 were substantially lower than those of Nafion 117, indicating that the branched polymer membranes were less susceptible to swell even under the same content of water absorption.

The WU-normalized SR-IP, SR-TP, and SR-volume of B-*x*-SPAEKS and B-10-SPAEKS-30 membranes at 80 ℃ as a function of IEC are shown in **Figure 4.4d**. All the SRs/WU of B-*x*-SPAEKS exhibited a slightly downward trend with the augment of IEC, which is due to the increased content of branching architecture contributing to reducing the swelling change of the membranes. [117] In a comparison of the B-10-SPAEKS and B-10-SPAEKS-30 with the same DB and almost equal IEC, B-10-SPAEKS presented a smaller SR-IP/WU but a larger SR-TP/WU than B-10-SPAEKS-30, illustrating that B-10-SPAEKS preferred to swell toward the TP direction, which was consistent with the anisotropic swelling phenomenon discussed above. Eventually, B-10-SPAEKS was more stable in terms of volumetric swelling due to a lower SR-volume/WU. The main reason is that branched centers tethered with sulfonic acid groups occupy only a few repeating units of the polymer, forming the more coherent hydrophobic polymer segments that maintain the integral stability of membranes. [90]

In summary, compared with the B-10-SPAEKS-30 membrane, the B-*x*-SPAEKS membranes exhibited less WU and SRs, more pronounced anisotropic swelling behavior, and better capability to inhibit the dimensional change in IP and volume under the same water content. In addition, the dimensional stability of B-*x*-SPAEKS was significantly greater than Nafion 117 in all directions.

Table 4.2. Data related to water uptake and swelling ratios of B-*x*-SPAEKS, B-10-SPAEKS-30, and Nafion 117 membranes. Adapted with permission from Ref. [145]. Copyright 2023 American Chemical Society.

Membrane	WU (%)		SR							SR/WU		
			IP (%)		TP (%)		TP /IP	volume (%)		IP /WU	TP /WU	volume /WU
	25 ℃	80 ℃	25 ℃	80 ℃	25 ℃	80 ℃	80 ℃	25 ℃	80 ℃	80 ℃	80 ℃	80 ℃
B-7.5-SPAEKS	6.0 ± 0.2	9.9 ± 0.4	1.6 ± 0.1	3.2 ± 0.1	3.5 ± 0.1	5.7 ± 0.1	1.78	6.8 ± 0.3	12.6 ± 0.3	0.32	0.58	1.27
B-10-SPAEKS	11.3 ± 0.3	20.7 ± 0.4	2.9 ± 0.1	6.0 ± 0.2	5.9 ± 0.2	9.4 ± 0.3	1.57	12.1 ± 0.5	23.0 ± 0.7	0.29	0.45	1.11
B-12.5-SPAEKS	24.4 ± 0.3	43.5 ± 0.5	6.4 ± 0.3	11.6 ± 0.4	10.0 ± 0.4	17.8 ± 0.2	1.53	24.4 ± 1.3	46.8 ± 1.2	0.27	0.41	1.08
B-10-SPAEKS-30	29.6 ± 0.8	43.3 ± 1.6	10.1 ± 0.2	14.2 ± 0.3	13.1 ± 0.2	15.8 ± 0.3	1.11	37.1 ± 0.7	51.1 ± 1.2	0.33	0.36	1.18
Nafion 117	19.2 ± 0.4	29.4 ± 0.9	13.1 ± 0.5	20.2 ± 0.6	15.0 ± 0.4	23.1 ± 0.7	1.14	47.1 ± 1.8	77.9 ± 2.8	0.69	0.79	2.65

4.3.5. Microscopic Morphology

The microscopic morphology is the crucial factor that determines various properties of PEMs, particularly proton conductivity. [155] The nanoscale morphology of B-*x*-SPAEKS and B-10-SPAEKS-30 membranes was investigated by small-angle X-ray scattering (SAXS) and transmission electron microscope (TEM). The SAXS profiles are depicted in **Figure 4.5a**, all membranes featured characteristic scattering peaks, which demonstrates a phase separation

between hydrophilic and hydrophobic phases. [156] Further details are revealed from the TEM images in **Figure 4.5b**, the hydrophilic phase was distributed as ionic clusters in the hydrophobic phase with clear boundaries between each other. Moreover, the characteristic separation lengths of membranes, i.e., *d* values were calculated according to the positions of the scattering peaks. The B-*x*-SPAEKS exhibited *d* values of 12.19-16.14 nm, which were approximately 2-3 times that of the B-10-SPAEKS-30 (5.66 nm), and followed an upward trend with the increase of IEC. Consistent phenomena also arose in the TEM images, the observed ion clusters of B-*x*-SPAEKS were significantly larger than those of B-10-SPAEKS-30, and the size of clusters expanded from B-7.5-SPAEKS to B-12.5-SPAEKS.

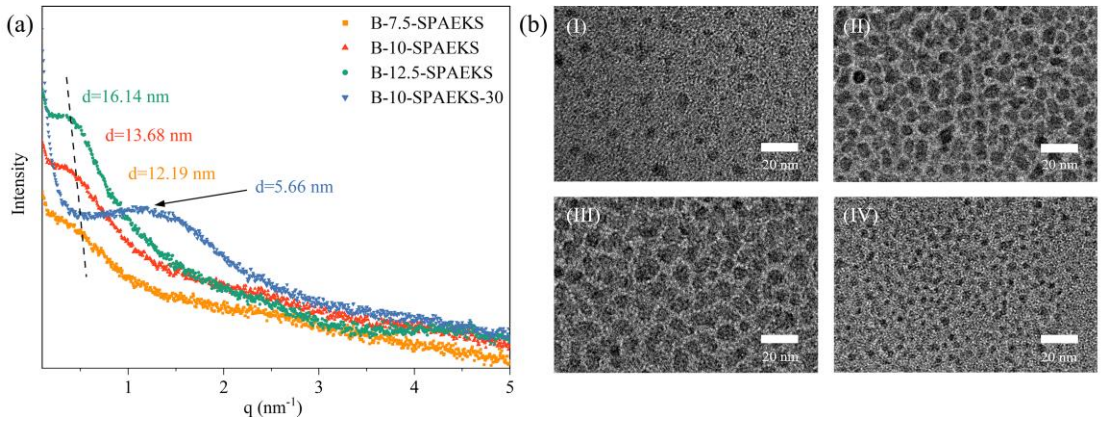

Figure 4.5. (a) The small-angle X-ray scattering profiles of the B-*x*-SPAEKS and B-10-SPAEKS-30 membranes (stained with Pb^{2+}); **(b)** The transmission electron microscope images of **(I)** B-7.5-SPAEKS, **(II)** B-10-SPAEKS, **(III)** B-12.5-SPAEKS, and **(IV)** B-10-SPAEKS-30 membranes (stained with Pb^{2+}). Adapted with permission from Ref. [145]. Copyright 2023 American Chemical Society.

The remarkable differences in *d* values and the status of clusters between two types of membranes are mainly attributed to the positions of sulfonic acid groups, which are ultra-densely tethered on the branched centers of B-*x*-SPAEKS, as opposed to the relatively random locations on the branched arms of B-10-SPAEKS-30. [157] Therefore, larger hydrophilic clusters are forming inside the B-*x*-SPAEKS membranes. In addition, as the IEC values of B-*x*-SPAEKS

increased, the sulfonic-acid-groups functionalized moieties tended to aggregate and lead to enlarged ionic clusters. [158]

4.3.6. Proton Conductivity

The proton conductivity (σ) of PEMs is vital for the performance of PEMFCs. [159] The σ values of B-*x*-SPAEKS and B-10-SPAEKS-30 membranes as a function of temperature are presented in **Figure 4.6a**, in which the curves of B-*x*-SPAEKS trended upward with increasing temperature. Although B-10-SPAEKS-30 and B-10-SPAEKS shared identical DB and similar IEC values, the former presented significantly higher proton conductivities over the whole temperature, which is attributed to the larger amount of water absorption. To thoroughly investigate the dependence of the proton conductivity of B-*x*-SPAEKS and B-10-SPAEKS-30 on the water content, the hydration number (λ), representing the number of water molecules bonded with each sulfonic acid group within the membrane, was calculated, as summarized in **Table 4.3**.

The proton conductivity of B-*x*-SPAEKS and B-10-SPAEKS-30 at 80 ℃ as a function of λ are depicted on the left of **Figure 4.6b**, where the B-*x*-SPAEKS showed a nearly linear and rapidly rising trend, reflecting a strong dependency of proton conductivity on the water content. The position of B-10-SPAEKS-30 was to the right of the curve of B-*x*-SPAEKS, suggesting that it requires more water molecules to achieve a similar proton conductivity compared to B-*x*-SPAEKS. The σ values at 80 ℃ were further normalized by λ to better visualize the difference between B-*x*-SPAEKS and B-10-SPAEKS-30. As shown on the right of **Figure 4.6b**, the curve of B-*x*-SPAEKS with the variation of IEC placed considerably above B-10-SPAEKS-30. The λ-normalized σ at 80 ℃ of B-10-SPAEKS was 10.49 mS cm^{-1}, which was 1.6 times that of B-

10-SPAEKS-30 (6.52 mS cm^{-1}), demonstrating that B-10-SPAEKS presents a better proton conductivity than B-10-SPAEKS-30 at the same water content.

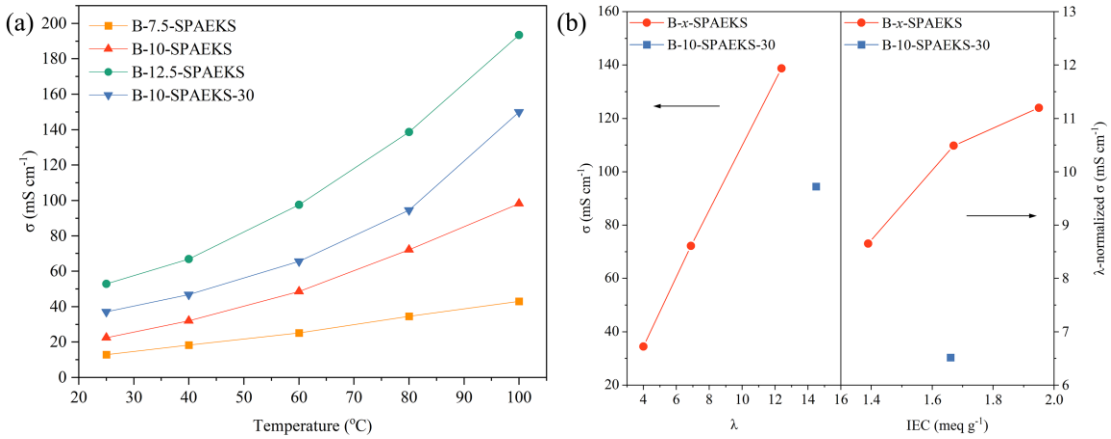

Figure 4.6. (a) Proton conductivity of the B-*x*-SPAEKS and B-10-SPAEKS-30 membranes as a function of temperature; **(b)** Proton conductivity of the B-*x*-SPAEKS and B-10-SPAEKS-30 membranes as a function of hydration number (left); hydration-number-normalized proton conductivity of the B-*x*-SPAEKS and B-10-SPAEKS-30 membranes as a function of IEC (right). Adapted with permission from Ref. [145]. Copyright 2023 American Chemical Society.

The possible reason for such a result is the larger size of ionic clusters inside the B-*x*-SPAEKS membranes, which facilitates the development of more coherent hydrophilic channels to enhance proton transportation. [41, 91] Consequently, the B-12.5-SPAEKS with the best-constructed microscopic morphology achieved a proton conductivity of 138.8 mS cm^{-1} at 80 °C, surpassing that of Nafion 117.

4.3.7. Stabilities and Mechanical Properties

Stability is essential to maintaining the durability of PEMs during practical operation in the PEMFCs. [160] The thermogravimetric analysis (TGA) curves of the B-*x*-SPAEKS and B-10-SPAEKS-30 membranes were measured and are illustrated in **Figure 4.7**, where two evident degradation steps were observed. The first started at around 280 °C, attributed to the

degradation of the sulfonic acid groups. As a result, the B-10-SPAEKS and B-10-SPAEKS-30 with almost equal IEC values displayed nearly coincident profiles in the range of 390 to 480 °C. Further decomposition occurred at approximately 480 °C, resulting from the fragmentation of the polymer backbone. All the membranes still retained about 50% of residual mass at 800 °C. The typical operating temperature of PEMFCs is 80 °C, thus the performance of the B-*x*-SPAEKS membrane fulfills the requirement of PEMFCs in terms of thermal stability until 280 °C.

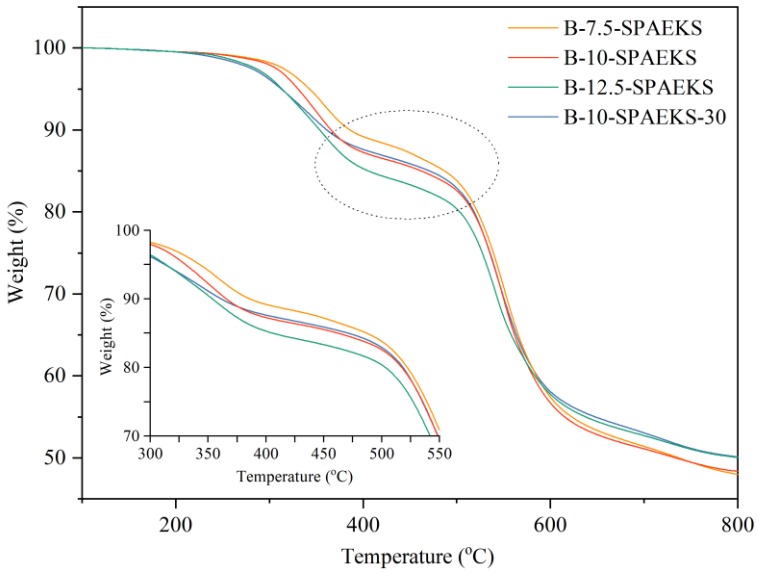

Figure 4.7. The thermogravimetric analysis curves of B-*x*-SPAEKS and B-10-SPAEKS-30 membranes. Adapted with permission from Ref. [145]. Copyright 2023 American Chemical Society.

The oxidative stability of the B-*x*-SPAEKS and B-10-SPAEKS-30 membranes was evaluated by immersion of the membranes in Fenton's reagent at 80 °C and recording the time to the onset of rupture (τ). [161] As listed in **Table 4.3**, the τ values followed a downward trend from B-7.5-SPAEKS to B-12.5-SPAEKS, which is due to the elevated WU that expands the opportunity for free radicals to attack the polymer. However, the B-10-SPAEKS-30, with a higher WU than B-10-SPAEKS at 80 °C, exhibited considerably better stability in Fenton's reagent. Typically,

the oxidative degradation of sulfonated aromatic polymer backbones primarily occurs at the ether bond in the *ortho* position of the sulfonic acid group or the carbon atom in the *meta* position of the sulfonic acid group. [162-164] Indeed, since the sulfonated tetraarylmethane units are randomly distributed on the branched arms of B-10-SPAEKS-30, the branched centers preserve the integrity of the polymer chains even though some polymer segments are damaged by free radicals due to the presence of sulfonic acid groups. On the contrary, once the sulfonated tetraarylmethane units concentrated on the branched centers of B-10-SPAEKS were disrupted, the degradation of the polymer chain accelerates.

Table 4.3. Proton conductivity, hydration number, hydration-number-normalized proton conductivity, oxidative stability, and mechanical properties of B-*x*-SPAEKS, B-10-SPAEKS-30, and Nafion 117 membranes. Adapted with permission from Ref. [145]. Copyright 2023 American Chemical Society.

Membrane	σ (mS cm^{-1})		λ	σ/λ (mS cm^{-1})	Oxidative stability	Mechanical properties	
	25 ℃	80 ℃	80 ℃	80 ℃	τ[a] (min)	Tensile Strength (MPa)	Elongation at break (%)
B-7.5-SPAEKS	12.8 ± 0.2	34.5 ± 1.2	3.99	8.65	300 ± 15	57.3 ± 3.3	18.1 ± 1.3
B-10-SPAEKS	22.4 ± 0.9	72.2 ± 1.9	6.88	10.49	180 ± 15	34.6 ± 3.2	9.4 ± 0.5
B-12.5-SPAEKS	52.8 ± 0.7	138.8 ± 2.4	12.39	11.20	45 ± 15	27.5 ± 1.6	7.1 ± 0.4
B-10-SPAEKS-30	37.1 ± 1.4	94.5 ± 3.1	14.50	6.52	510 ± 15	24.9 ± 2.7	10.8 ± 1.6
Nafion 117	59.0 ± 3.0	122.0 ± 4.5	17.95	6.80	> 600	15.5 ± 0.6	106.3 ± 6.3

[a] τ is the time required for the sample immersed in Fenton's reagent to start to rupture.

The tensile testing results of the hydrated B-*x*-SPAEKS and B-10-SPAEKS-30 membranes at 25 ℃ are summarized in **Table 4.3**. Both tensile strength and elongation at break values of B-*x*-SPAEKS declined with the increased IEC and DB, due to the reduction of chain entanglement

derived from the elevation of water content and branching architecture within the membranes. [165] Similarly, the higher WU of B-10-SPAEKS-30 contributed to an inferior tensile strength to B-10-SPAEKS. However, in comparison to Nafion 117, B-*x*-SPAEKS displayed better tensile strength, demonstrating they are sufficiently robust.

4.3.8. H_2/air Single-cell Performance and Durability

The B-*x*-SPAEKS and B-10-SPAEKS-30 membranes were manufactured as membrane electrode assemblies (MEAs), and the H_2/air fuel cells performance was investigated under 100% relative humidity at 80 °C. The resultant polarization curves are presented in **Figure 4.8a**, where the maximum power densities of B-*x*-SPAEKS were 185.9, 283.2, and 407.9 mW cm^{-2}, respectively, following an uptrend with the increase of proton conductivity. In addition, the B-10-SPAEKS-30 reached a maximum power density of 351.1 mW cm^{-2}, which was significantly higher than that of the B-10-SPAEKS.

The durability of H_2/air fuel cells assembled with B-10-SPAEKS and B-10-SPAEKS-30 was further analyzed. As shown in **Figure 4.8b**, both B-10-SPAEKS and B-10-SPAEKS-30 operated relatively stable for 48 hours, but the former exhibited a faster voltage decay, presumably resulting from inferior oxidative stability. [166]

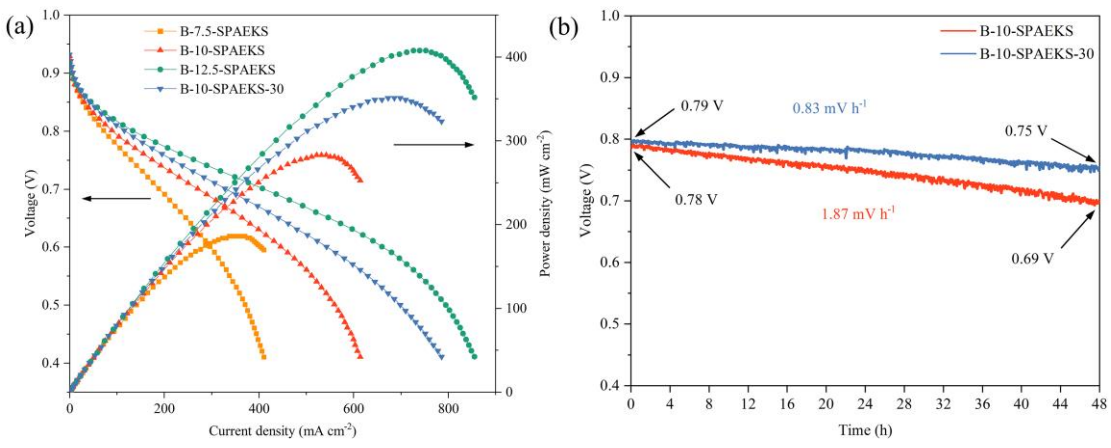

Figure 4.8. (a) The polarization curves of H_2/air fuel cells assembled with B-*x*-SPAEKS and B-10-SPAEKS-30 membranes under 100% relative humidity at 80 ℃; **(b)** Durability of H_2/air fuel cells assembled with B-10-SPAEKS and B-10-SPAEKS-30 membranes under 100% relative humidity at 80 ℃. Adapted with permission from Ref. [145]. Copyright 2023 American Chemical Society.

4.4. Recapitulation

Branching monomer **c** containing tri-tetraarylmethane was synthesized as the branching agent, which was copolymerized with 4,4'-difluorobenzophenone and 4,4'-dihydroxydiphenylsulfone, followed by post-sulfonation. A series of branched poly(arylene ether ketone sulfone)s with sulfonic acid groups ultra-densely tethered on the branched center was afforded, identifying as B-*x*-SPAEKS, with a maximum DB value of 12.5% was achieved.

In comparison with analogous branched polymer PEM with branched arms, the B-*x*-SPAEKS membranes presented reduced water affinity, resulting in less swelling change in all directions and proton conductivity. For instance, with nearly identical DB and IEC values of B-10-SPAEKS and B-10-SPAEKS-30, the WU, SR-IP, and proton conductivity of the former at 80 ℃ were 52.2, 57.7, and 23.6% lower than those of B-10-SPAEKS-30, respectively.

Further analysis revealed that B-*x*-SPAEKS membranes featured better dimensional stability (IP and volume) and proton conduction ability under the same water content. The main reason is the concentration of sulfonic acid groups on the branched centers, which contributes to the formation of coherent hydrophobic polymer segments and large-size ionic clusters, thereby inhibiting dimensional change and promoting proton conductivity at the same time. The B-12.5-SPAEKS exhibited superior proton conductivity and dimensional stability at 80 ℃ to Nafion 117, which were 138.8 mS cm^{-1} and 11.6% (SR-IP), respectively. In addition, a decent

maximum power density of 407.9 mW cm^{-2} was also achieved.

However, the oxidative stability of B-*x*-SPAEKS was observed to be relatively inferior, due to the presence of sulfonic acid groups on branched centers enhancing the degradation risk of polymer chains. This result may affect the strategy of centralizing sulfonic acid groups on the branched center.

5. Branched poly(arylene ether ketone sulfone)s bearing flexible sulfoalkyl side chains for proton exchange membranes

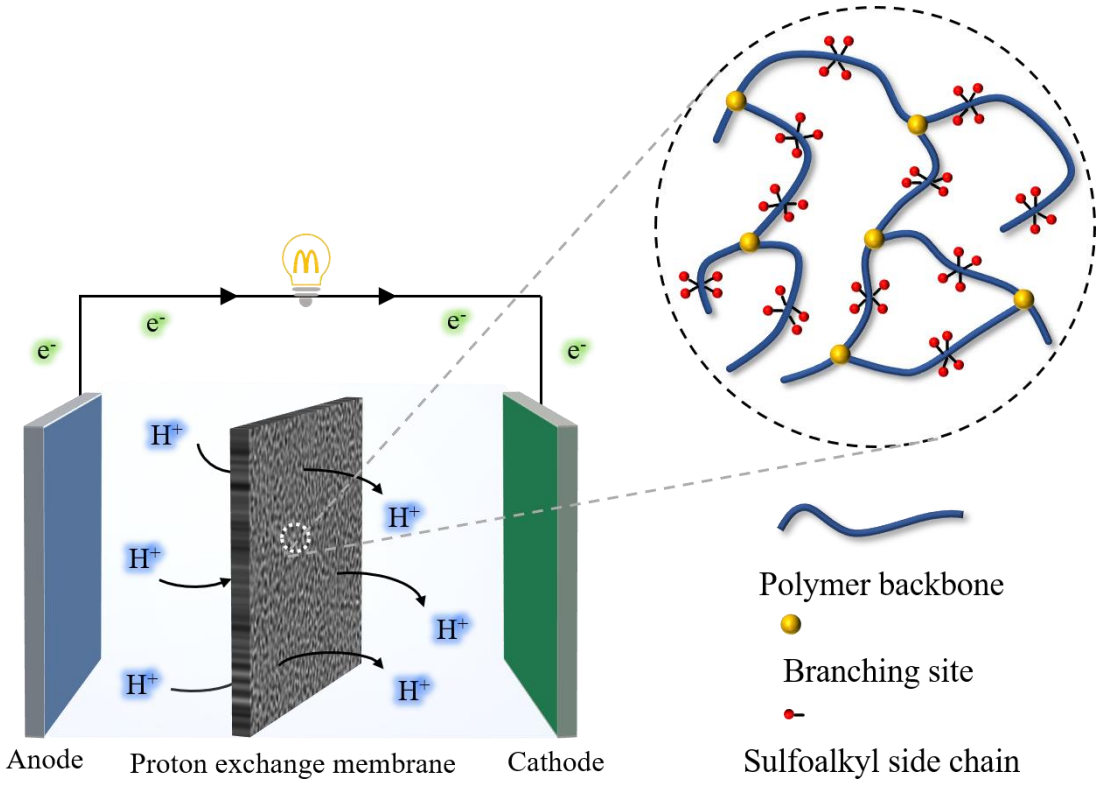

This chapter and the corresponding parts in the experimental section are adapted with permission from Ref. [167]: Yunji Xie, Di Liu, Anna Ringuette, Jinhui Pang, Hatice Mutlu, Dominik Voll, and Patrick Théato*. Highly branched poly(arylene ether ketone sulfone)s bearing flexible sulfoalkyl side chains for proton exchange membranes, *ACS Applied Energy Materials*, 2023, 6 (1), 564-572. Copyright 2023 American Chemical Society.

5.1. Introduction

Over the course of more than two decades, continuous advancements in research have led the focus of sulfonated aromatic polymer PEMs progressively shifted toward practical applications. [11, 168] Although many studies have reported branched sulfonated polymer PEMs with excellent properties, few examples are comparable to commercial PFSA membranes in terms of fuel cell performance. [169] Likewise, the H_2/air single-cell performance of B-*x*-SPAEKS-*y* and B-*x*-SPAEKS membranes fabricated in **Chapters 3** and **4** was inferior to that of Nafion 117. Consequently, the architecture of sulfonated branched aromatic polymer needs to be further optimized to improve proton conductivity, thus achieving superior fuel cell performance of PEMs.

Drawing inspiration from the classic architecture of PFSA polymers, attaching aromatic or aliphatic sulfonic acid groups to the main chain via flexible alkyl chains proves advantageous for enhancing the mobility of functional groups. [170, 171] Pang et al. synthesized a series of poly(arylene ether ketone)s bearing sulfonated tetraarylmethane pendants on alkyl spacers. The prepared PEMs exhibited outstanding proton conductivity, one of which reached 147 mS cm^{-1} at 80 °C with an ion exchange capacity (IEC) value of only 1.43 meq g^{-1}. [148] Wang and co-workers grafted sulfobutyl side chains to the polymer backbone through the nucleophilic ring-opening reaction, resulting in an approximately 20% improvement in the proton conductivity for PEMs, compared to analogous polymers with sulfophenyl groups directly attached to the polymer skeleton. [172]

In **Chapter 4**, a triphenol monomer with tri-tetraarylmethane, i.e., branching monomer **c** was designed as the branching agent. Although the strategy of tethering sulfonic acid groups to the

branched centers may be constrained by reduced oxidative stability, a high degree of branching (DB) value of 12.5% was achieved using this monomer in the polymerization process. Higher DB values promote water affinity, proton conductivity, and oxidative stability of PEMs with sulfonated branched arms, as evidenced by the results in **Chapter 3**. Consequently, grafting flexible side chains functionalized with sulfonic acid groups to the arms of branched polymers with a high DB value appears to be a promising approach for improving the proton conductivity of PEMs, potentially leading to superior fuel cell performance.

5.2. Strategy

In this chapter, the branching monomer **c** is still employed as the branching agent, and a bisfluoride monomer with tetra-methoxyphenyl is synthesized. Following copolymerization with 4,4'-difluorobenzophenone and 4,4'-dihydroxydiphenylsulfone, a series of branched poly(arylene ether ketone sulfone)s with a DB value of 12.5% was afforded. Subsequently, a two-step post-modification reaction, comprising demethoxylation and sulfobutylation, was performed to graft the sulfobutyl side chains to the branched arms. Various properties, such as water uptake, swelling ratio, microscopic morphology, proton conductivity, thermal and oxidative stability, mechanical properties, and H_2/air single-cell performance of the fabricated PEMs were investigated and further compared to those of Nafion 117.

5.3. Results and Discussion

5.3.1. Synthesis of Monomer

The synthetic route of monomer **d** is depicted in **Scheme 5.1**. A bromination reaction of 4,4'-difluorobenzophenone (DFBP) mediated by 1,3-dibromo-5,5-dimethylhydantoin (DBDMH)

was performed under the acidic condition to yield compound **3**, with the molar ratio of DFBP to DBDHM maintained at 1:2.5 to achieve the desired degree of bromination. Subsequently, the monomer **d** was synthesized via a Suzuki coupling reaction between compound **3** and 4-methoxyphenylboronic acid. Despite the purification process of the above reaction involving recrystallization and column chromatography, the yields remained at a satisfactory level, exceeding 60%.

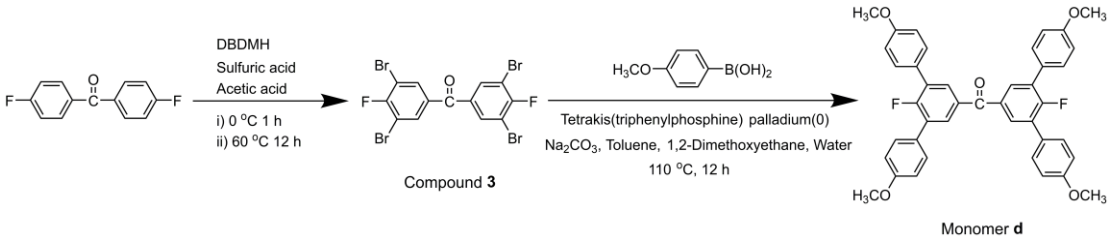

Scheme 5.1. Synthesis of monomer **d**. Adapted with permission from Ref. [167]. Copyright 2023 American Chemical Society.

The chemical structures of compound **3** and branching monomer **d** were confirmed by ^{1}H NMR spectroscopy. As shown in **Figure 5.1**, which depicts the zoomed region between 6.0-9.0 ppm, a sole signal peak (H_1) was observed at 8.07 ppm in the ^{1}H NMR spectrum of compound **3**, demonstrating that the proton located in the *meta* position of the carbonyl group of DFBP had been completely substituted. Furthermore, several new signal peaks arose in the ^{1}H NMR spectrum of monomer **d**. The integral area ratio of signal peaks at 7.79 ppm (H_1), 7.55 ppm (H_2), 7.06 ppm (H_3), and 3.81 ppm (H_4) was 1:2:2:3, which indicated that the Suzuki coupling reaction had been conducted successfully and all four bromine atoms of compound **3** were reacted.

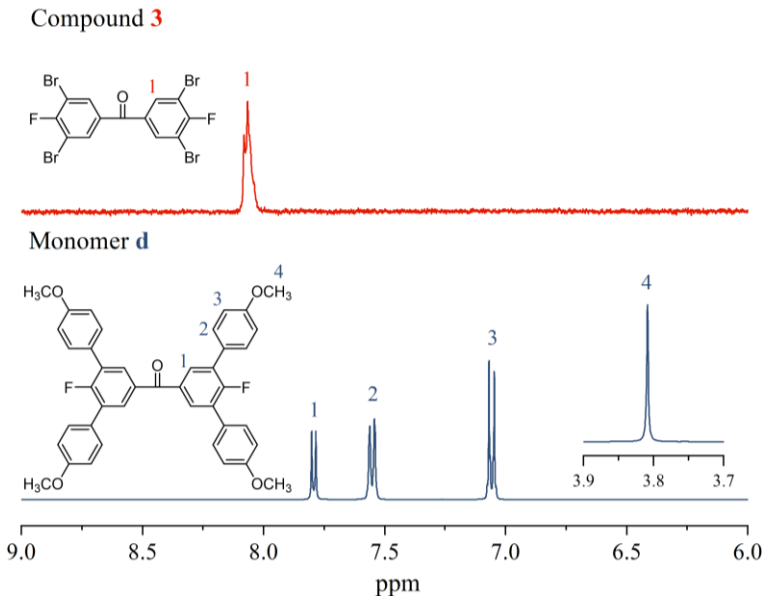

Figure 5.1. ^{1}H NMR spectra (DMSO-d_6) of compound **3** and monomer **d**. Adapted with permission from Ref. [167]. Copyright 2023 American Chemical Society.

5.3.2. Synthesis of Copolymers

The synthesis of a series of branched poly(arylene ether ketone sulfone)s with different functional groups is depicted in **Scheme 5.2**, and the ^{1}H NMR spectra of exemplary copolymers are exhibited in **Figure 5.2**. The branched poly(arylene ether ketone sulfone)s with methoxy groups were initially synthesized via nucleophilic polycondensation, i.e., B-12.5-SPAEKS-M-*y*, where 12.5 signifies the degree of branching (DB), determined by the molar ratio of branching monomer **c** to the employed bisfluoride monomers, and *y* represents the molar ratio of monomer **d** to the employed bisfluoride monomers. As illustrated in the ^{1}H NMR spectrum of B-12.5-PAEKS-M-30, the presence of the signal peaks at 8.27 ppm (H_1), 6.62-6.78 ppm (H_{15}), and 3.61-3.70 ppm (H_{16}) indicated the successful incorporation of branching monomer **c** and monomer **d** into the copolymer. Furthermore, the integral area ratio of these signal peaks corroborated that the composition was nearly consistent with the initial feed ratio.

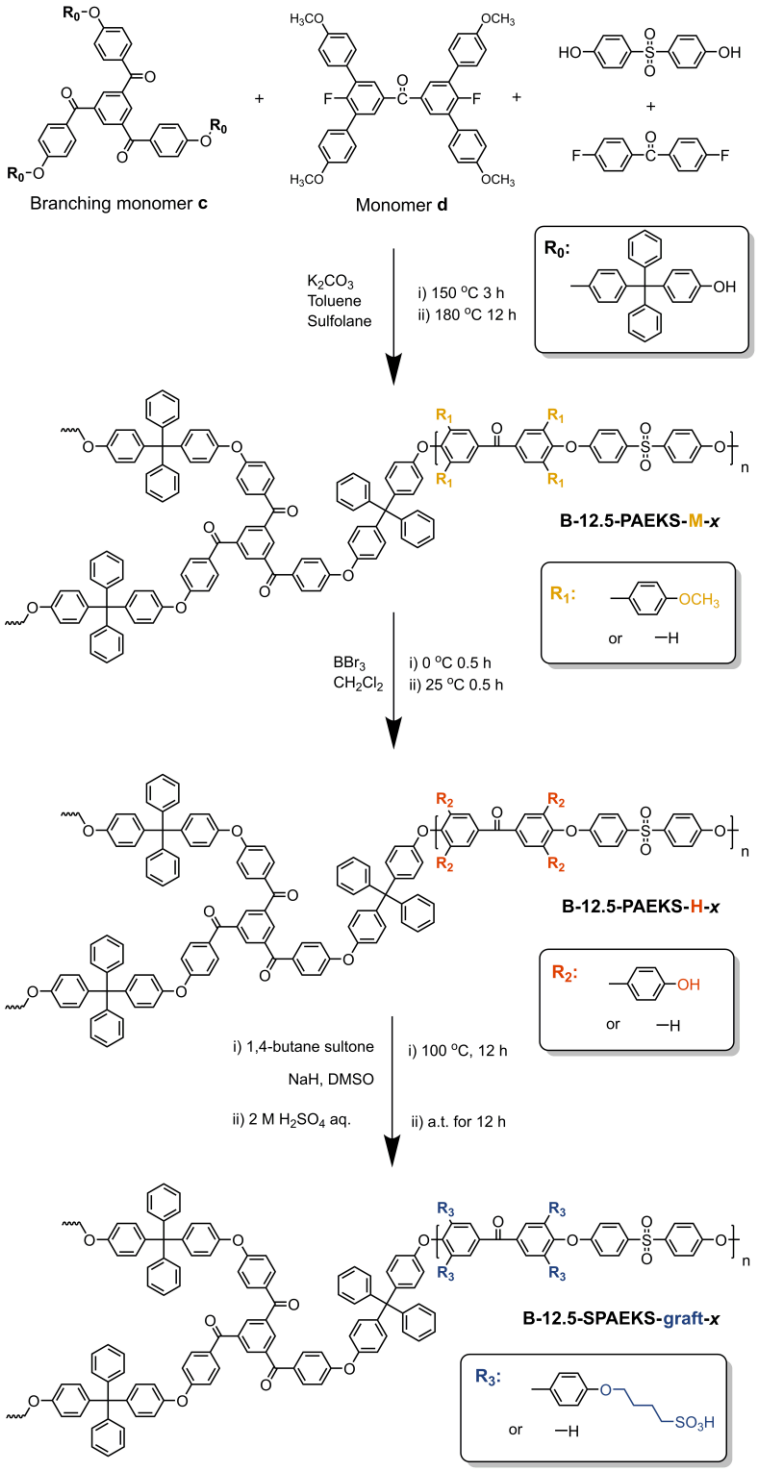

Scheme 5.2. Synthesis of branched poly(arylene ether ketone sulfone)s with different functional groups B-12.5-PAEKS-M-*y*, B-12.5-PAEKS-H-*y*, and B-12.5-SPAEKS-graft-*y* copolymers, with 12.5 and *y* representing the molar ratio of branching monomer **c** and monomer **d** to the employed bisfluoride monomers, respectively. Adapted with permission from Ref. [167]. Copyright 2023 American Chemical Society.

Subsequently, the demethoxylation reaction of B-12.5-PAEKS-M-*y* copolymers was conducted to yield the branched copolymers with hydroxyl groups, i.e., B-12.5-PAEKS-H-*y*. The complete conversion of the methoxy groups to the hydroxyl groups was evidenced by the ^{1}H NMR spectrum of B-12.5-PAEKS-H-30, in which a new signal peak arose at 9.52 ppm ($H_{16'}$), and the signal peak at 3.61-3.70 ppm (H_{16}) had fully vanished.

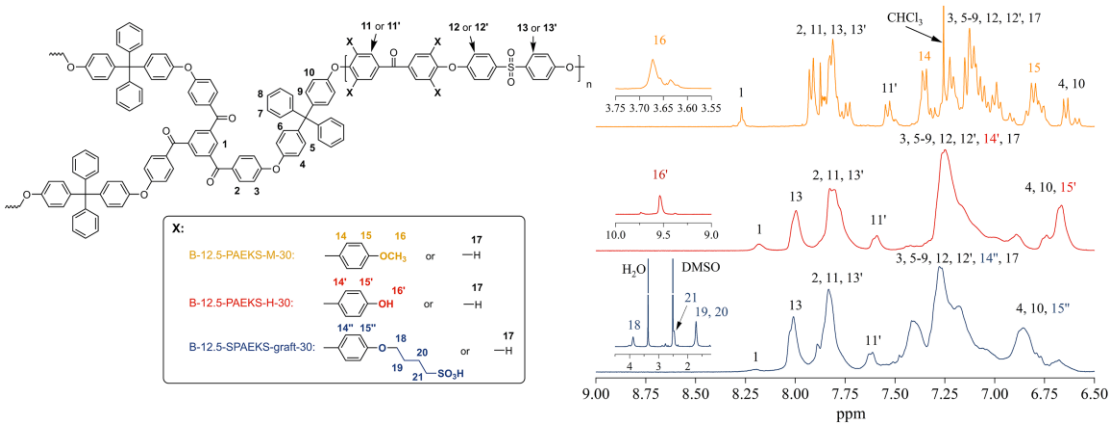

Figure 5.2. ^{1}H NMR spectra of B-12.5-PAEKS-M-30 ($CDCl_3$), B-12.5-PAEKS-H-30 (DMSO-d_6), and B-12.5-SPAEKS-graft-30 (DMSO-d_6). Adapted with permission from Ref. [167]. Copyright 2023 American Chemical Society.

Ultimately, the B-12.5-PAEKS-H-*y* copolymers were sulfobutylated through the nucleophilic ring-opening reaction, affording the branched copolymers grafted with sulfoalkyl side chains, i.e., B-12.5-SPAEKS-graft-*y*. The vanishing signal peak at 9.52 ppm ($H_{16'}$) in the ^{1}H NMR spectrum of B-12.5-SPAEKS-graft-30 demonstrated that the hydroxyl groups had quantitively reacted with 1,4-butane sultone, and several new signal peaks arose in the range of 1.59-3.97 ppm, which were vest in the sulfoalkyl side chain. Moreover, the FT-IR spectra of B-12.5-SPAEKS-graft-*y* and B-12.5-PAEKS-H-30 are displayed in **Figure 5.3**, depicting the band of sulfonic acid groups (S=O) at 1033 cm^{-1}, which further indicates that the sulfonic acid groups were successfully introduced to the B-12.5-SPAEKS-graft-*y*.

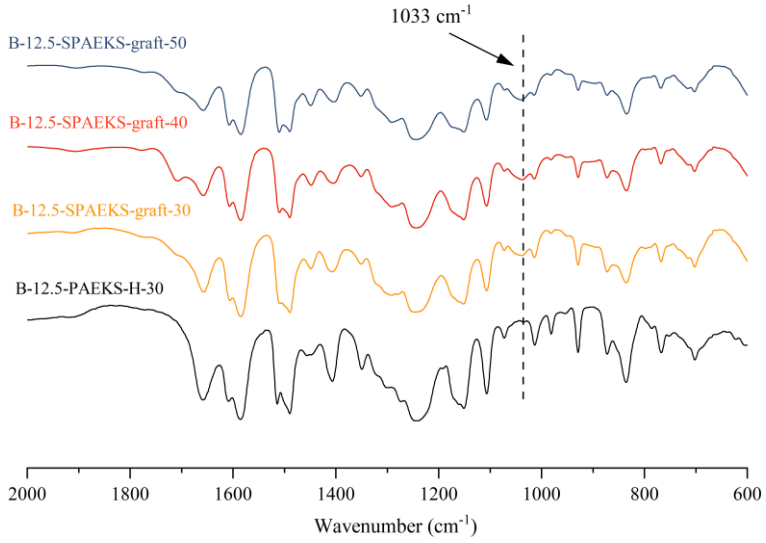

Figure 5.3. FT-IR spectra of B-12.5-SPAEKS-graft-*y* and B-12.5-PAEKS-H-30. Adapted with permission from Ref. [167]. Copyright 2023 American Chemical Society.

Additionally, the series of copolymers exhibited good solubility in the common polar solvents, such as *N,N*-dimethylacetamide (DMAc), dimethyl sulfoxide (DMSO), and *N*-methyl-2-pyrrolidone (NMP), without insoluble gel was observed. The inherent viscosities of copolymers are listed in **Table 5.1**, with an uptrend of the molecular weights from B-12.5-PAEKS-M-*y* to B-12.5-SPAEKS-graft-*y*, which is presumably due to the different intermolecular interactions of the three types of functional groups and polyelectrolyte effect of B-12.5-SPAEKS-graft-*y*. [173, 174]

5.3.3. Preparation of Membranes and Ion Exchange Capacity

B-12.5-SPAEKS-graft-*y* membranes with thicknesses of approximately 40 μm (**Table 5.1**) were fabricated from solution casting, and subsequently immersed in a 2 M H_2SO_4 aqueous solution for 12 h to fully protonate. The visual image of dry B-12.5-SPAEKS-graft-40 membrane at ambient temperature is representatively shown in **Figure A.1** (**Appendix**). As illustrated in **Table 5.1**, the IEC_{Titr} values of B-12.5-SPAEKS-graft-*y* membranes were in the

range of 1.45 to 1.94 meq g^{-1}, which were close to the IEC_{Theo} values, indicating a high degree of protonation. Consequently, IEC values shown hereinafter are represented by IEC_{Theo}.

Table 5.1. Degree of branching, inherent viscosity, ion exchange capacity, thickness, and density of B-12.5-SPAEKS-graft-*y* membranes. Adapted with permission from Ref. [167]. Copyright 2023 American Chemical Society.

Membrane	DB (%)	η[a] (dL g^{-1})	IEC (meq g^{-1})		Thickness[d] (μm)	Density[e] (g cm^{-3})
			Theo[b]	Titr[c]		
B-12.5-SPAEKS-graft-30	12.5	0.86 (0.49, 0.35)	1.44	1.41	45 ± 2	0.95 ± 0.04
B-12.5-SPAEKS-graft-40	12.5	1.00 (0.57, 0.40)	1.73	1.68	34 ± 3	0.94 ± 0.03
B-12.5-SPAEKS-graft-50	12.5	1.15 (0.51, 0.35)	1.96	1.91	37 ± 2	0.92 ± 0.03

[a] The inherent viscosity of B-12.5-SPAEKS-graft-*y*, number in parenthesis represents the viscosity of corresponding B-12.5-SPAEKS-H-*y* and B-12.5-SPAEKS-M-*y* in sequence.

[b] Calculated from the repeating unit of chemical structural formula.

[c] Obtained by acid-base titration.

[d] Thickness of dry membrane.

[e] Density of dry membrane.

5.3.4. Water Uptake and Swelling Ratio

The water uptake (WU) of PEMs directly determines the proton conductivity and swelling ratio (SR). Enhancing the water absorption typically promotes the proton conductivity, but the excessive water within the membrane leads to unrestrained swelling change and ion dilution. [175] The WU of B-12.5-SPAEKS-graft-*y* and Nafion 117 membranes as a function of temperature is shown in **Figure 5.4a**. As can be observed, the WU of B-12.5-SPAEKS-graft-*y* increased with elevating temperature and IEC, respectively. Indeed, the curves of B-12.5-

SPAEKS-graft-30 and B-12.5-SPAEKS-graft-40 presented a smoothly upward trend with an augment of temperature from 25 to 100 °C, which were in the range of 27.9-44.2% and 48.2-99.1%, respectively. In contrast, the WU of B-12.5-SPAEKS-graft-50 maintained a relatively steady variation (66.6-133.2%) from 25 to 80 °C, but dramatically rose to 412.5% at 100 °C, exhibiting an excessive water absorption behavior. Indeed, all the B-12.5-SPAEKS-graft-*y* membranes demonstrated enhanced WU compared to other analogous linear polymer PEMs with sulfoalkyl side chains, [176, 177] presumably due to the formation of large free volumes within the former as a consequence of the 12.5% DB value. This is supported by the densities listed in **Table 5.2**, ranging from 0.92 to 0.95 g cm^{-3}.

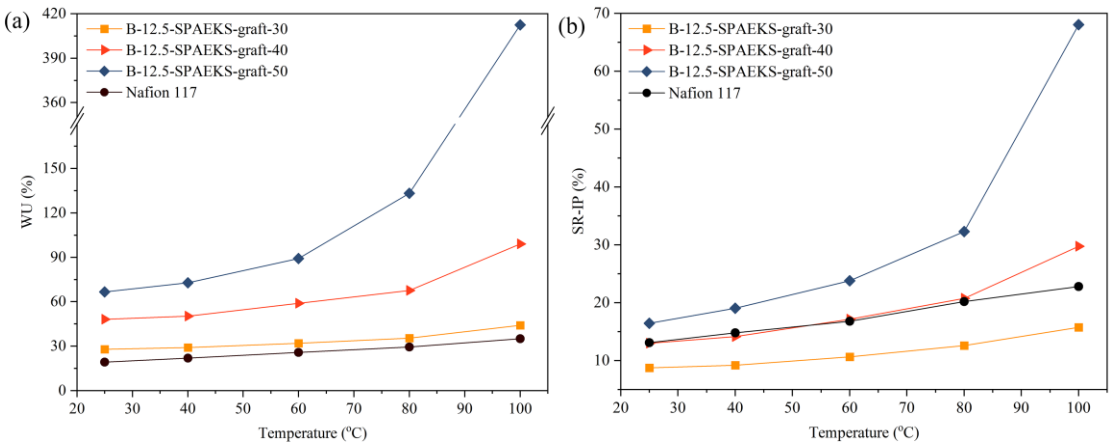

Figure 5.4. (a) Water uptake and **(b)** swelling ratio in the in-plane direction of B-12.5-SPAEKS-graft-*y* and Nafion 117 membranes as a function of temperature. Adapted with permission from Ref. [167]. Copyright 2023 American Chemical Society.

Anisotropic swelling phenomena were not observed from B-12.5-SPAEKS-graft-*y* membranes, which might be attributed to the high DB value. Therefore, the SR only in the in-plane (IP) direction of B-12.5-SPAEKS-graft-*y* membranes as a function of temperature is depicted in **Figure 5.4b**, which presents similar profiles with those of WU. Noteworthy, the B-12.5-SPAEKS-graft-40 and B-12.5-SPAEKS-graft-30 membranes exhibited nearly similar or lower

SR compared to Nafion 117, although both of them possessed higher WU. For instance, at the typical operating temperature of PEMFCs, i.e., 80 ℃, the WU of B-12.5-SPAEKS-graft-40 membrane (67.5%) was almost two times than that of Nafion 117 (29.4%), but the SRs of these two membranes were 20.8% and 20.2%, respectively. The reason is due to the restraint of branching architecture on the motion of polymer chains, thereby reducing the swelling change of the membranes. [178, 179] The SR of B-12.5-SPAEKS-graft-50 remained relatively reasonable in the range of 25-80 ℃, however, the massive WU at 100 ℃ resulted in uncontrollable dimensional variation, leading to a maximum SR of 68.1%. [126]

Table 5.2. Water uptake, swelling ratio in the in-plane direction, and proton conductivity of B-12.5-SPAEKS-graft-*y* and Nafion 117 membranes. Adapted with permission from Ref. [167]. Copyright 2023 American Chemical Society.

Membrane	WU (%)		SR-IP (%)		Proton conductivity (mS cm^{-1})			
	25 ℃	80 ℃	25 ℃	80 ℃	25 ℃	80 ℃	30% RH	95% RH
B-12.5-SPAEKS-graft-30	27.9 ± 1.2	35.4 ± 1.5	8.8 ± 0.2	12.6 ± 0.3	37.1 ± 1.7	87.0 ± 3.5	-	-
B-12.5-SPAEKS-graft-40	48.2 ± 1.8	67.5 ± 2.4	13.0 ± 0.3	20.7 ± 0.5	56.2 ± 2.3	118.6 ± 3.8	0.46 ± 0.05	100.4 ± 3.6
B-12.5-SPAEKS-graft-50	66.6 ± 2.6	133.2 ± 3.9	16.5 ± 0.5	32.3 ± 1.1	80.3 ± 3.2	155.4 ± 4.4	1.4 ± 0.2	131.2 ± 4.1
Nafion 117	19.2 ± 0.4	29.4 ± 0.9	13.1 ± 0.5	20.2 ± 0.6	59.0 ± 3.0	122.0 ± 4.5	3.3 ± 0.4	108.3 ± 3.3

5.3.5. Microscopic Morphology

The microscopic morphology of membranes crucially affects various macroscopic properties including proton conductivity. [180] The B-12.5-SPAEKS-graft-*y* membranes were stained with lead ions, then measured by small-angle X-ray scattering (SAXS) and transmission electron microscope (TEM) under a vacuum condition to investigate the nanoscale morphology. As

shown in **Figure 5.5a**, all membranes exhibited distinct characteristic peaks, indicating the existence of well-defined phase separation between the hydrophilic and hydrophobic phases inside membranes. [181] And the intensities of the peaks tended to be stronger with the increasing IEC values of B-12.5-SPAEKS-graft-*y* membranes. Furthermore, the characteristic separation length, i.e., *d* values presented a slight downward trend from 2.65 to 2.49 nm.

The above phenomena were consistent with the results of TEM images in **Figure 5.5b**, where the hydrophilic phase (black region) in the form of the ionic cluster was evenly distributed in the hydrophobic phase (bright region), revealing an evident hydrophilic-hydrophobic phase separation morphology. [182] As the IEC values elevated, the hydrophilic phase area of B-12.5-SPAEKS-graft-*y* membranes enlarged, leading to stronger contrast with the hydrophobic phase, thus higher peak height of SAXS. Moreover, the dispersion of ionic clusters turned to be denser, reducing the distance between the center of the hydrophilic phase, which resulted in lower *d* values. [183]

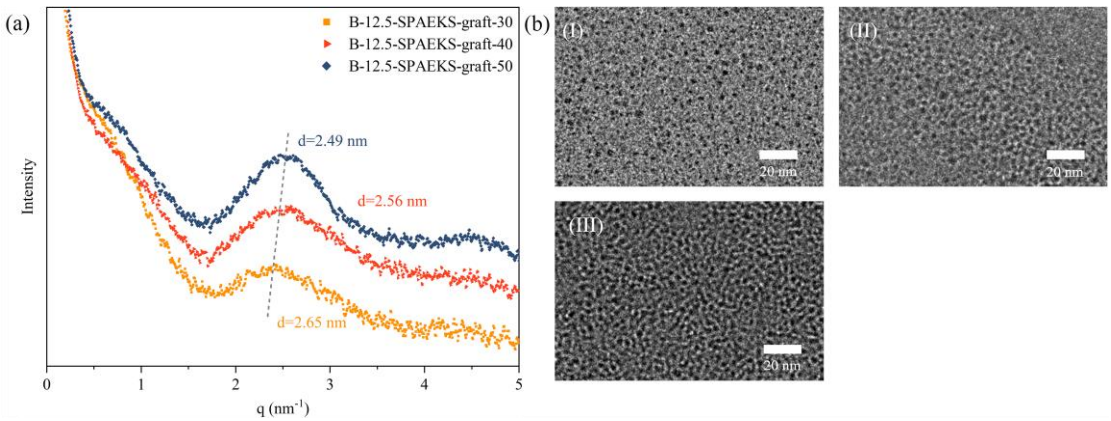

Figure 5.5. (a) The small-angle X-ray scattering profiles of B-12.5-SPAEKS-graft-*y* membranes. **(b)** The transmission electron microscope images of the **(I)** B-12.5-SPAEKS-graft-30, **(II)** B-12.5-SPAEKS-graft-40, and **(III)** B-12.5-SPAEKS-graft-50 membranes. Adapted with permission from Ref. [167]. Copyright 2023 American Chemical Society.

Noteworthy, the B-12.5-SPAEKS-graft-*y* membranes exhibited lower *d* values and smaller ionic cluster sizes compared to B-*x*-SPAEKS-*y* and B-*x*-SPAEKS membranes reported in **Chapters 3** and **4**, which is attributed to the reduced volume of aliphatic sulfonic acid groups relative to aromatic sulfonic acid groups. [184, 185]

5.3.6. Proton Conductivity

Proton conductivity (σ) is an important parameter that crucially determines the performance of PEMFCs. [186] The proton conductivity of B-12.5-SPAEKS-graft-*y* membranes was investigated under two different environments and further compared with Nafion 117, part details of which are summarized in **Table 5.2**. All membranes were firstly measured in a fully hydrated state, as can be observed from **Figure 5.6a**, the σ values of B-12.5-SPAEKS-graft-*y* membranes rose with increasing temperature and IEC value, respectively. Indeed, the B-12.5-SPAEKS-graft-40 and B-12.5-SPAEKS-graft-50 exhibited considerably satisfactory performance. The proton conductivity of the B-12.5-SPAEKS-graft-40 ranged from 56.2 to 149.7 mS cm^{-1} over the entire temperature range, which was nearly consistent with that of Nafion 117 (59.0-151.2 mS cm^{-1}). Moreover, the B-12.5-SPAEKS-graft-50 showed the highest proton conductivity among all the membranes, which was in the range of 80.3–173.7 mS cm^{-1} from 25 to 100 °C. It is worth noting that an abrupt downward fluctuation of the curve occurred from 80 to 100 °C, presumably due to the ion dilution within the membrane as a result of excessive WU. [187, 188]

Moreover, the proton conductivity of B-12.5-SPAEKS-graft-40 and B-12.5-SPAEKS-graft-50 membranes as a function of relative humidity (RH) at 80 °C was further tested. As shown in **Figure 5.6b**, the B-12.5-SPAEKS-graft-40 realized a comparable σ value of 100.4 mS cm^{-1} to Nafion 117 (108.3 mS cm^{-1}) at 95% RH, however, the proton conductivity rapidly reduced with

the declining RH. In contrast, the B-12.5-SPAEKS-graft-50 remained outstanding performance across a broader RH range, presenting σ values of 131.2, 83.9, and 27.1 mS cm^{-1} at 95%, 75%, and 50% RH, respectively. Although the proton conductivity at 35% RH was lower than that of Nafion 117, which still maintained within the same order of magnitude.

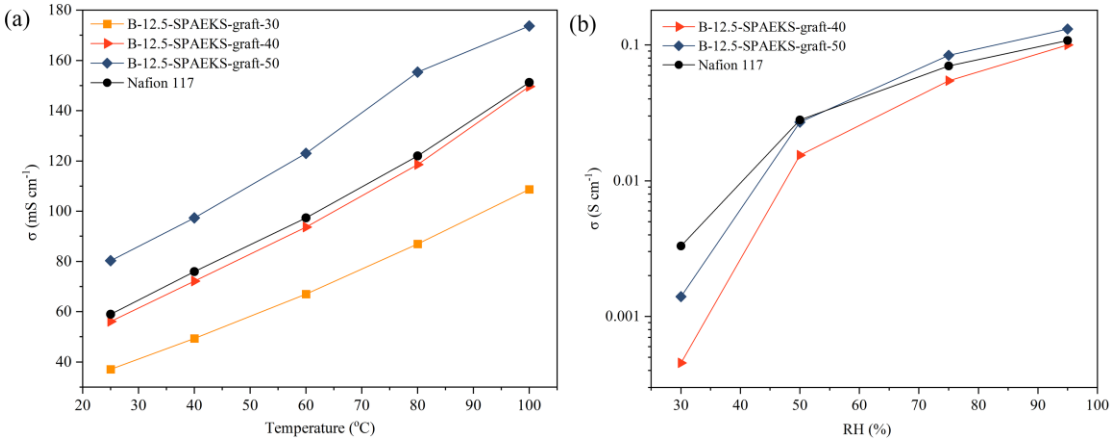

Figure 5.6. (**a**) Proton conductivity of B-12.5-SPAEKS-graft-*y* and Nafion 117 membranes as a function of temperature in a fully hydrated state; (**b**) Proton conductivity of B-12.5-SPAEKS-graft-40, B-12.5-SPAEKS-graft-50, and Nafion 117 membranes as a function of relative humidity at 80 °C. Adapted with permission from Ref. [167]. Copyright 2023 American Chemical Society.

In summary, the B-12.5-SPAEKS-graft-*y* membranes, especially B-12.5-SPAEKS-graft-50, illustrated excellent proton conduction ability, achieving significantly higher proton conductivity than B-*x*-SPAEKS-*y* and B-*x*-SPAEKS membranes prepared in **Chapters 3** and **4** under the similar IEC levels. This is presumably due to the exceptional water affinity and enhanced mobility of sulfonic acid groups, [189, 190] which result from the high DB value and the presence of flexible side chains, respectively.

5.3.7. Stabilities and Mechanical Properties

It is critical that the PEMs possess sufficient thermal and oxidative stabilities during long-term operation in PEMFCs. [191] The thermogravimetric analysis (TGA) curves of B-12.5-SPAEKS-

y membranes are depicted in **Figure 5.7**. As can be observed, the initial degradation temperature of all membranes was higher than 170 ℃, since the typical operating temperature of PEMFCs is 80 ℃, the remarkable stability of B-12.5-SPAEKS-*y* membranes is able to meet the thermal requirement of PEMFCs. Furthermore, two evident degradation stages were observed, the first occurred at around 200 ℃, which was generated by the elimination of the sulfoalkyl side chains, thus the thermal weight loss of the B-12.5-SPAEKS-*y* membranes at this stage elevated with the augment of IEC. Subsequently, the second step appeared at approximately 400 ℃, attributing to the decomposition of the polymer main chains. After the heating ceased at 800 ℃, the residue weights of membranes were still higher than 45%.

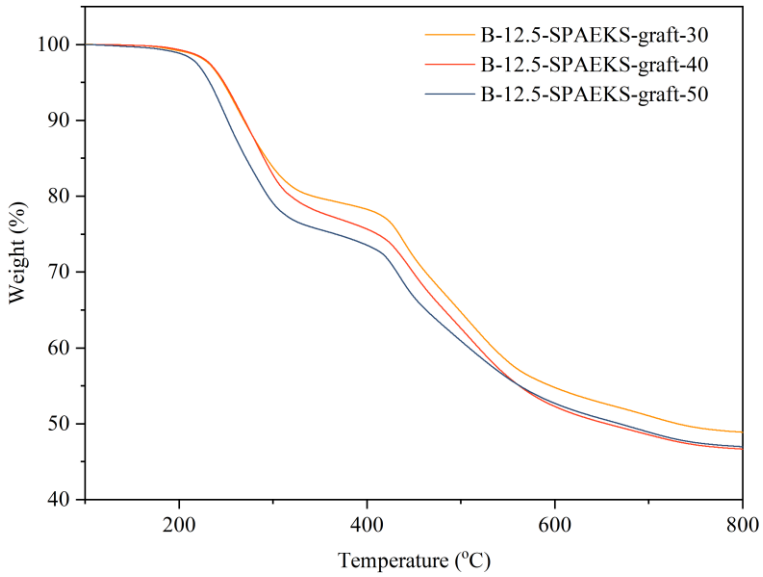

Figure 5.7. The thermogravimetric analysis curves of B-12.5-SPAEKS-graft-*y* membranes. Adapted with permission from Ref. [167]. Copyright 2023 American Chemical Society.

The oxidative stability of B-12.5-SPAEKS-*y* membranes was evaluated again by immersing in Fenton's reagent at 80 ℃ to simulate an accelerated degradation condition. [192] As listed in **Table 5.3**, the time of B-12.5-SPAEKS-graft-*y* membranes required to break (τ) exhibited a downward trend with rising the IEC value, which is attributed to the growing water absorption

leading to an incremental risk of polymer degradation upon attack of free radicals. Nevertheless, the minimum τ value of the B-12.5-SPAEKS-graft-50 still reached 240 min. Generally, PEMs with τ value higher than 200 min are considered to survive in the operating environment of PEMFCs, therefore, the B-12.5-SPAEKS-graft-*y* membranes present satisfactory oxidative stability. [115] Furthermore, the resistance to oxidation of B-12.5-SPAEKS-graft-*y* membranes was considerably better than other reported linear polymer PEMs bearing sulfoalkyl side chains, which is owing to the branching architecture maintaining the integrity of the polymer chain, even though part of the polymer segments ruptured by the free radicals. [193]

Table 5.3. Oxidative stability and mechanical properties of B-12.5-SPAEKS-graft-*y* and Nafion 117 membranes. Adapted with permission from Ref. [167]. Copyright 2023 American Chemical Society.

Membrane	Oxidative stability	Mechanical properties	
	τ[a] (min)	Tensile Strength (MPa)	Elongation at break (%)
B-12.5-SPAEKS-graft-30	450 ± 15	21.6 ± 2.3	14.0 ± 2.1
B-12.5-SPAEKS-graft-40	360 ± 15	17.3 ± 0.9	8.5 ± 1.1
B-12.5-SPAEKS-graft-50	240 ± 15	10.3 ± 0.7	6.4 ± 0.8
Nafion 117	> 600	15.5 ± 0.6	106.3 ± 6.3

[a] τ is the time required for the sample immersed in Fenton's reagent to start to rupture.

The robust mechanical properties are another important parameter that ensures the feasibility of PEMs for long-term operation in PEMFCs. [194] Therefore, tensile testing experiments of hydrated B-12.5-SPAEKS-graft-*y* membranes were performed at 25 °C and the results are listed in **Table 5.3**. Both tensile strength and elongation at break of B-12.5-SPAEKS-graft-*y* membranes decreased with the enhancement of the IEC value, due to the increasing water

absorption impairs the chain entanglements. [195] Nevertheless, the tensile strength of B-12.5-SPAEKS-graft-30 (21.6 MPa) and B-12.5-SPAEKS-graft-40 (17.3 MPa) was comparable to or even better than that of Nafion 117 (15.5 MPa), indicating they are sufficiently strong.

5.3.8. H_2/air Single-cell Performance and Durability

Considering the abovementioned excellent proton conductivity of the B-12.5-SPAKES-graft-*y* membranes, the membrane electrode assemblies (MEAs) were manufactured to investigate the H_2/air fuel cells performance, with the resulting polarization curves depicted in **Figure 5.8a**. It was observed that the maximum power density of the B-12.5-SPAEKS-graft-*y* membranes exhibited an upward trend with increasing proton conductivity, which were 363.0, 438.9, and 529.5 mW cm^{-2}, respectively. The performance of B-12.5-SPAEKS-graft-50 successfully surpassed that of Nafion 117 (507.2 mW cm^{-2}), which was the best among all prepared membranes in this thesis. It is worth noting that the gap between the B-12.5-SPAEKS-graft-40 and Nafion 117 on the maximum power density was apparently bigger than that of proton conductivity. This is presumably due to the worse compatibility between the fabricated membranes and catalyst layers. [196, 197]

The durability of the H_2/air fuel cell assembled with B-12.5-SPAEKS-graft-40 was further evaluated, and the result is illustrated in **Figure 5.8b**. As can be observed, the voltage of B-12.5-SPAEKS-graft-40 exhibited a relatively evident downward tendency before 16 h, then turned to steady until the end. The overall attenuation was nearly 9% throughout the 48-h test. The durability performance of B-12.5-SPAEKS-graft-40 reflected a certain application potential of the fabricated membranes in H_2/air fuel cells.

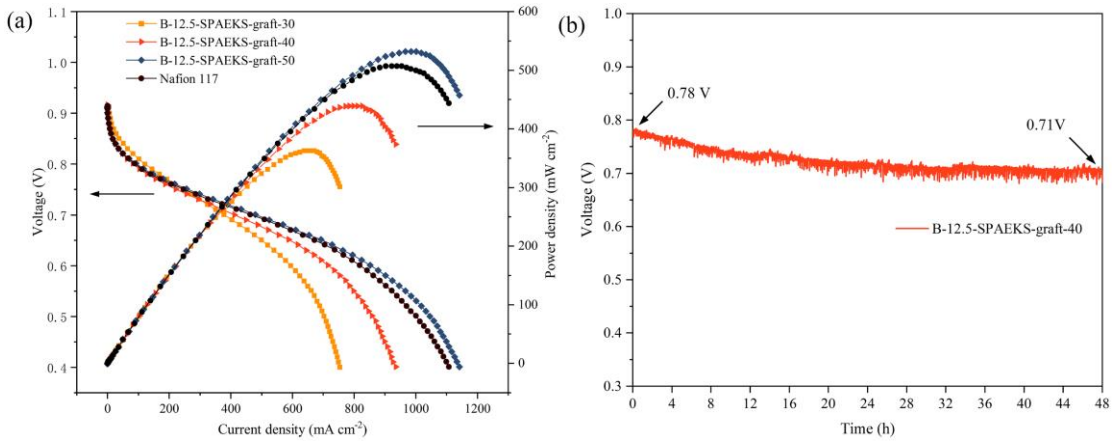

Figure 5.8. (a) The polarization curves of H_2/air fuel cell assembled with B-12.5-SPAEKS-graft-*y* and Nafion 117 membranes under 100% RH at 80 °C; **(b)** Durability of H_2/air fuel cell assembled with B-12.5-SPAEKS-graft-40 under 100% RH at 80 °C. Adapted with permission from Ref. [167]. Copyright 2023 American Chemical Society.

5.4. Recapitulation

Monomer **d** featuring tetra-methoxyphenyl was synthesized and copolymerized with branching monomer **c**, 4,4'-difluorobenzophenone, and 4,4'-dihydroxydiphenylsulfone. Subsequent post-modification comprising demethoxylation and sulfobutylation was performed. A series of branched poly(arylene ether ketone sulfone)s bearing flexible sulfoalkyl side chains was obtained, exhibiting a DB value of 12.5% and denoted as B-12.5-SPAEKS-graft-*y*.

The B-12.5-SPAEKS-graft-*y* membranes presented exceptional water affinity attributed to the high DB value, and the mobility of sulfonic acid groups was enhanced by flexible side chains. As a result, outstanding proton conductivity, significantly higher than other branched polymer PEMs fabricated in the previous two chapters with similar IEC levels, was achieved.

The B-12.5-SPAEKS-graft-40 membrane exhibited comparable proton conductivity to Nafion 117 at 80 °C in a fully hydrated state, registering 118.6 mS cm^{-1}. With a similar SR-IP to Nafion 117 and satisfactory oxidative stability, this membrane realized a trade-off between proton

conductivity, dimensional stability, and durability. Moreover, the proton conductivity of the B-12.5-SPAEKS-graft-50 membrane exceeded Nafion 117 in both a fully hydrated state and a broad range of RH at 80 ℃, leading to superior single H_2/air single-cell performance to Nafion 117.

Therefore, employing a combination of high DB value and grafting flexible sulfoalkyl side chains to the branched arms proves to be an effective strategy for achieving performance surpassing that of commercial PFSA membranes.

6. Conclusion and Outlook

In this thesis, with the branched poly(arylene ether ketone sulfone) as the basic skeleton, the polymer architecture was progressively optimized by introducing different monomers during the polymerization and improving the post-modification process. The research focused on the structure-property relationship of branched sulfonated polymer PEMs, achieving superior performance to commercial PFSA membranes ultimately.

Chapter 3 revealed the effects of DB and IEC on the branched sulfonated polymer PEMs. Two series of branched poly(arylene ether ketone sulfone)s containing sulfonated tetraarylmethane units, namely B-*x*-SPAEKS-*y*, were synthesized. Increasing the DB and IEC exerted the same impact on promoting water absorption, proton conductivity, single-cell performance, and formation of denser distribution of ionic clusters while reducing the mechanical properties of the B-*x*-SPAEKS-*y* membranes. Distinctly different effects of DB and IEC occurred on dimensional variation and oxidative stability, as elevated DB led to isotropic swelling change and enhanced oxidative stability, whereas the influence of IEC was totally the opposite. To optimize oxidative stability and ensure satisfactory proton conductivity of PEMs, increasing DB to 12.5% and then suitably raising IEC appears to be a good option.

Chapter 4 demonstrated the effect of sulfonic acid group positioning within the branched polymer architecture on PEMs. A series of branched poly(arylene ether ketone sulfone)s with ultra-densely sulfonated branched centers was synthesized, identified as B-*x*-SPAEKS, with a maximum DB value of 12.5% being achieved. Compared to analogous branched polymer PEM with relatively random sulfonation of branched arms, concentrating sulfonic acid groups on the branched centers decreased the water affinity of B-*x*-SPAEKS membranes, resulting in less

swelling change in all directions and proton conductivity. Upon normalizing the water content, these membranes indeed exhibited improved dimensional stability (IP and volume) and proton conduction ability. The primary reason is the formation of coherent hydrophobic polymer segments and large-size ionic clusters. However, the oxidative stability was significantly inferior due to the enhanced degradation risk of polymer chains.

Chapter 5 accomplished the development of branched sulfonated polymer PEMs with superior performance compared to Nafion 117. A series of branched poly(arylene ether ketone sulfone)s bearing sulfoalkyl side chains was synthesized, exhibiting a DB value of 12.5% and denoted as B-12.5-SPAEKS-graft-*y*. The water affinity and mobility of sulfonic acid groups in B-12.5-SPAEKS-graft-*y* membranes were improved due to the high DB value and flexible side chains, respectively. Consequently, outstanding proton conductivity, significantly higher than other branched polymer PEMs fabricated in the previous two chapters with similar IEC levels, was achieved. The B-12.5-SPAEKS-graft-40 membrane presented proton conductivity and swelling change comparable to Nafion 117, as well as satisfactory oxidative stability, achieving a trade-off between proton conductivity, dimensional stability, and durability. Furthermore, the proton conductivity of the B-12.5-SPAEKS-graft-50 membrane surpassed Nafion 117 in both a fully hydrated state and a broad range of RH at 80 ℃, leading to superior H_2/air single-cell performance compared to Nafion 117.

In summary, branched sulfonated aromatic polymers demonstrate considerable potential for application as PEMs, however, further advancements are necessary to substitute commercial PFSA membranes in a practical context. For instance, increasing the DB values of branched polymers improves various performance aspects of PEMs but concurrently weakens polymer

chain entanglement, resulting in diminished mechanical properties that may negatively affect long-term durability. Moreover, the assembly technology for branched polymer PEMFCs demands additional refinement. PEMFC assembly design is highly complex, and failure of any factors may impede branched polymer PEMs from achieving fuel cell performance commensurate with their inherent capabilities.

7. Experimental Section

7.1. Materials

Chlorosulfonic acid, sulfolane, 1,3-dibromo-5,5-dimethylhydantoin (DBDMH), 1,4-butane sultone, sodium hydride (60% dispersion in mineral oil) (NaH), and 1,2-dimethoxyethane (DME) were purchased from Sigma Aldrich. Boron tribromide (BBr_3), fluorobenzene, 4,4'-dihydroxydiphenylsulfone (DHDPS), anhydrous sodium carbonate (Na_2CO_3), anhydrous potassium carbonate (K_2CO_3), and anhydrous aluminum chloride ($AlCl_3$) were purchased from Fischer scientific. Tetrakis(triphenylphosphine)palladium(0), 4-methoxytriphenylmethyl chloride, and 4-methoxyphenylboronic acid were purchased from ABCR. Phenol, 4,4'-difluorobenzophenone (DFBP), and 1,3,5-benzenetricarbonyl trichloride were purchased from TCI. Concentrated sulfuric acid (98%) (H_2SO_4) and acetic acid (96%) were purchased from Carl Roth. Other commercial solvents such as dimethyl sulfoxide (DMSO), *N,N*-dimethylacetamide (DMAc), and *N*-methyl-2-pyrrolidone (NMP), and chemicals were purchased from the VWR and used without further purification.

7.2. Synthetic Procedures

7.2.1. Synthesis of benzene-1,3,5-triyltris((4-fluorophenyl)methanone) (Branching monomer a)

$AlCl_3$ (40.0 g, 30.0 mmol) and fluorobenzene (50.0 ml) were charged into a 250 mL three-necked flask equipped with a nitrogen inlet, a magnetic stirrer, a dropping funnel, and a reflux condenser. After the temperature was cooled to 0 ℃, 1,3,5-benzenetricarbonyl trichloride (13.27 g, 50.0 mmol) dissolved in the fluorobenzene (50.0 mL) was added dropwise into the

reaction system under vigorous stirring. The temperature was heated to 80 °C and maintained for 8 h, then most of the fluorobenzene was removed by distillation. The rest of the mixture was poured into a large amount of ice-deionized water containing a few drops of hydrochloric acid. The resultant precipitate was filtered, washed several times with deionized water, and dried in a vacuum oven at 80 °C for 12 h. The branching monomer **a** was afforded by recrystallization with acetone. Yield: 94%. MP: 187.3 °C. ^{1}H NMR (400 MHz, DMSO-d_6): δ = 8.24 (s, 3H), 8.02 – 7.91 (m, 6H), 7.51 – 7.40 (m, 6H).

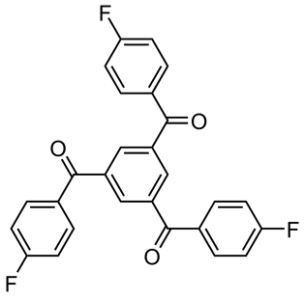

Figure 7.1. Chemical structure of branching monomer **a**.

7.2.2. Synthesis of 4,4'-(diphenylmethylene)diphenol (Monomer b)

4-Methoxy-tritylchlorid (15.44 g, 50.0 mmol) and phenol (28.23 g, 300.0 mmol) were charged into a 250 mL two-necked flask equipped with a nitrogen inlet, a magnetic stirrer, and an air condenser. The temperature was initially heated to 80 °C. After the mixture had melted for 1 h, the temperature was further raised to 150 °C and maintained for 6 h. The solution was cooled to ambient temperature and poured into cold ethanol. The resultant precipitate was collected, washed several times with cold ethanol, and dried in a vacuum oven at 80 °C for 12 h to obtain compound **1**. Yield: 84%. MP: 199.9 °C. ^{1}H NMR (400 MHz, DMSO-d_6): δ = 9.35 (s, 1H), 7.32 – 7.07 (m, 10H), 7.05 – 6.97 (m, 2H), 6.95 – 6.80 (m, 4H), 6.72 – 6.64 (m, 2H), 3.72 (s, 3H).

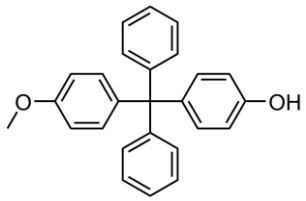

Figure 7.2. Chemical structure of compound **1**.

Compound **1** (3.66 g, 10.0 mmol) and dichloromethane (100.0 mL) were charged into a 250 mL three-necked flask equipped with a nitrogen inlet, a magnetic stirrer, a dropping funnel, and an anhydrous $CaCl_2$ drying tube. After the temperature was cooled to 0 ℃, BBr_3 (2.85 mL, 30.0 mmol) mixed with dichloromethane (30.0 mL) was added dropwise into the reaction system under vigorous stirring. Then the temperature was maintained at ambient temperature to allow the reaction to proceed smoothly for 6 h. The mixture was poured into a large amount of ice-deionized water, and the resultant organic layer was separated and washed several times with brine. Monomer **b** was collected by rotary evaporation and dried in a vacuum oven at 60 °C for 12 h. Yield: 94%. MP: 201.8 ℃. ^{1}H NMR (400 MHz, DMSO-d_6): δ = 9.33 (s, 2H), 7.32 – 7.05 (m, 10H), 6.93 – 6.84 (m, 4H), 6.72 – 6.62 (m, 4H).

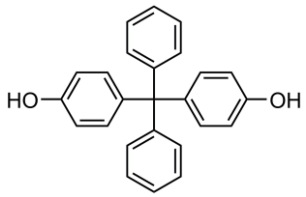

Figure 7.3. Chemical structure of monomer **b**.

7.2.3. Synthesis of benzene-1,3,5-triyltris((4-(4-((4-hydroxyphenyl) diphenylmethyl)phenoxy)phenyl)methanone) (Branching monomer c)

Branching monomer **a** (4.44 g, 10.0 mmol), compound **1** (12.09 g, 33.0 mmol), K_2CO_3 (2.74 g, 20.0 mmol), sulfolane (38.10 mL), and toluene (26.50 mL) were charged into a 100 mL three-necked flask equipped with a nitrogen inlet, a mechanical stirrer, a Dean-Stark trap, and a reflux

condenser. The temperature was heated to 150 ℃ and maintained for 3 h to ensure complete dehydration of the reaction system. Subsequently, the temperature was raised to 180 ℃, enabling the reaction to proceed smoothly for 6 h. After cooling to ambient temperature, the mixture was poured into a large amount of ethanol. The precipitate was dissolved in dichloromethane and filtered through a 0.45 μm organic filter. Then the filtrate was precipitated into ethanol again, and the resultant white powder was collected and washed several times with deionized water and ethanol. Compound **2** was obtained after being dried in a vacuum oven at 60 ℃ for 12 h. Yield: 75%. ^{1}H NMR (400 MHz, DMSO-d_6): δ = 8.19 (s, 3H), 7.94 – 7.82 (m, 6H), 7.35 – 6.95 (m, 54H), 6.87 – 6.78 (m, 6H), 3.70 (s, 9H).

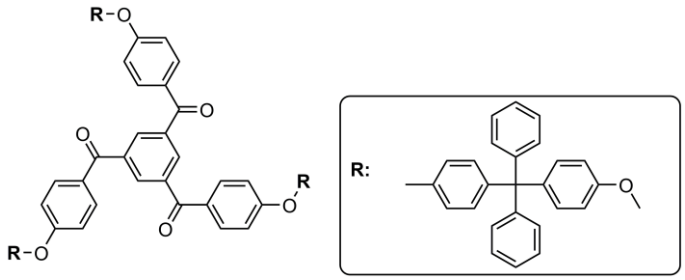

Figure 7.4. Chemical structure of compound **2**.

Subsequently, compound **2** (5.93 g, 4.0 mmol) and dichloromethane (120.0 mL) were charged into a 250 mL three-necked flask equipped with a nitrogen inlet, a magnetic stirrer, a dropping funnel, and an anhydrous $CaCl_2$ drying tube. After the temperature was cooled to 0 ℃, BBr_3 (3.42 mL, 36.0 mmol) mixed with dichloromethane (30.0 mL) was added dropwise into the reaction system under vigorous stirring. Then the temperature was maintained at ambient temperature to allow the reaction to proceed smoothly for 1 h. The mixture was poured into a large amount of ice-deionized water, the resultant organic layer was separated and washed several times with brine. Branching monomer **c** was collected by rotary evaporation and dried

in a vacuum oven at 60 °C for 12 h. Yield: 92%. ^{1}H NMR (400 MHz, DMSO-d_6): δ = 9.38 (s, 3H), 8.20 (s, 3H), 7.95 – 7.84 (m, 6H), 7.34 – 6.83 (m, 54H), 6.74 – 6.61 (m, 6H).

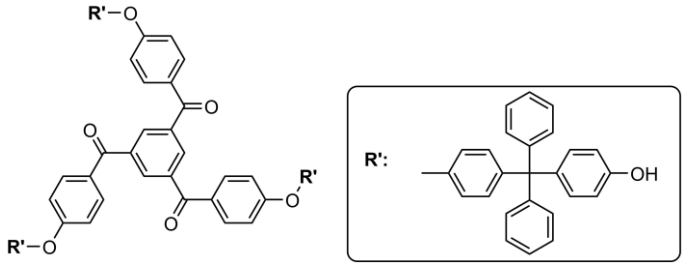

Figure 7.5. Chemical structure of branching monomer **c**.

7.2.4. Synthesis of 3,3',5,5'-tetra(4''-methoxyphenyl)-4,4'-difluorodiphenyl ketone (Monomer d)

DFBP (10.90 g, 50.0 mmol), acetic acid (20.0 mL), and concentrated sulfuric acid (100.0 mL) were charged into a 250 mL three-necked flask equipped with a nitrogen inlet, a mechanical stirrer, and a reflux condenser. After the temperature was cooled to 0 ℃, 1,3-dibromo-5,5-dimethylhydantoin (35.74 g, 125.0 mmol) was divided equally into six portions and added to the reaction system every 10 min in sequence. The temperature was heated to 60 ℃ and maintained for 12 h. The mixture was poured into a large amount of ice-deionized water, and the resultant precipitate was washed with deionized water several times and recrystallized with tetrahydrofuran. Compound **3** was afforded after being dried in a vacuum oven at 60 ℃ for 12 h. Yield: 60%. MP: 217.6 ℃. ^{1}H NMR (400 MHz, DMSO-d_6): δ = 8.10 – 8.02 (m, 4H).

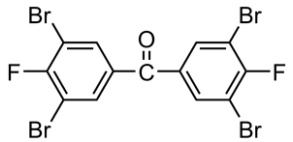

Figure 7.6. Chemical structure of compound **3**.

Compound **3** (3.20 g, 6.0 mmol), 4-methoxyphenylboronic acid (4.56 g, 30.0 mmol), Na_2CO_3

(6.36 g, 60.0 mmol), and tetrakis(triphenylphosphine)palladium(0) (0.35 g, 0.30 mmol) were charged into a 100 mL two-necked flask equipped with a nitrogen inlet, a magnetic stirrer, and a reflux condenser. After strict de-oxygen, a solvent mixture of toluene (25.0 mL), deionized water (25.0 mL), and DME (5.0 mL) was added to the reaction system. The temperature was heated to 110 ℃ and maintained for 12 h. After removing the solvents by rotary evaporation, the crude product was purified by column chromatography with dichloromethane as the eluent. Monomer **d** was obtained after being dried in a vacuum oven at 60 ℃ for 12 h. Yield: 76%. MP: 178.2 ℃. ^{1}H NMR (400 MHz, DMSO-d_6): δ = 7.79 (d, 4H), 7.60 – 7.51 (m, 8H), 7.10 – 7.01 (m, 8H), 3.81 (s, 12H).

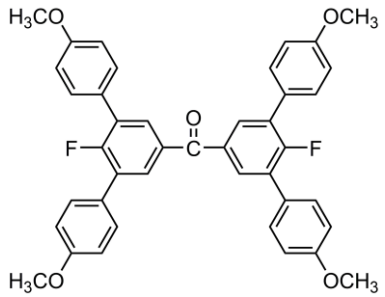

Figure 7.7. Chemical structure of monomer **d**.

7.2.5. Synthesis of branched poly(arylene ether ketone sulfone)s (B-*x*-PAEKS-*y*) and linear poly(arylene ether ketone sulfone) (L-PAEKS-30) containing tetraarylmethane units

The typical polycondensation procedure of B-*x*-PAEKS-*y* and L-PAEKS-30, where *x* = branching monomer **a** / (monomer **b** + DHDPS) × 100, *y* and 30 = monomer **b** / (monomer **b** + DHDPS) × 100, is illustrated by the synthesis of B-7.5-PAEKS-30. Branching monomer **a** (0.33 g, 0.750 mmol), monomer **b** (1.06 g, 3.0 mmol), DFBP (1.94 g, 8.875 mmol), DHDPS (1.75 g, 7.0 mmol), K_2CO_3 (1.66 g, 12.0 mmol), sulfolane (16.10 mL), and toluene (10.0 mL) were

charged into a 50 mL three-necked flask equipped with a nitrogen inlet, a mechanical stirrer, a Dean-Stark trap, and a reflux condenser. The temperature was heated to 150 ℃ and maintained for 3 h to ensure complete dehydration of the reaction system. Subsequently, the temperature was raised to 210 ℃, enabling the reaction to proceed smoothly for 7 h. By pouring the viscous mixture into a large amount of deionized water, a white fibrous precipitate was obtained. The resultant product was pulverized and washed several times with hot deionized water and ethanol. The B-7.5-PAEKS-30 was obtained after being dried in a vacuum oven at 80 ℃ for 12 h. Yield: 94%.

7.2.6. Synthesis of branched poly(arylene ether ketone sulfone)s (B-*x*-SPAEKS-*y*) and linear poly(arylene ether ketone sulfone) (L-SPAEKS-30) containing sulfonated tetraarylmethane units

The typical sulfonation procedure is illustrated by the synthesis of B-7.5-SPAEKS-30. The B-7.5-PAEKS-30 (1.0 g) was dissolved in dichloromethane (30.0 mL), and the polymer solution was filtered through a G4 glass sand core funnel, and charged into a 100 mL two-necked flask equipped with a nitrogen inlet, a magnetic stirrer, and a dropping funnel. After the temperature was cooled at 0 ℃ for 0.5 h, chlorosulfonic acid (0.68 mL, 10.42 mmol) mixed with dichloromethane (20.0 mL) was added dropwise to the reaction system. Then the mixture was vigorously stirred at ambient temperature to allow the sulfonation reaction to proceed smoothly for 2 h 20 min, meanwhile, a purple product was precipitated from the solution. After decanting the supernatant, the resultant product was washed several times with hexane and deionized water. The B-7.5-SPAEKS-30 was obtained after being dried in a vacuum oven at 80 ℃ for 12 h. Yield: 95%.

7.2.7. Synthesis of branched poly(arylene ether ketone sulfone)s with tetraarylmethane moieties concentrated on the branched centers (B-*x*-PAEKS)

The typical polymerization procedure of B-*x*-PAEKS, where *x* = branching monomer **c** / DFBP × 100, is illustrated by the synthesis of B-10-PAEKS. Branching monomer **c** (0.72 g, 0.50 mmol), DFBP (1.10 g, 5.0 mmol), DHDPS (1.06 g, 4.250 mmol), K_2CO_3 (0.83 g, 6.0 mmol), TMS (9.10 mL) and toluene (6.0 mL) were charged into a 25 mL three-necked flask equipped with a nitrogen inlet, a mechanical stirrer, a Dean-Stark trap, and a reflux condenser. The temperature was heated to 150 ℃ and maintained for 3 h to ensure complete dehydration of the reaction system. Subsequently, the temperature was raised to 210 ℃, enabling the reaction to proceed smoothly for 6 h. By pouring the viscous mixture into a large amount of deionized water, a white fibrous precipitate was obtained. The resultant polymer was pulverized and washed several times with hot deionized water and ethanol. The B-10-PAEKS was obtained after being dried in a vacuum oven at 80 ℃ for 12 h. Yield: 95%.

7.2.8. Synthesis of branched poly(arylene ether ketone sulfone)s with ultra-densely sulfonated branched centers (B-*x*-SPAEKS)

The typical sulfonation procedure is illustrated by the synthesis of B-10-SPAEKS. The B-10-PAEKS (1.0 g) was dissolved in dichloromethane (30.0 mL), and the polymer solution was filtered through a G4 glass sand core funnel, and charged into a 100 mL two-necked flask equipped with a nitrogen inlet, a magnetic stirrer, and a dropping funnel. After the temperature was cooled at 0 ℃ for 0.5 h, chlorosulfonic acid (0.59 mL, 8.96 mmol) mixed with dichloromethane (20.0 mL) was added dropwise to the reaction system. Then the mixture was vigorously stirred at ambient temperature to allow the sulfonation reaction to proceed smoothly

for 2 h, meanwhile, a purple product was precipitated from the solution. After decanting the supernatant, the resultant product was washed several times with hexane and deionized water. The B-10-SPAEKS was obtained after being dried in a vacuum oven at 80 ℃ for 12 h. Yield: 94%.

7.2.9. Synthesis of branched poly(arylene ether ketone sulfone)s with methoxy groups (B-12.5-PAEKS-M-*y*)

The typical polycondensation procedure of B-12.5-PAEKS-M-*y*, where 12.5 = branching monomer **c** / (monomer **d** + DFBP) × 100, *y* = monomer **d** / (monomer **d** + DFBP) × 100, is illustrated by the synthesis of B-12.5-PAEKS-M-30. Branching monomer **c** (0.90 g, 0.625 mmol), DHDPS (1.02 g, 4.0625 mmol), monomer **d** (0.96 g, 1.50 mmol), DFBP (0.76 g, 3.50 mmol), K_2CO_3 (0.83 g, 6.0 mmol), sulfolane (11.60 mL), and toluene (10.0 mL) were charged into a 50 mL three-necked flask equipped with a nitrogen inlet, a mechanical stirrer, a Dean-Stark trap, and a reflux condenser. The temperature was heated to 150 ℃ and maintained for 3 h to ensure complete dehydration of the reaction system. Subsequently, the temperature was raised to 180 ℃, enabling the reaction to proceed smoothly for 12 h. By pouring the viscous mixture into a large amount of deionized water, a white fibrous precipitate was obtained. The resultant polymer was pulverized and washed several times with hot deionized water and ethanol. The B-12.5-PAEKS-M-30 was obtained after being dried in a vacuum oven at 80 ℃ for 12 h. Yield: 95%.

7.2.10. Synthesis of branched poly(arylene ether ketone sulfone)s with hydroxyl groups (B-12.5-PAEKS-H-*y*)

The typical synthetic route of B-12.5-PAEKS-H-*y* is illustrated by that of B-12.5-PAEKS-H-30. The B-12.5-PAEKS-M-30 (1.0 g) and dichloromethane (30.0 mL) were charged into a 50 mL three-necked flask equipped with a nitrogen inlet, a magnetic stirrer, a dropping funnel, and an anhydrous $CaCl_2$ drying tube. After the temperature was cooled to 0 ℃, BBr_3 (0.83 mL, 8.75 mmol) mixed with dichloromethane (10.0 mL) was added dropwise into the reaction system under vigorous stirring. Then the temperature was maintained at ambient temperature to allow the reaction to proceed smoothly for 0.5 h. The mixture was poured into a large amount of ice-deionized water, the precipitated polymer was pulverized and washed several times with deionized water. The B-12.5-PAEKS-H-30 was obtained after being dried in a vacuum oven at 80 ℃ for 12 h. Yield: 93%.

7.2.11. Synthesis of branched poly(arylene ether ketone sulfone)s grafted with flexible sulfoalkyl groups (B-12.5-SPAEKS-graft-*y*)

The typical synthesis process of B-12.5-SPAEKS-graft-*y* is illustrated by that of B-12.5-SPAEKS-graft-30. The B-12.5-PAEKS-H-30 (1.0 g) and DMSO (20.0 mL) were charged into a 50 mL three-necked flask equipped with a nitrogen inlet, a magnetic stirrer, a dropping funnel, and a reflux condenser. After a homogenous solution was formed, NaH (0.14 g, 3.52 mmol) was quickly added, then 1,4-butane sultone (0.72 mL, 7.04 mmol) was dropwise added into the reaction system. The temperature was heated to 80 ℃ and maintained for 10 h. The mixture was poured into a large amount of isopropanol, then the precipitated polymer was washed several times with isopropanol and deionized water. The B-12.5-SPAEKS-graft-30 was

obtained after being dried in a vacuum oven at 80 ℃ for 12 h. Yield: 91%.

7.3. Membrane Preparation

The sulfonated copolymers were dissolved in DMAc to form homogeneous solutions (6 wt%), filtered through G4 glass sand core funnels, and cast onto horizontal glass plates (8 cm×8 cm). The temperature was maintained at 100 ℃ for 24 h to evaporate most of the solvent and raised to 120 ℃ for 12 h under vacuum to remove the residual solvent. After cooling to ambient temperature, the membranes were soaked in deionized water to let them peel off the glass plates. The membranes were immersed in 2 M H_2SO_4 solution at ambient temperature for 12 h to ensure the completion of acidification, then washed with deionized water several times until neutral. The membranes in proton form were stored in deionized water for further testing. The thicknesses of dry membranes are around 40 μm, which is reproducible.

7.4. Characterization Methods

The proton nuclear magnetic resonance (^{1}H NMR) spectra of compounds, monomers, and copolymers were investigated by a Bruker Ascend 400 NMR spectrometer with $CDCl_3$ and DMSO-d_6 as the deuterated solvent. The Fourier-transform infrared (FT-IR) spectra of polymers were measured by a Bruker Vector 22 FT-IR spectrometer. The inherent viscosities of polymers were evaluated by an Ubbelohde viscometer in a thermostatic container at 25 ± 0.1 ℃, and the polymers were dissolved in *N*-methyl-2-pyrrolidone (NMP) to form homogenous solutions at the concentration of 0.5 g L^{-1} before the test. The densities of membranes were calculated by the masses and volumes.

7.4.1. Ion Exchange Capacity (IEC)

The experimental IEC values of membranes were determined by the acid-base titration method. The samples were dried in the vacuum oven at 120 ℃ for 12 h and weighed to obtain accurate weights. After being re-protonated, the samples were soaked in 2 M NaCl aqueous solutions for at least 7 days to ensure all the H^+ ions were replaced by Na^+ ions. The solutions containing H^+ ions were titrated by a 0.02 M NaOH aqueous solution with phenolphthalein as the indicator.

The IEC_{Titr} (meq g^{-1}) was calculated using the following equation:

$$IEC_{Titr} = \frac{c_{NaOH} V_{NaOH}}{W_{dry}}$$

where the c_{NaOH} (mmol mL^{-1}) and V_{NaOH} (mL) are the molarity and consumed volume of NaOH aqueous solution, respectively; and W_{dry} (g) represents the weight of the dried sample.

7.4.2. Small-angle X-ray Scattering (SAXS)

The SAXS measurements of membranes were conducted by a Labmate SAXS ess mc^2 system (Anton Paar) equipped with a hermetic pipe X-ray generator (40 kV/40 mA) at 25 ℃. The ionic regions of samples (40 × 5 mm) were selectively stained by soaking in a saturated lead acetate solution for 12 h, then thoroughly washed with deionized water. The resultant samples were dehydrated in a vacuum chamber for several minutes prior to the test.

The scattering vector q (nm^{-1}) is expressed by the formula:

$$q = \frac{4\pi sin\theta}{\lambda}$$

where the θ is the scattering angle, and the λ is the wavelength of 0.1542 nm.

The Bragg spacing d (nm) was obtained based on the scattering vector:

$$d = \frac{2\pi}{q}$$

7.4.3. Transmission Electron Microscope (TEM)

The TEM images of membranes were taken on a JEM-2100F electron microscope under an acceleration voltage of 200 kV. Before the measurement, the samples were immersed in the saturated lead acetate aqueous solution for 12 h to stain the ionic regions with Pb^{2+}. After carefully washing with deionized water, the samples (10 × 1 mm) were strictly dried in the vacuum oven and embedded with epoxy resin, then sliced onto the copper grids.

7.4.4. Water Uptake (WU), Swelling Ratio (SR), and Hydration Number (λ)

The samples (40 × 10 mm) were dried in the vacuum oven at 120 ℃ for 12 h and recorded accurate weights, lengths, widths, and thicknesses. Then the samples were soaked in the deionized water at the specified temperature (25 ℃, 40 ℃, 60 ℃, 80 ℃, and 100 ℃) for at least 2 h until the equilibrium was reached. After carefully wiping off excess water from the surfaces, the weights, lengths, widths, and thicknesses of samples were noted again. The WU, the SRs in the in-plane (SR-IP), through-plane (SR-TP), and volume (SR-volume) directions were determined by calculating the difference between the weights, the lengths, thicknesses, and volumes of pre- and post-immersion samples, respectively.

Here is the equation for calculating the WU (%):

$$WU = \frac{W_{wet}\text{-}W_{dry}}{W_{dry}} \times 100$$

where the W_{wet} (g) and W_{dry} (g) are the weights of the wet and dry samples, respectively.

And the formula of SR-IP, SR-TP, and SR-volume (%) are shown as follows:

$$SR\text{-}IP = \frac{L_{wet}\text{-}L_{dry}}{L_{dry}} \times 100$$

$$SR\text{-}TP = \frac{T_{wet}\text{-}T_{dry}}{t_{dry}} \times 100$$

$$SR\text{-}volume = \frac{V_{wet}\text{-}V_{dry}}{V_{dry}} \times 100$$

where the L_{wet} (mm), T_{wet} (mm), and V_{wet} (mm^3) represent the lengths, thicknesses, and volumes of the wet samples, respectively; and the L_{dry} (mm), T_{dry} (mm), and V_{dry} (mm^3) refer to the lengths, thicknesses, and volumes of the dry samples, respectively.

The hydration number λ, denoting the number of water molecules bonded with each sulfonic acid group, can be calculated by:

$$\lambda = \frac{WU}{M_{H_2O} \times IEC} \times 10$$

where the M_{H_2O} (g mol^{-1}) is the molar mass of the water molecular.

7.4.5. Proton Conductivity (σ)

The σ values of membranes were measured with a Princeton Applied Research potentiostat (model 273 A) equipped with a frequency response detector (Model 5210, EG&G GPARC, Princeton) by the AC impedance method from 0.1 Hz to 100 kHz. The AC perturbation and the DC rest voltage are 10 mV and 0.0 V, respectively. The sample (40 × 10 mm) was immobilized in a sealed cell consisting of four electrodes and two PTFE plates, which was placed in deionized water with different temperatures (25 ℃, 40 ℃, 60 ℃, 80 ℃, and 100 ℃) or in varying relative humidity (RH) environments (30%, 50%, 75% and 95% RH) at 80 ℃ until equilibrium was reached before starting the test.

The proton conductivity σ (mS cm^{-1}) was determined with the following equation:

$$\sigma = \frac{D}{R \times A}$$

where D is the distance between the two working electrodes, R represents the measured resistance, and A refers to the cross-sectional area of the sample.

7.4.6. Thermogravimetric Analysis (TGA)

The thermal stability of membranes was analyzed by a TGA 550 (TA instrument). The samples (3-5 mg) were dried in the vacuum oven at 120 ℃ for 12 h to remove the residual water prior to the test. And the heating procedure was set starting from 100 to 800 ℃ with a speed of 10 ℃ min^{-1} under the nitrogen atmosphere.

7.4.7. Oxidative Stability

The samples (20 × 10 mm) were soaked in Fenton's reagent (aqueous solution containing 3% H_2O_2 and 2 ppm $FeSO_4$) at 80 ℃. The oxidative stability of membranes was evaluated by the consumption time (τ) required for the samples to rupture upon exposure to Fenton's reagent. And the integrity of the samples was checked every 15 min by gently shaking the containers.

7.4.8. Mechanical Properties

The tensile tests of membranes proceeded with a Shimadzu AG-I 20-kN Universal Tester at a stretching rate of 2 mm min^{-1} at 25 ℃. Prior to the test, the samples (40 × 5 mm) were soaked in the deionized water for 12 h to reach the equilibrium, then wiped the excess water from the surfaces.

7.4.9. H_2/air Single-cell Performance and Durability

The Pt/C catalyst (HiSPEC 9100) was mixed with 5 wt% Nafion isopropanol solution to form the ink, which was sprayed evenly on both sides of the membranes by an ExactaCoat sprayer (SONO-TEK Corporation), the resultant catalyst loading and effective area were 0.5 mg cm^{-2}

and 6.25 cm^{-2}, respectively. After being air-dried, the catalyst-sprayed membranes were sandwiched by carbon papers under a pressure of 5-8 bar. The prepared membrane electrolyte assembly (MEA) was mounted in a HORIBA FuelCon instrument, with 200 mL min^{-1} of hydrogen and 400 mL min^{-1} of air supplied to the anode and cathode, respectively. The system was activated (80 °C, 100% relative humidity) for at least 4 h until full equilibrium, then the polarization curve was started to record. The durability test was conducted under the same conditions with a constant current density of 100 mA cm^{-2} for 48 h.

7.5. Task Distribution

The author, Yunji Xie, based in KIT, completed all synthesis work and membrane preparation, along with undertaking part of the characterization tasks, which included ^{1}H NMR, IEC, density, WU, SR, hydration number, TGA, and oxidative stability.

The collaborator, Dr. Di Liu, stationed at Jilin University, China, conducted the remaining characterization procedures such as FT-IR, viscosity, SAXS, TEM, proton conductivity, mechanical properties, and H_2/air single-cell performance.

References

[1] S. Chu, A. Majumdar, *Nature* **2012**, *488*, 294.

[2] M. S. Dresselhaus, I. L. Thomas, *Nature* **2001**, *414*, 332.

[3] M. Wise, K. Calvin, A. Thomson, L. Clarke, B. Bond-Lamberty, R. Sands, S. J. Smith, A. Janetos, J. Edmonds, *Science* **2009**, *324*, 1183.

[4] L. A. Colombo, M. Pansera, R. Owen, *J Clean Prod* **2019**, *214*, 653.

[5] O. Z. Sharaf, M. F. Orhan, *Renewable and Sustainable Energy Reviews* **2014**, *32*, 810.

[6] M. I. Hoffert, K. Caldeira, G. Benford, D. R. Criswell, C. Green, H. Herzog, A. K. Jain, H. S. Kheshgi, K. S. Lackner, J. S. Lewis, H. D. Lightfoot, W. Manheimer, J. C. Mankins, M. E. Mauel, L. J. Perkins, M. E. Schlesinger, T. Volk, T. M. L. Wigley, *Science* **2002**, *298*, 981.

[7] M. Winter, R. J. Brodd, *Chem. Rev.* **2004**, *104*, 4245.

[8] O. Gröger, H. A. Gasteiger, J.-P. Suchsland, *J. Electrochem. Soc.* **2015**, *162*, A2605.

[9] W. R. Grove, *The London, Edinburgh, and Dublin Philosophical Magazine and Journal of Science* **1839**, *14*, 127.

[10] B. C. H. Steele, A. Heinzel, *Nature* **2001**, *414*, 345.

[11] A. Sajid, E. Pervaiz, H. Ali, T. Noor, M. M. Baig, *Int J Energ Res* **2022**, *46*, 6953.

[12] S. Mekhilef, R. Saidur, A. Safari, *Renewable and Sustainable Energy Reviews* **2012**, *16*, 981.

[13] L. Fan, Z. Tu, S. H. Chan, *Energy Reports* **2021**, *7*, 8421.

[14] H. Chen, X. Zhao, T. Zhang, P. Pei, *Energy Convers. Manage.* **2019**, *182*, 282.

[15] D. A. Cullen, K. C. Neyerlin, R. K. Ahluwalia, R. Mukundan, K. L. More, R. L. Borup, A. Z. Weber, D. J. Myers, A. Kusoglu, *Nat Energy* **2021**, *6*, 462.

[16] A. Kraytsberg, Y. Ein-Eli, *Energ Fuel* **2014**, *28*, 7303.

[17] Y. Luo, K. Jiao, *Prog. Energy Combust. Sci.* **2018**, *64*, 29.

[18] M. Tang, S. Zhang, S. Chen, *Chem. Soc. Rev.* **2022**, *51*, 1529.

[19] A. C. Fărcaş, P. Dobra, *Procedia Technology* **2014**, *12*, 42.

[20] D. Chen, P. Pei, Y. Li, P. Ren, Y. Meng, X. Song, Z. Wu, *Energy Convers. Manage.* **2022**, *261*, 115651.

[21] F. Xiao, Y.-C. Wang, Z.-P. Wu, G. Chen, F. Yang, S. Zhu, K. Siddharth, Z. Kong, A. Lu, J.-C. Li, C.-J. Zhong, Z.-Y. Zhou, M. Shao, *Adv. Mater.* **2021**, *33*, 2006292.

[22] M. A. Hickner, H. Ghassemi, Y. S. Kim, B. R. Einsla, J. E. McGrath, *Chem. Rev.* **2004**, *104*, 4587.

[23] R. Devanathan, *Energ Environ Sci* **2008**, *1*, 101.

[24] P. Sharma, O. P. Pandey, "Chapter 1 - Proton exchange membrane fuel cells: fundamentals, advanced technologies, and practical applications", in *PEM Fuel Cells*, G. Kaur, Ed., Elsevier, 2022, p. 1.

[25] M. Pan, C. Pan, C. Li, J. Zhao, *Renewable and Sustainable Energy Reviews* **2021**, *141*, 110771.

[26] S. J. Peighambardoust, S. Rowshanzamir, M. Amjadi, *Int. J. Hydrogen Energy* **2010**, *35*, 9349.

[27] S. Banerjee, D. E. Curtin, *J. Fluorine Chem.* **2004**, *125*, 1211.

[28] M. Adamski, N. Peressin, S. Holdcroft, *Materials Advances* **2021**, *2*, 4966.

[29] M. B. Karimi, F. Mohammadi, K. Hooshyari, *Int. J. Hydrogen Energy* **2019**, *44*, 28919.

[30] B. E. Erickson, *C&EN Global Enterprise* **2023**, *101*, 12.
[31] H. W. Zhang, P. K. Shen, *Chem. Rev.* **2012**, *112*, 2780.
[32] C. H. Park, C. H. Lee, M. D. Guiver, Y. M. Lee, *Progress in Polymer Science* **2011**, *36*, 1443.
[33] J. H. Pang, H. B. Zhang, X. F. Li, Z. H. Jiang, *Macromolecules* **2007**, *40*, 9435.
[34] T. Xu, D. Wu, L. Wu, *Progress in Polymer Science* **2008**, *33*, 894.
[35] P. Xing, G. P. Robertson, M. D. Guiver, S. D. Mikhailenko, K. Wang, S. Kaliaguine, *Journal of Membrane Science* **2004**, *229*, 95.
[36] Z. Wang, H. Z. Ni, C. J. Zhao, M. Y. Zhang, H. Na, *J. Appl. Polym. Sci.* **2009**, *112*, 858.
[37] A. Kausar, *Polym-Plast Technol* **2017**, *56*, 1375.
[38] K. Miyatake, H. Furuya, M. Tanaka, M. Watanabe, *Journal of Power Sources* **2012**, *204*, 74.
[39] M. P. Kulkarni, T. J. Peckham, O. D. Thomas, S. Holdcroft, *J. Polym. Sci., Part A: Polym. Chem.* **2013**, *51*, 3654.
[40] B. Huang, X. Wang, H. Fang, S. Jiang, H. Hou, *Mater. Lett.* **2019**, *234*, 354.
[41] S. G. Jo, T. H. Kim, S. J. Yoon, S. G. Oh, M. S. Cha, H. Y. Shin, J. M. Ahn, J. Y. Lee, Y. T. Hong, *Journal of Membrane Science* **2016**, *510*, 326.
[42] E. G. Sorte, B. A. Paren, C. G. Rodriguez, C. Fujimoto, C. Poirier, L. J. Abbott, N. A. Lynd, K. I. Winey, A. L. Frischknecht, T. M. Alam, *Macromolecules* **2019**, *52*, 857.
[43] C. Genies, R. Mercier, B. Sillion, R. Petiaud, N. Cornet, G. Gebel, M. Pineri, *Polymer* **2001**, *42*, 5097.
[44] M. A. Hickner, H. Ghassemi, Y. S. Kim, B. R. Einsla, J. E. McGrath, *Chem. Rev.* **2004**, *104*, 4587.
[45] S.-W. Chuang, S. L.-C. Hsu, Y.-H. Liu, *Journal of Membrane Science* **2007**, *305*, 353.
[46] T.-H. Kim, S.-K. Kim, T.-W. Lim, J.-C. Lee, *Journal of Membrane Science* **2008**, *323*, 362.
[47] A. J. Berresheim, M. Müller, K. Müllen, *Chem. Rev.* **1999**, *99*, 1747.
[48] A. Abdulkarim, F. Hinkel, D. Jänsch, J. Freudenberg, F. E. Golling, K. Müllen, *J. Am. Chem. Soc.* **2016**, *138*, 16208.
[49] W. F. G. Saleha, N. Nalajala, M. Neergat, *Polym. Int.* **2021**, *70*, 1026.
[50] M. G. Dhara, S. Banerjee, *Progress in Polymer Science* **2010**, *35*, 1022.
[51] P. Wang, X. Liu, D. Wang, M. Wang, D. Zhang, J. Chen, K. Li, Y. Li, K. Jia, Z. Wang, W. Feng, Q. Liu, J. Courtois, X. Yang, *Materials Research Express* **2021**, *8*, 122003.
[52] M. A. Hickner, B. S. Pivovar, *Fuel Cells* **2005**, *5*, 213.
[53] P. Khomein, W. Ketelaars, T. Lap, G. Liu, *Renew Sust Energ Rev* **2021**, *137*.
[54] Y. S. Kim, M. A. Hickner, L. Dong, B. S. Pivovar, J. E. McGrath, *Journal of Membrane Science* **2004**, *243*, 317.
[55] H. Ghassemi, J. E. McGrath, T. A. Zawodzinski, *Polymer* **2006**, *47*, 4132.
[56] H.-S. Lee, A. S. Badami, A. Roy, J. E. McGrath, *J. Polym. Sci., Part A: Polym. Chem.* **2007**, *45*, 4879.
[57] G. Alberti, M. Casciola, L. Massinelli, B. Bauer, *Journal of Membrane Science* **2001**, *185*, 73.
[58] B. Liu, G. P. Robertson, D.-S. Kim, M. D. Guiver, W. Hu, Z. Jiang, *Macromolecules* **2007**, *40*, 1934.
[59] B. Lafitte, L. E. Karlsson, P. Jannasch, *Macromol. Rapid Commun.* **2002**, *23*, 896.

[60] M. Schuster, K.-D. Kreuer, H. T. Andersen, J. Maier, *Macromolecules* **2007**, *40*, 598.
[61] F. Wang, M. Hickner, Y. S. Kim, T. A. Zawodzinski, J. E. McGrath, *Journal of Membrane Science* **2002**, *197*, 231.
[62] F. Wang, M. Hickner, Q. Ji, W. Harrison, J. Mecham, T. A. Zawodzinski, J. E. McGrath, *Macromolecular Symposia* **2001**, *175*, 387.
[63] K. D. Kreuer, *Solid State Ionics* **2000**, *136-137*, 149.
[64] E. M. W. Tsang, S. Holdcroft, "10.35 - Alternative Proton Exchange Membranes by Chain-Growth Polymerization", in *Polymer Science: A Comprehensive Reference*, K. Matyjaszewski and M. Möller, Eds., Elsevier, Amsterdam, 2012, p. 651.
[65] A. Z. Weber, J. Newman, *Chem. Rev.* **2004**, *104*, 4679.
[66] A. K. Sahu, S. Pitchumani, P. Sridhar, A. K. Shukla, *Bull. Mater. Sci.* **2009**, *32*, 285.
[67] T. A. Zawodzinski, T. E. Springer, F. Uribe, S. Gottesfeld, *Solid State Ionics* **1993**, *60*, 199.
[68] C. H. Lee, H. B. Park, Y. M. Lee, R. D. Lee, *Industrial & Engineering Chemistry Research* **2005**, *44*, 7617.
[69] K. D. Kreuer, *Journal of Membrane Science* **2001**, *185*, 29.
[70] N. W. Li, M. D. Guiver, *Macromolecules* **2014**, *47*, 2175.
[71] D. W. Shin, M. D. Guiver, Y. M. Lee, *Chem. Rev.* **2017**, *117*, 4759.
[72] F. Wang, M. Hickner, Y. S. Kim, T. A. Zawodzinski, J. E. McGrath, *Journal of Membrane Science* **2002**, *197*, 231.
[73] W. L. Harrison, F. Wang, J. B. Mecham, V. A. Bhanu, M. Hill, Y. S. Kim, J. E. McGrath, *J. Polym. Sci., Part A: Polym. Chem.* **2003**, *41*, 2264.
[74] X. Li, H. Na, H. Lu, *J. Appl. Polym. Sci.* **2004**, *94*, 1569.
[75] Y. S. Kim, B. Einsla, M. Sankir, W. Harrison, B. S. Pivovar, *Polymer* **2006**, *47*, 4026.
[76] P. P. Zuo, Z. A. Xu, Q. Zhu, J. Ran, L. Ge, X. L. Ge, L. Wu, Z. J. Yang, T. W. Xu, *Adv. Funct. Mater.* **2022**.
[77] B. Bae, K. Miyatake, M. Watanabe, *Macromolecules* **2009**, *42*, 1873.
[78] Z. Wang, H. Ni, C. Zhao, M. Zhang, H. Na, *J. Appl. Polym. Sci.* **2009**, *112*, 858.
[79] H.-S. Lee, A. Roy, O. Lane, S. Dunn, J. E. McGrath, *Polymer* **2008**, *49*, 715.
[80] K. Nakabayashi, K. Matsumoto, M. Ueda, *J. Polym. Sci., Part A: Polym. Chem.* **2008**, *46*, 3947.
[81] H.-S. Lee, A. Roy, O. Lane, M. Lee, J. E. McGrath, *J. Polym. Sci., Part A: Polym. Chem.* **2010**, *48*, 214.
[82] Q. Li, Y. Chen, J. R. Rowlett, J. E. McGrath, N. H. Mack, Y. S. Kim, *Acs Appl Mater Inter* **2014**, *6*, 5779.
[83] Y. Fan, C. J. Cornelius, H.-S. Lee, J. E. McGrath, M. Zhang, R. Moore, C. L. Staiger, *Journal of Membrane Science* **2013**, *430*, 106.
[84] K. Nakabayashi, T. Higashihara, M. Ueda, *J. Polym. Sci., Part A: Polym. Chem.* **2010**, *48*, 2757.
[85] A. S. Badami, O. Lane, H.-S. Lee, A. Roy, J. E. McGrath, *Journal of Membrane Science* **2009**, *333*, 1.
[86] X. Yu, A. Roy, S. Dunn, A. S. Badami, J. Yang, A. S. Good, J. E. McGrath, *J. Polym. Sci., Part A: Polym. Chem.* **2009**, *47*, 1038.
[87] A. Roy, X. Yu, S. Dunn, J. E. McGrath, *Journal of Membrane Science* **2009**, *327*, 118.
[88] S. Takamuku, P. Jannasch, *Adv Energy Mater* **2012**, *2*, 129.

[89] S. H. Tian, Y. Z. Meng, A. S. Hay, *J Polym Sci Pol Chem* **2009**, *47*, 4762.
[90] D. Y. Chen, S. J. Wang, M. Xiao, Y. Z. Meng, A. S. Hay, *J. Mater. Chem.* **2011**, *21*, 12068.
[91] S. Matsumura, A. R. Hlil, N. Y. Du, C. Lepiller, J. Gaudet, D. Guay, Z. Q. Shi, S. Holdcroft, A. S. Hay, *J Polym Sci Pol Chem* **2008**, *46*, 3860.
[92] S. Matsumura, A. R. Hlil, C. Lepiller, J. Gaudet, D. Guay, A. S. Hay, *Macromolecules* **2008**, *41*, 277.
[93] S. Matsumura, A. R. Hlil, C. Lepiller, J. Gaudet, D. Guay, Z. Q. Shi, S. Holdcroft, A. S. Hay, *Macromolecules* **2008**, *41*, 281.
[94] K. Matsumoto, T. Higashihara, M. Ueda, *Macromolecules* **2009**, *42*, 1161.
[95] S. H. Tian, Y. Z. Meng, A. S. Hay, *Macromolecules* **2009**, *42*, 1153.
[96] B. Bae, K. Miyatake, M. Watanabe, *Macromolecules* **2010**, *43*, 2684.
[97] T. B. Norsten, M. D. Guiver, J. Murphy, T. Astill, T. Navessin, S. Holdcroft, B. L. Frankamp, V. M. Rotello, J. Ding, *Adv. Funct. Mater.* **2006**, *16*, 1814.
[98] J. Parvole, P. Jannasch, *Macromolecules* **2008**, *41*, 3893.
[99] B. Lafitte, P. Jannasch, *Adv. Funct. Mater.* **2007**, *17*, 2823.
[100] Y. Zhang, Y. Wan, C. J. Zhao, K. Shao, G. Zhang, H. T. Li, H. D. Lin, H. Na, *Polymer* **2009**, *50*, 4471.
[101] J. H. Pang, H. B. Zhang, X. F. Li, D. F. Ren, Z. H. Jiang, *Macromol. Rapid Commun.* **2007**, *28*, 2332.
[102] N. Li, C. Wang, S. Y. Lee, C. H. Park, Y. M. Lee, M. D. Guiver, *Angew Chem Int Edit* **2011**, *50*, 9158.
[103] T. Dong, J. Hu, M. Ueda, Y. Wu, X. Zhang, L. Wang, *J Mater Chem A* **2016**, *4*, 2321.
[104] S. N. Feng, G. B. Wang, H. B. Zhang, J. H. Pang, *J Mater Chem A* **2015**, *3*, 12698.
[105] H. A. Elwan, M. Mamlouk, K. Scott, *Journal of Power Sources* **2021**, *484*, 229197.
[106] R. Haider, Y. Wen, Z.-F. Ma, D. P. Wilkinson, L. Zhang, X. Yuan, S. Song, J. Zhang, *Chem. Soc. Rev.* **2021**, *50*, 1138.
[107] H. Hou, M. L. Di Vona, P. Knauth, *Journal of Membrane Science* **2012**, *423-424*, 113.
[108] S. D. Mikhailenko, K. Wang, S. Kaliaguine, P. Xing, G. P. Robertson, M. D. Guiver, *Journal of Membrane Science* **2004**, *233*, 93.
[109] S. Gu, G. He, X. Wu, Y. Guo, H. Liu, L. Peng, G. Xiao, *Journal of Membrane Science* **2008**, *312*, 48.
[110] P. Wen, Z. Zhong, L. Li, F. Shen, X.-D. Li, M.-H. Lee, *Journal of Membrane Science* **2014**, *463*, 58.
[111] M. Xu, H. Xue, Q. Wang, L. Jia, *Int. J. Hydrogen Energy* **2021**, *46*, 31727.
[112] X. Zhang, Z. Hu, L. Luo, S. Chen, J. Liu, S. Chen, L. Wang, *Macromol. Rapid Commun.* **2011**, *32*, 1108.
[113] C. Fang, X. N. Toh, Q. Yao, D. Julius, L. Hong, J. Y. Lee, *Journal of Power Sources* **2013**, *226*, 289.
[114] S. Y. Lee, N. R. Kang, D. W. Shin, C. H. Lee, K.-S. Lee, M. D. Guiver, N. Li, Y. M. Lee, *Energ Environ Sci* **2012**, *5*, 9795.
[115] S. Neelakandan, L. Wang, B. P. Zhang, J. P. Ni, M. S. Hu, C. M. Gao, W. Y. Wong, L. Wang, *Polym Rev* **2021**.
[116] H. X. Xie, D. Tao, J. P. Ni, X. Z. Xiang, C. M. Gao, L. Wang, *Journal of Membrane Science* **2016**, *497*, 55.

[117] F. Ahmed, S. C. Sutradhar, T. Ryu, H. Jang, K. Choi, H. Yang, S. Yoon, M. M. Rahman, W. Kim, *Int. J. Hydrogen Energy* **2018**, *43*, 5374.
[118] R. Chatterjee, A. Singh, A. G. Kumar, B. Voit, S. Banerjee, *Eur. Polym. J.* **2020**, *123*.
[119] W. Guo, X. Li, H. Wang, J. Pang, G. Wang, Z. Jiang, S. Zhang, *Journal of Membrane Science* **2013**, *444*, 259.
[120] H. Xie, D. Wang, D. Tao, L. Wang, *Journal of Power Sources* **2014**, *262*, 328.
[121] H. Xie, D. Tao, X. Xiang, Y. Ou, X. Bai, L. Wang, *Journal of Membrane Science* **2015**, *473*, 226.
[122] D. Liu, D. Tao, J. P. Ni, X. Z. Xiang, L. Wang, J. Y. Xi, *J Mater Chem C* **2016**, *4*, 1326.
[123] Y. Xie, A. Ringuette, D. Liu, J. Pang, H. Mutlu, D. Voll, P. Théato, *Eur. Polym. J.* **2023**, *186*, 111837.
[124] C. Liu, D. Wang, W. Wang, Y. Song, Y. Li, H. Zhou, C. Chen, X. Zhao, *Polym. J.* **2013**, *45*, 318.
[125] D. Liu, Y. J. Xie, N. Cui, X. C. Han, J. R. Zhang, J. H. Pang, Z. H. Jiang, *Journal of Membrane Science* **2021**, *620*.
[126] Y. J. Xie, D. Liu, D. Q. Li, X. C. Han, S. Li, Z. Chen, H. B. Zhang, J. H. Pang, Z. H. Jiang, *J Polym Sci Pol Chem* **2018**, *56*, 25.
[127] D. Liu, Y. J. Xie, S. Li, X. C. Han, H. B. Zhang, Z. Chen, J. H. Pang, Z. H. Jiang, *Acs Applied Energy Materials* **2019**, *2*, 1646.
[128] J. H. Pang, X. Jin, Y. Wang, S. N. Feng, K. Z. Shen, G. B. Wang, *Journal of Membrane Science* **2015**, *492*, 67.
[129] K. D. Kreuer, *Chem. Mater.* **2014**, *26*, 361.
[130] Y. S. Kim, *Acs Appl Polym Mater* **2021**, *3*, 1250.
[131] G. W. Crabtree, M. S. Dresselhaus, *MRS Bull.* **2008**, *33*, 421.
[132] H. Y. Hou, M. L. Di Vona, P. Knauth, *Chemsuschem* **2011**, *4*, 1526.
[133] S. Takamuku, P. Jannasch, *Macromolecules* **2012**, *45*, 6538.
[134] D. Liu, Y. Xie, J. Zhong, F. Yang, J. Pang, Z. Jiang, *Journal of Membrane Science* **2022**, *650*, 120413.
[135] M. A. Shehzad, A. Yasmin, X. L. Ge, L. Wu, T. W. Xu, *Adv Mater Technol-Us* **2021**.
[136] S. Takamuku, E. A. Weiber, P. Jannasch, *Chemsuschem* **2013**, *6*, 308.
[137] T. Higashihara, K. Matsumoto, M. Ueda, *Polymer* **2009**, *50*, 5341.
[138] M. J. Park, K. H. Downing, A. Jackson, E. D. Gomez, A. M. Minor, D. Cookson, A. Z. Weber, N. P. Balsara, *Nano Lett.* **2007**, *7*, 3547.
[139] Q. Liu, S. H. Zhang, Z. Q. Wang, J. H. Han, C. Song, P. Q. Xu, X. Wang, S. K. Fu, X. G. Jian, *PCCP* **2022**, *24*, 1760.
[140] T. Holmes, T. J. G. Skalski, M. Adamski, S. Holdcroft, *Chem. Mater.* **2019**, *31*, 1441.
[141] Y. Liang, C. L. Gong, Z. G. Qi, H. Li, Z. Y. Wu, Y. K. Zhang, S. J. Zhang, Y. F. Li, *Journal of Power Sources* **2015**, *284*, 86.
[142] X. L. Ge, F. Zhang, L. Wu, Z. J. Yang, T. W. Xu, *Macromolecules* **2022**, *55*, 3773.
[143] J. P. Ni, M. S. Hu, D. Liu, H. X. Xie, X. Z. Xiang, L. Wang, *J Mater Chem C* **2016**, *4*, 4814.
[144] L. M. Lin, Z. Chen, Z. P. Zhang, S. N. Feng, B. Liu, H. B. Zhang, J. H. Pang, Z. H. Jiang, *Polymer* **2016**, *96*, 188.
[145] Y. Xie, D. Liu, A. Ringuette, P. Théato, *Acs Appl Mater Inter* **2023**, *15*, 24517.

[146] L. Wang, D. G. Wang, G. M. Zhu, J. Q. Li, *Eur. Polym. J.* **2011**, *47*, 1985.
[147] X. C. Han, J. H. Pang, D. Liu, H. B. Zhang, Z. H. Jiang, *Int. J. Hydrogen Energy* **2020**, *45*, 4644.
[148] J. H. Pang, S. N. Feng, Y. Y. Yu, H. B. Zhang, Z. H. Jiang, *Polym Chem-Uk* **2014**, *5*, 1477.
[149] J. Ran, L. Wu, Y. B. He, Z. J. Yang, Y. M. Wang, C. X. Jiang, L. Ge, E. Bakangura, T. W. Xu, *Journal of Membrane Science* **2017**, *522*, 267.
[150] X. Liu, J. T. Wu, J. B. Huo, X. Y. Meng, L. S. Cui, Q. Zhou, *Prog Chem* **2015**, *27*, 395.
[151] M. S. Jung, T. H. Kim, Y. J. Yoon, C. G. Kang, D. M. Yu, J. Y. Lee, H. J. Kim, Y. T. Hong, *Journal of Membrane Science* **2014**, *459*, 72.
[152] Y. Chen, C. H. Lee, J. R. Rowlett, J. E. McGrath, *Polymer* **2012**, *53*, 3143.
[153] A. Roy, X. Yu, S. Dunn, J. E. McGrath, *Journal of Membrane Science* **2009**, *327*, 118.
[154] K. Matsumoto, T. Higashihara, M. Ueda, *Macromolecules* **2008**, *41*, 7560.
[155] G. Gebel, O. Diat, *Fuel Cells* **2005**, *5*, 261.
[156] T. J. Peckham, S. Holdcroft, *Adv. Mater.* **2010**, *22*, 4667.
[157] C. Wang, D. W. Shin, S. Y. Lee, N. R. Kang, G. P. Robertson, Y. M. Lee, M. D. Guiver, *J. Mater. Chem.* **2012**, *22*, 25093.
[158] C. F. Kins, E. Sengupta, A. Kaltbeitzel, M. Wagner, I. Lieberwirth, H. W. Spiess, M. R. Hansen, *Macromolecules* **2014**, *47*, 2645.
[159] J. Miyake, M. Sakai, M. Sakamoto, M. Watanabe, K. Miyatake, *Journal of Membrane Science* **2015**, *476*, 156.
[160] R. Borup, J. Meyers, B. Pivovar, Y. S. Kim, R. Mukundan, N. Garland, D. Myers, M. Wilson, F. Garzon, D. Wood, P. Zelenay, K. More, K. Stroh, T. Zawodzinski, J. Boncella, J. E. McGrath, M. Inaba, K. Miyatake, M. Hori, K. Ota, Z. Ogumi, S. Miyata, A. Nishikata, Z. Siroma, Y. Uchimoto, K. Yasuda, K. I. Kimijima, N. Iwashita, *Chem. Rev.* **2007**, *107*, 3904.
[161] M. Danilczuk, S. Schlick, F. D. Coms, *Macromolecules* **2013**, *46*, 6110.
[162] A. Panchenko, H. Dilger, E. Moller, T. Sixt, E. Roduner, *Journal of Power Sources* **2004**, *127*, 325.
[163] L. Wang, Y. Z. Meng, S. J. Wang, A. S. Hay, *J Polym Sci Pol Chem* **2004**, *42*, 1779.
[164] L. Wang, Y. Z. Meng, S. J. Wang, X. Y. Shang, L. Li, A. S. Hay, *Macromolecules* **2004**, *37*, 3151.
[165] D. Liu, J. H. Peng, Z. Y. Li, B. Liu, L. Wang, *Journal of Power Sources* **2018**, *378*, 451.
[166] L. Gubler, S. M. Dockheer, W. H. Koppenol, *J. Electrochem. Soc.* **2011**, *158*, B755.
[167] Y. Xie, D. Liu, A. Ringuette, J. Pang, H. Mutlu, D. Voll, P. Théato, *ACS Applied Energy Materials* **2023**, *6*, 564.
[168] A. Jamil, S. Rafiq, T. Iqbal, H. A. A. Khan, H. M. Khan, B. Azeem, M. Z. Mustafa, A. S. Hanbazazah, *Chemosphere* **2022**, *303*.
[169] M. Adamski, T. J. G. Skalski, E. M. Schibli, M. Killer, Y. Wu, N. Peressin, B. J. Frisken, S. Holdcroft, *Journal of Membrane Science* **2020**, *595*.
[170] I. a. t. t. u. n. separa-, t. a. a. i. n. i. channels, n. o. b. S.-a. S.-a. responsible, C. Y. for the high proton conductivities and low dimensional swelling.Wang, N. Li, D. W. Shin, S. Y. Lee, N. R. Kang, Y. M. Lee, M. D. Guiver, *Macromolecules* **2011**, *44*, 7296.
[171] B. L. Wang, L. H. Hong, Y. F. Li, L. Zhao, Y. X. Wei, C. J. Zhao, H. Na, *Acs Appl Mater Inter* **2016**, *8*, 24079.
[172] C. Wang, D. W. Shin, S. Y. Lee, N. R. Kang, Y. M. Lee, M. D. Guiver, *Journal of*

Membrane Science **2012**, *405*, 68.
[173] B. L. Wang, Z. Z. Cai, N. Zhang, B. Zhang, D. Qi, C. J. Zhao, H. Na, *Rsc Adv* **2015**, *5*, 536.
[174] G. B. Li, C. J. Zhao, X. F. Li, D. Qi, C. Liu, F. Z. Bu, H. Na, *Polym Chem-Uk* **2015**, *6*, 5911.
[175] T. D. Dong, B. He, X. Z. Li, C. C. Wu, N. W. Li, M. Ueda, X. Zhang, L. J. Wang, *J Polym Sci Pol Chem* **2017**, *55*, 1940.
[176] D. Liu, M. Z. Xu, M. L. Fang, J. L. Chen, L. Wang, *J Mater Chem A* **2018**, *6*, 10879.
[177] M. L. Fang, D. Liu, S. Neelakandan, M. Z. Xu, D. Q. Liu, L. Wang, *Appl. Surf. Sci.* **2019**, *493*, 1306.
[178] S. S. Li, R. J. Gan, L. Li, L. D. Li, F. X. Zhang, G. H. He, *Ionics* **2018**, *24*, 189.
[179] L. J. Li, T. Jiang, S. Wang, S. Cheng, X. L. Li, H. B. Wei, Y. S. Ding, *Acs Applied Energy Materials* **2022**, *5*, 2462.
[180] T. D. Dong, J. H. Hu, M. Ueda, Y. M. Wu, X. Zhang, L. J. Wang, *J Mater Chem A* **2016**, *4*, 2321.
[181] E. P. Jutemar, P. Jannasch, *Journal of Membrane Science* **2010**, *351*, 87.
[182] B. Bae, K. Miyatake, M. Watanabe, *Acs Appl Mater Inter* **2009**, *1*, 1279.
[183] X. F. Li, F. P. V. Paoloni, E. A. Weiber, Z. H. Jiang, P. Jannasch, *Macromolecules* **2012**, *45*, 1447.
[184] L. Y. Zhang, G. Zhang, C. J. Zhao, Z. G. Liu, H. Jiang, S. Xu, M. Y. Li, D. Xu, H. Na, *Int. J. Hydrogen Energy* **2013**, *38*, 12363.
[185] K. Shao, J. Zhu, C. J. Zhao, X. F. Li, Z. M. Cui, Y. Zhang, H. T. Li, D. Xu, G. Zhang, T. Z. Fu, J. Wu, H. Na, W. Xing, *J Polym Sci Pol Chem* **2009**, *47*, 5772.
[186] K. Miyatake, T. Shimura, T. Mikami, M. Watanabe, *Chem. Commun.* **2009**, 6403.
[187] Y. Chang, G. F. Brunello, J. Fuller, M. L. Disabb-Miller, M. E. Hawley, Y. S. Kim, M. A. Hickner, S. S. Jang, C. Bae, *Polym Chem-Uk* **2013**, *4*, 272.
[188] S. Takamuku, A. Wohlfarth, A. Manhart, P. Rader, P. Jannasch, *Polym Chem-Uk* **2015**, *6*, 1267.
[189] L. Y. Zhang, D. Qi, G. Zhang, C. J. Zhao, H. Na, *Rsc Adv* **2014**, *4*, 51916.
[190] L. Y. Zhang, G. Zhang, C. J. Zhao, H. Jiang, J. Wang, D. Xu, Y. Zhang, K. Shao, Z. G. Liu, W. J. Ma, H. T. Li, M. Y. Li, S. Wang, H. Na, *Journal of Power Sources* **2012**, *201*, 142.
[191] C. Perrot, L. Gonon, C. Marestin, A. Morin, G. Gebel, *Journal of Power Sources* **2010**, *195*, 493.
[192] C. Perrot, L. Gonon, M. Bardet, C. Marestin, A. Pierre-Bayle, G. Gebel, *Polymer* **2009**, *50*, 1671.
[193] S. Y. Moon, J. H. Kim, B. J. Chang, *J. Appl. Polym. Sci.* **2020**, *137*.
[194] D. Liu, L. M. Lin, Y. J. Xie, J. H. Pang, Z. H. Jiang, *Journal of Membrane Science* **2021**, *623*.
[195] S. A. Feng, J. H. Pang, X. W. Yu, G. B. Wang, A. Manthiram, *Acs Appl Mater Inter* **2017**, *9*, 24527.
[196] X. T. Pu, Y. T. Duan, J. L. Li, C. Y. Ru, C. J. Zhao, *Journal of Power Sources* **2021**, *493*.
[197] S. Ahmad, T. Nawaz, A. Ali, M. F. Orhan, A. Samreen, A. M. Kannan, *Int. J. Hydrogen Energy* **2022**, *47*, 19086.

Appendix

Additional Figure

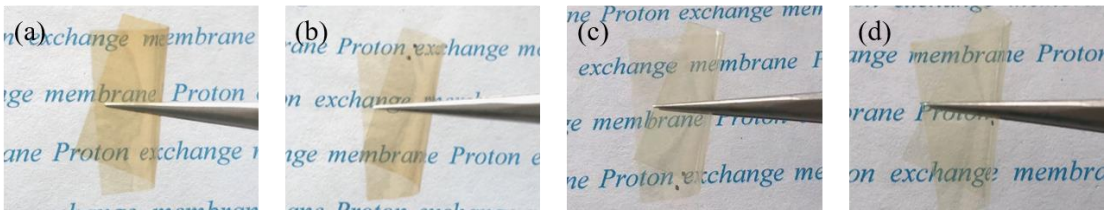

Figure A.1. The visual images of **(a)** B-10-SPAEKS-30; **(b)** L-SPAEKS-30; **(c)** B-10-SPAEKS; **(d)** B-12.5-SPAEKS-graft-40 membranes.

List of Abbreviations

PEMs	proton exchange membranes
PFSA	perfluorosulfonic acid
DB	degree of branching
IEC	ion exchange capacity
SOFCs	solid oxide fuel cells
MCFCs	molten carbonate fuel cells
PAFCs	phosphoric acid fuel cells
PEMFCs	proton exchange membrane fuel cells
AFCs	alkaline fuel cells
PAEs	poly(arylene ether)s
SPAEs	sulfonated poly(arylene ether)s
SAXS	small-angle X-ray scattering
TEM	transmission electron microscope
AFM	atomic force microscope
RH	relative humidity
PAEKS	poly(arylene ether ketone sulfone)
SPAEKS	sulfonated poly(arylene ether ketone sulfone)
DS	degree of sulfonation
WU	water uptake
SR	swelling ratio
IP	in-plane
TP	through-plane
SEC	size exclusion chromatography
^{1}H NMR	proton nuclear magnetic resonance
FT-IR	Fourier-transform infrared
TGA	thermogravimetric analysis
MEA	membrane electrolyte assembly
NMP	*N*-methyl-2-pyrrolidone

DMAc	*N,N*-dimethylacetamide
DMSO	dimethyl sulfoxide
DFBP	4,4'-difluorobenzophenone
DHDPS	4,4'-dihydroxydiphenylsulfone
DBDMH	1,3-dibromo-5,5-dimethylhydantoin
NaH	sodium hydride
DME	1,2-dimethoxyethane
BBr_3	boron tribromide
Na_2CO_3	anhydrous sodium carbonate
K_2CO_3	anhydrous potassium carbonate
$AlCl_3$	anhydrous aluminum chloride

List of Publications

[1] **Yunji Xie**, Di Liu, Anna Ringuette, and Patrick Théato*. Branched poly(arylene ether ketone sulfone)s with ultradensely sulfonated branched centers for proton exchange membranes: Effect of the positions of the sulfonic acid groups. *ACS Applied Materials & Interfaces*, 2023, 15 (20), 24517-24527.

[2] **Yunji Xie**, Di Liu, Anna Ringuette, Jinhui Pang, Hatice Mutlu, Dominik Voll, and Patrick Théato*. Highly branched poly(arylene ether ketone sulfone)s bearing flexible sulfoalkyl side chains for proton exchange membranes, *ACS Applied Energy Materials*, 2023, 6 (1), 564-572.

[3] **Yunji Xie**, Anna Ringuette, Di Liu, Jinhui Pang, Hatice Mutlu, Dominik Voll, and Patrick Théato*. Sulfonated branched poly(arylene ether ketone sulfone) proton exchange membranes: Effects of degree of branching and ion exchange capacity, *European Polymer Journal*, 2023, 186, 111837.

Conference Contributions

[1] *2023 Macromolecular Colloquium Freiburg*

Poster presentation: Structure and properties of branched poly(arylene ether ketone sulfone) proton exchange membranes: Effect of position of the sulfonic acid group

Acknowledgments

As I pen down this acknowledgment, I am taken back to 28.12.2018, when I first stepped onto German soil, alone yet hopeful. The initial sights of Karlsruhe Hbf Vorplatz are still imprinted on my mind. It is incredible how swiftly four and a half years have elapsed, and I am on the brink of concluding my Ph.D. Reflecting on this journey, I have been fortunate to meet with many incredible individuals whose support and company have shaped my experiences. Each of you truly deserves my heartfelt gratitude.

My deepest appreciation goes to my supervisor, Prof. Dr. Patrick Théato. Your faith in me opened doors to invaluable opportunities, allowing me to join your esteemed team, explore my research interests, and grow academically. Your guidance, assistance, and financial support during my Ph.D. have been invaluable. I am enthusiastic about potential collaborations and accomplishments with you in the future.

I would also like to acknowledge JProf. Dr. Hatice Mutlu and Dr. Dominik Voll for their indispensable assistance in manuscript preparation and daily lab affairs. Special thanks go to our lab technician, Mrs. Katharina Kuppinger, for managing the lab supplies and helping overcome daily lab challenges. I owe my gratitude to Prof. Dr. Jinhui Pang and Dr. Di Liu from Jilin University, China, for their tremendous support in performance measurements. My intern, Anna Ringuette, deserves special recognition for her help in the synthesis of monomers and polymers.

Dr. Wenyuan Dong and Dr. Hongxin Zhang, my apartment mates and travel companions. Our shared living experiences, commutes, and cooking sessions constituted some of my most

cherished memories. To Victoria, Dr. Johannes Scheiger, and Dr. Yosuke Akae, our mutual support and camaraderie at Lab 209 over these years have been instrumental in my Ph.D. journey. Meryem, your kindness and encouragement during difficult times have been a beacon of light to me.

I extend my appreciation to my dear friends and esteemed colleagues, whose presence and assistance, be it momentary or consistent, have left indelible imprints on my life. Thank you, Dr. Wenwen Xue, Dr. Shouliang Nie, Dr. Bo Chen, Dr. Qiyang Jiang, Dr. Zengwen Li, Dr. Xiaohui Li, Dr. Xia Huang, Dr. Marvin Subarew, Dr. Isabella Weiß, Prof. Dr. Weigui Fu, Prof. Dr. Xiang Zhang, Dr. Martin Gauthier-Jaques, Dr. Sergej Baraban, Dr. Edgar Molle, Dr. Stefan Frech, Dr. Andreas Butzelaar, Vaishali, David, Daniel, Alex, Nico, Sven, Klara, Cornelius, Tiechen, Yibo, Dr. Azra Kocaarslan, Dr. Miriam Khodeir, and many others.

I express my sincere gratitude to the China Scholarship Council (CSC) for funding my Ph.D. research, and to DAAD STIBET for the pre-graduate scholarship during the final stage of my Ph.D.

My deepest affection goes out to my girlfriend, Dr. Di Liu. Our journey, beginning on 27.11.2017, has been a constant source of strength and inspiration. Words fall short of expressing my profound love for you. Hence, at this juncture, I take the opportunity to ask, “Will you marry me?”

Finally, I owe an immense debt of gratitude to my parents, whose unwavering support and patience have been the bedrock of my achievements. I can only aspire to embody the principles and values you’ve instilled in me.